$AD\!/\!COM$

INTERMODULATION DISTORTION FROM RECEIVER
NON-LINEAR PHASE CHARACTERISTICS

Final Report

Tasks I and II

of

Radio Communications Study on
Noise Threshold Reduction

Contract NAS 5-9742

December 2, 1966

Prepared for

National Aeronautics and Space Administration
Goddard Space Flight Center
Greenbelt, Maryland

Submitted by

ADCOM, Inc.
808 Memorial Drive
Cambridge, Massachusetts 02139

ADVANCED COMMUNICATIONS • RESEARCH AND DEVELOPMENT

INTERMODULATION DISTORTION FROM RECEIVER NON-LINEAR PHASE CHARACTERISTICS

Final Report

Tasks I and II

of

Radio Communications Study on
Noise Threshold Reduction

Contract NAS 5-9742

December 2, 1966

Authors

Ahmad F. Ghais
Charles J. Boardman
Bert D. Nelin

Prepared for

National Aeronautics and Space Administration
Goddard Space Flight Center
Greenbelt, Maryland

Approved by *Steven M. Sussman*
Steven M. Sussman
Director of Research

Submitted by

ADCOM, Inc.
808 Memorial Drive
Cambridge, Massachusetts 02139

G-63

ABSTRACT

In Part I of this report the effect of predetection-filter characteristics on telemetry-data quality is studied. Intermodulation distortion is recognized as the primary data-degrading effect. A realistic, practical and tractable method of characterizing this type of distortion is shown to be the noise-loading technique.

Mathematical models are formulated for angle-modulation systems, and distortion mechanisms are identified. Narrowband angle-modulation signals are found to suffer no intermodulation distortion in predetection filters. The distortion mechanism for other signals is found to hinge on the ratio of video-signal bandwidth to filter bandwidth. Two cases are identified: the quasi-stationary case, when this ratio is much less than unity, and the general case when it is not.

In the quasi-stationary case, the distortion is determined entirely by the filter phase characteristic, whereas in the general case the whole transfer function determines the distortion. The distortion spectrum is computed for each case, and the contributions caused by filter asymmetry are isolated.

The preceding results are applied in Part II of this report to the computation of intermodulation distortion levels produced by predetection filters in telemetry systems. Filter types commonly employed in telemetry receivers are catalogued along with their distortion levels, shape factors and noise bandwidths. The tradeoffs between these performance measures are considered, leading to meaningful and effective methods of specifying filter performance.

The noise-loading technique is also applied to the characterization of nonlinearities in modulators and demodulators. The intermodulation distortion levels are evaluated in terms of these nonlinearities and the signal parameters.

Advanced types of filters are considered for use in future telemetry systems in order to improve data quality, and a study and development effort is recommended to achieve this end.

TABLE OF CONTENTS

PART I

TELEMETRY RECEIVER PHASE CHARACTERISTICS AND DATA DISTORTION

TABLE OF CONTENTS - PART I (Cont.)

ADVANCED COMMUNICATIONS • RESEARCH AND DEVELOPMENT

TABLE OF CONTENTS

PART II

COMPUTATION AND SPECIFICATION OF
INTERMODULATION DISTORTION

LIST OF ILLUSTRATIONS
PART I

LIST OF ILLUSTRATIONS

PART II

LIST OF NOTATIONS

(Arranged in order of appearance in the main text.)

t	time variable
$x(t)$	waveform at system input; also, telemetry video signal at input to FM modulator (Fig. 10)
$y(t)$	waveform at system output; also, telemetry video signal at output of FM demodulator (Fig. 10)
$h(t)$	system (or filter) impulse response; also, impulse response of predetection filter (Fig. 10)
ω	angular-frequency variable
$X(\omega)$	Fourier transform of $x(t)$
$Y(\omega)$	Fourier transform of $y(t)$
$H(\omega)$	Fourier transform of $h(t)$, hence filter transfer function
$z(t)$	waveform at equalizer output
$h_e(t)$	linear-equalizer impulse response
$Z(\omega)$	Fourier transform of $z(t)$
$H_e(\omega)$	Fourier transform of $h_e(t)$, hence linear-equalizer transfer function
$S_w(\omega)$	power-density spectrum of any waveform $w(t)$
$F[\cdot]$	function appearing in transfer relation of a memoryless nonlinear system (Eq. (7))
$F\{\cdot\}$	functional appearing in transfer relation of a nonlinear system with memory (Eq. (18))
τ	time-shift variable in correlation operations
$R_w(\tau)$	autocorrelation function of any waveform $w(t)$
$\delta(\cdot)$	impulse "function"
$G[\cdot]$	function appearing in transfer relation of a memoryless nonlinear equalizer (Eq. (17))
I/S	intermodulation-to-signal power-density ratio, a function of frequency within the video band

$u(t)$	angle-modulated signal at input to predetection filter (Eq. (35) and Fig. 10)
A	peak amplitude of $u(t)$
ω_c	carrier frequency at IF or RF
$\phi(t)$	instantaneous phase modulation on $u(t)$
ω_e	rms frequency deviation in FM system
$v(t)$	output of predetection filter when $u(t)$ is the input (Eq. (38))
$B(t)$	instantaneous amplitude of $v(t)$, hence AM introduced by predetection filter
$\theta(t)$	instantaneous phase modulation on $v(t)$
$h_p(t)$	cophasal component of $h(t)$ (Eq. (41))
$h_q(t)$	quadrature component of $h(t)$ (Eq. (41))
$H_1(\omega)$	positive-frequency part of $H(\omega)$ (Eq. (42))
$H_2(\omega)$	negative-frequency part of $H(\omega)$ (Eq. (42))
$H_p(\omega)$	Fourier transform of $h_p(t)$, hence symmetric part of lowpass equivalent of $H(\omega)$ (Eq. (43))
$H_q(\omega)$	Fourier transform of $h_q(t)$, hence antisymmetric part of lowpass equivalent of $H(\omega)$ (Eq. (44))
$\Phi(\omega)$	phase characteristic of predetection filter
c_i	power-series coefficients of $\Phi(\omega)$ (Eq. (57))
B	half bandwidth of predetection filter
$\theta_1(t), \theta_2(t), \theta_3(t)$	first-, second- and third-order terms in the functional Taylor series expansion of $\theta(t)$, respectively (Eqs. (63) - (70))
$I_w(\omega)$	power density spectrum of intermodulation distortion contained in any waveform $w(t)$; a function of frequency within the video band (Eq. (71))
$\hat{\omega}$	video signal bandwidth rad/sec.

ν	normalized angular-frequency variable for video signals, given by $\omega/\hat{\omega}$
$\otimes$	denotes convolution operation
$H_i(x)$	Hermite-polynomials (Eqs. (78) - (80))
h_i	Hermite coefficients (Eqs. (78) - (81))
$\psi(t,\sigma)$	a modified phase-modulation waveform (Eq. (88))
$*$	asterisk denotes complex conjugate
T_i	terms in the expansion of R_ψ (Eq. (95))
m_i	moments of $h_p(t)$ (Eq. (96))
a_i	power-series coefficients of $H_p(\omega)$ (Eqs. (98), (99))
n_i	moments of $h_q(t)$ (Eq. (101))
b_i	power-series coefficients of $H_q(\omega)$ (Eqs. (102), (103))

PART I

TELEMETRY RECEIVER PHASE CHARACTERISTICS AND DATA DISTORTION

1. INTRODUCTION

1.1 Purpose

This part comprises the second final task report on the results of a program of investigations carried out at ADCOM, Inc. under Contract No. NAS 5-9742 for NASA. This work was conducted in close coordination with, and in direct support of, activities of members of the RF Systems Branch, Advanced Development Division of the Goddard Space Flight Center.

The effort during the quarter 1 December 1964 - 28 February 1965 was allocated exclusively to performing the second task of the study program. Since the task was completed in one quarter, no quarterly reports are contractually required for the second quarter.

1.2 Scope

Task II of the study program is defined in the task requirements of the subject contract as follows:

> The nonlinear phase characteristic and phase distortion exhibited by conventional telemetry receivers deteriorate the fidelity of data recovery. Some of the undesirable products of this phase distortion are recognized as crosstalk between frequency multiplexed channels and degradation of bit error rates of PCM signals.

> The object of this task is to determine and report on the effects of nonlinear phase variations on various circuit operations. In addition to the analysis, the report should contain handbook-type information, tables and graphs showing the relation between phase nonlinearity expressed in an easily interpreted fashion to such functions as the generation of intermodulation products, deterioration of bit error rates, et al.

> The results of this task were presented orally to the technical staff of the RF Systems Branch on three occasions:

Date of Presentation	ADCOM Staff Participating
1 December 1964	Ahmad F. Ghais Bert D. Nelin
5 February 1965	Ahmad F. Ghais Bert D. Nelin
22 February 1965	Ahmad F. Ghais

In addition, most of the contents of Secs. 2 and 3 were presented in the form of an informal technical memorandum to the technical representative of the contracting officer. This was numbered G-63-3, and entitled "Intermodulation Distortion in FDM-FM Systems."

The remainder of this introductory section is devoted to a general discussion of the problem of telemetry data distortion caused by receiver phase nonlinearity. We describe our approach to the problem, and preview the contents of the main body of the report.

1.3   Telemetry Modulation Techniques and Data Distortion

The need for increased reliability and accuracy in the extraction of telemetry data under adverse conditions has become acute with the increased magnitude and complexity of spacecraft missions. It is known that nonlinearities in the phase characteristics of receivers and recorders can produce data distortion, but until recently very little effort has been devoted to determining the quantitative relationships between phase nonlinearities and data distortion.

Figure 1 illustrates the general configuration of an angle-modulation telemetry system. Two subsystems depicted in this figure incorporate filters that may distort the telemetry data because of their nonlinear phase characteristics. We use the generic term predetection filters to refer to all these filters.

The manner in which each of the phase characteristics may distort the telemetry data depends on the way the data are modulated on the signal passing
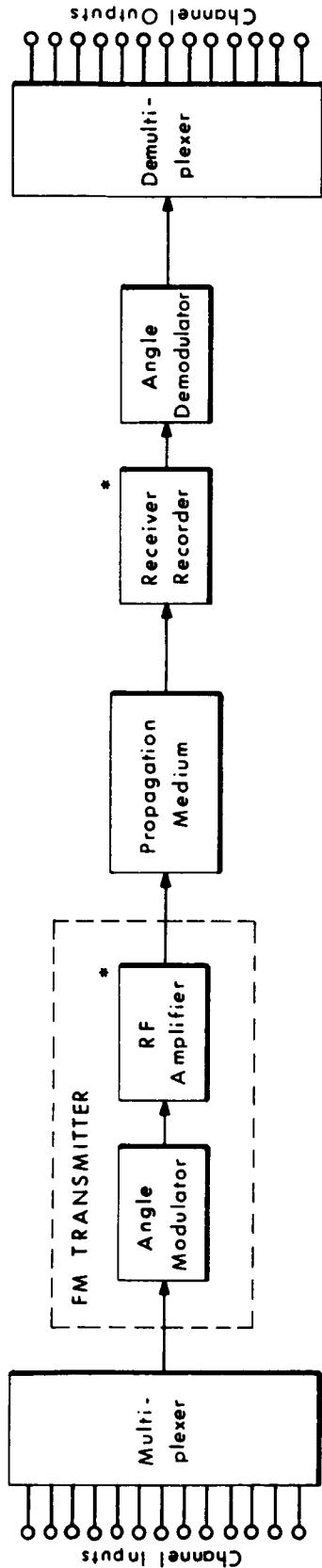
Fig. 1 Typical Angle-modulation Telemetry System.
(*Asterisks mark locations of predetection filters).

R-662

through the filter. All standard telemetry formats employ frequency or phase modulation on the transmitted carrier, and many also have FM or PM sub-carriers. Now, there is no fundamental difference between phase and frequency modulation. Appropriate baseband filtering can convert one type of modulation to the other. Indeed, FM with conventional pre-emphasis and de-emphasis filtering represents an intermediate type of modulation between pure FM and PM. We use the generic term <u>angle modulation</u> to include all these types of modulation, and concentrate the discussion in this document on the distortion of angle-modulated data.

Although amplitude modulation on the transmitted carrier is seldom (if ever) used in space telemetry, we briefly discuss in Sec. 3.2 the effects of phase nonlinearities on it, because the effects are very similar to those observed on low-deviation angle-modulation signals.

1.4   <u>Sources of Data Degradation in Telemetry Systems</u>

In this section, we briefly review the sources of data degradation in telemetry systems, in order to:

a) place the problem of distortion caused by phase non-linearities in perspective, and

b) identify the subsystems in the receiving system that contribute to distortion by their nonlinear phase characteristics.

Referring to Fig. 1, we note that the video output of the receiving system is still in its multiplexed form. In order to extract the telemetry data, the video is fed to the demultiplexer. Now suppose that one of the data channels is kept empty at the transmitter by eliminating the appropriate subcarrier, and all the other channels are fully loaded. Ideally, the corresponding demultiplexer output remains zero. However, because of practical system imperfections this is not the case. A certain amount of undesired signal (or noise) is always present at the output of the presumably empty channel. Had the channel been loaded, this undesired signal would have degraded the channel signal by superposition.

These undesired signals can be separated into three groups, namely:

a) noise caused by additive noise at the receiver input,

b) interchannel crosstalk, and

c) intermodulation distortion.

a) The noise caused by additive receiver and antenna noise is a well-known phenomenon. Characteristic of this type of output noise is the fact that it is relatively independent of the video signal and will always occur even when all channels are empty. In the following we will assume that the received signal strength is so large that the effects of additive noise can be ignored.

b) Interchannel crosstalk is caused by imperfect channel filtering, as opposed to imperfect predetection filtering. Interchannel crosstalk in a given channel consists mainly of components from the two adjacent channels which are not sufficiently attenuated by the skirts of the given channel filter. It can readily be evaluated by applying linear system theory.

The interchannel crosstalk can be easily distinguished from intermodulation distortion by placing the multiplexer back-to-back with the demultiplexer and only loading the two channels adjacent to the observed (empty) channel. Intermodulation distortion is negligible under these conditions.

c) Intermodulation distortion is caused by nonlinearities in the telemetry system. By nonlinearity we mean here any operation which creates spectral components in the video output that were absent in the video input. We shall show in Sec. 3.1 that a frequency modulator is inherently nonlinear, even though it may have a perfectly linear voltage-to-frequency characteristic, because it spreads the spectrum of the modulating signal in the process of transferring it

to a higher frequency band. We shall also show how, and to what extent, a common RF filter inserted in the receiver between a frequency modulator and a frequency demodulator has a nonlinear effect on the data and produces intermodulation distortion of the video signal. The intermodulation distortion in a channel is very much dependent (in a complicated way) on the signals in all the other channels and will essentially vanish if all other channels are empty.

The following sources of intermodulation distortion may occur in an angle-modulation telemetry system:

a) nonlinearities in baseband and multiplex circuits,

b) (FM or PM) modulator nonlinearity,

c) predetection filtering at the receiver system,

d) antenna feeder mismatch at the transmitter or receiver,

e) multipath effects in the propagation medium
(e. g., frequency-selective fading),

f) FM demodulator nonlinearity,

g) time-base fluctuations in the predetection recorder/
reproducer (wow and flutter), and finally,

h) FM-to-AM conversion in predetection filters, fol-
lowed by AM-to-video conversion by demodulators
(incorporating limiters) that are not completely
amplitude insensitive.

The fundamental objective of the present task is to evaluate the effects of nonlinear phase characteristics exhibited by telemetry receivers on telemetry data quality. Thus, of the sources listed in (a) to (h) above, we are primarily concerned with intermodulation distortion caused by predetection filters.

Figure 2 is a functional block diagram of a typical telemetry receiving system; the possible locations of predetection filters are identified in this figure.

6
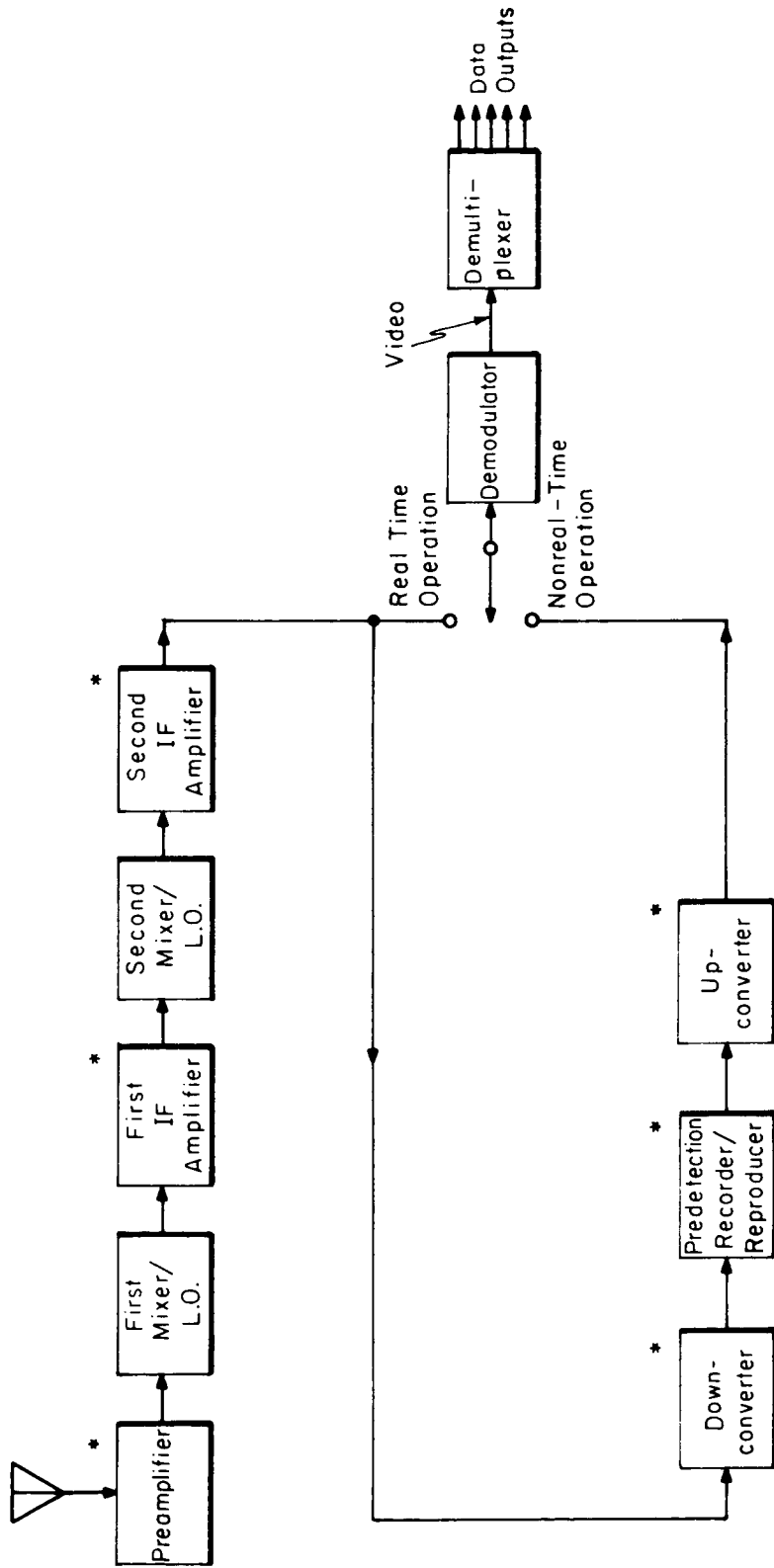
Fig. 2 Typical Telemetry Receiving System.
(* Asterisks mark locations of predetection filters).

R-661

7

The functions of predetection filters are:

    a) to reduce the total additive noise power appearing
       at the demodulator input,

    b) to reject interfering signals from adjacent telemetry
       bands, and

    c) to reject undesired mixer products.

All these functions are best achieved by narrowing the filter bandwidth as far as possible without causing undue distortion of the telemetry data. It is customary to specify the amplitude characteristic of the desired filter, without much regard to the associated phase characteristic. And yet it is well-known that the phase characteristic can exhibit gross nonlinearities, especially at the edges of the passband, resulting in message distortion. It is essential for the telemetry system designer to have at his disposal clear and concise information relating the filter characteristics with resultant data distortion.

Customarily, all but one of the predetection-filtering blocks depicted in Fig. 2 are wideband designs whose function is primarily to reject undesired mixer and spurious components. The remaining block, usually the second IF amplifier, is carefully designed to restrict the bandwidth of the entire receiver, and hence to perform functions (a) and (b) listed above. Phase nonlinearities over the telemetry signal bandwidth are concentrated in this one block. It is therefore sufficient to evaluate the intermodulation distortion caused by this one block; the results will not be materially changed by the presence of the other predetection filters. Of course, if several predetection filters together restrict the bandwidth of the receiver, then it is necessary to consider the cascade of these filters in determining the intermodulation distortion.

1.5   Outline of Analytical Approach

The conventional approach to the problem of phase characteristics and their effects on message transmission has been to evaluate the distortion of the

RF (or IF) signal, and then to attempt to relate this distortion to data (or message) degradation. We believe that the results of the second step in this approach have been inconclusive, which accounts for the complete lack of design information that relates phase characteristics and data quality. We take a novel approach to the problem, and demonstrate that it yields the desired design information. This novel approach,which is based in part on the work of Magnusson,[1,2] directly relates video signal degradation to phase characteristics, completely bypassing the RF distortion problem.

In order to coherently present our technique for evaluating intermodulation distortion in terms of the configurations and parameters of the system, it is necessary to begin in Sec. 2 by identifying and characterizing various general classes of distortion mechanisms, and introducing the analytical tools appropriate to each class. Readers familiar with these techniques may wish to skip over Sec. 2 and proceed directly to Sec. 3. Three classes of distortion mechanisms are identified:

    a) distortion in linear systems,
    b) distortion in memoryless nonlinear systems, and
    c) distortion in nonlinear systems with memory.

In Sec. 3, we show that the nature of the transfer relation for an angle-modulation system depends on the deviation ratio involved. Thus the distortion mechanism of the predetection filter corresponds to those listed above for low, high and medium deviation ratios respectively:

Case I: Narrowband Angle Modulation

By narrowband angle modulation (FM or PM) of the carrier is meant the case in which the resulting phase deviation is small compared to one radian. (See Ref. 3, Ch. 19.) An FM deviation ratio much smaller than unity satisfies this

condition. We show in Sec. 3.2 that the transmitted signal can then be viewed as the result of a <u>linear</u> modulation operation very similar to amplitude modulation. The predetection filter has a linear distortion effect on the modulation just like a video filter. Thus no intermodulation distortion is caused by the predetection filter, irrespective of its phase characteristic.

Case II: The Quasi-stationary Case

If the message bandwidth is much smaller than the predetection filter bandwidth, then the instantaneous frequency of the FM signal can be viewed as tracing the static phase characteristic of the predetection filter. This is the case if the FM deviation ratio is much greater than unity. We find in this case that the intermodulation distortion is determined only by the filter nonlinear phase characteristic, and not by its amplitude characteristic (assuming that the demodulator is amplitude insensitive, of course). The distortion mechanism is thus memoryless nonlinearity. This is discussed in Sec. 3.3. A distortion equalizer for the quasi-stationary distortion is also described in Sec. 3.3.

Case III: General Angle Modulation

By deriving the transfer relation for a general angle modulation system, we show in Sec. 3.1 that general angle modulation is fundamentally a nonlinear modulation technique, and that predetection filtering introduces memory in such a system. Thus the distortion mechanism is nonlinearity with memory. We find that the entire transfer function of the filter (i.e., both its amplitude and phase response) is involved in the intermodulation distortion mechanism. The general case is particularly applicable to telemetry systems employing intermediate values of deviation ratio (in the order of 1 to 3), where the ratio of filter bandwidth to message bandwidth is not much larger than unity.

In Sec. 3.4 we develop a simple approximation to the transfer relation, using the functional Taylor series technique. We are then able to identify the

distortion terms in the expansion of the demodulated video, thus paving the way for subsequent evaluation of intermodulation distortion in terms of filter characteristics. The functional Taylor series technique also facilitates the derivation of distortion equalizers. One such equalizer, operating on the demodulated video signal, is outlined in Sec. 3.4.

The results of Sec. 3 are employed in Secs. 4 and 5 to compute intermodulation distortion levels. We begin in Sec. 4 by selecting a suitable measure of video distortion, and describing a simple method of measuring it. This measure is the power-density spectrum of the intermodulation distortion, a particularly suitable measure for multi-channel telemetry systems employing frequency-division multiplexing. The objective is to relate the distortion spectrum to the parameters characterizing the video signal and the predetection filter.

Next, we choose to model the video signal by a gaussian noise process having a power-density spectrum similar to the message spectrum found in practice. It can be shown that the statistical properties of gaussian noise are very similar to those of a complex multichannel FDM video signal. Thus it is meaningful to simulate the video signal by a gaussian noise process.

In addition to being analytically convenient, this so-called noise-loading approach greatly simplifies experimental verification. Intermodulation distortion tests can be standardized and the measurements easily reproduced. In contrast, we believe that the customary method of simulating the video signal by a set of unmodulated subcarriers is inadequate. It is both mathematically intractable (except in the trivial case of one or two subcarriers) and experimentally cumbersome.

The remainder of Sec. 4 is devoted to the computation of the intermodulation spectrum in the quasi-stationary case. The static phase characteristic

is a sufficient characterization of the filter in this case. We expand the phase characteristic in a power series, and use a truncated series as an approximation. The distortion spectrum is found to involve multiple convolutions of the input video spectrum (see Eqs. (76) and (77)). The filter characteristic comes in only as constant factors determined by the phase power-series coefficients. Thus, given a video spectrum, we first compute the necessary convolutions (which can often be obtained in closed form), and then by finding the phase power-series coefficients of the predetection filter we can immediately write down the distortion spectrum. Any change of filter characteristic would not necessitate an elaborate recomputation.

A second method of computing the distortion spectrum in the quasi-stationary case is presented in Sec. 4.3. This has certain computational advantages over the power-series method. The phase characteristic is expanded in a series of Hermite polynomials, thus greatly simplifying the form of the final results (see Eqs. (84) and (85)).

In Sec. 5 we use the results of Sec. 3 to determine the intermodulation-distortion spectrum in the general case. The second-order distortion term may predominate over higher-order distortion terms in the general case of asymmetric filters; it vanishes for symmetric filters. An exact result is attained for the distortion spectrum in the second-order term, involving convolutions of the input video spectrum and the filter transfer function (see Eq. (92)). These convolutions would have to be evaluated numerically for each combination of input video spectrum and predetection filter of interest.

A method is described in Sec. 5.2 for bypassing the arduous numerical computation of the distortion spectrum for each case of interest. The filter transfer function is characterized by a set of coefficients of its power-series expansion, and an approximation to the distortion spectrum is obtained involving convolutions of the input video spectrum alone. The filter characteristic comes

in only as constant factors determined by the power-series coefficients (see Eqs. (104) and (105)). As in the quasi-stationary case of Sec. 4, the results of this approximation are flexible enough to accommodate any filter characteristic without elaborate recomputation.

The intermodulation-distortion spectrum for a symmetric filter is determined in Sec. 5.3. In this case the third-order distortion term predominates over higher-order distortion terms. Here again, an exact result is attained, involving double convolutions of the input video spectrum and the filter transfer function (see Eq. (110)). An approximation is obtained involving double convolutions of the input video spectrum alone, the filter characteristic coming in only as constant factors determined by the power-series coefficients (see Eqs. (112) and (113)).

2. GENERAL CLASSES OF DISTORTION MECHANISMS

2.1 Distortion in Linear Systems

A signal passed through a linear system suffers certain changes, often called linear distortion. A linear system (or network) does not create any new spectral components or intermodulation products. Thus, if the impulse response of a linear time-invariant system is h(t) then the system output y(t) for an input x(t) is given by the linear convolution

$$y(t) = \int_{-\infty}^{\infty} h(\tau) \, x(t-\tau) \, d\tau \tag{1}$$

The Fourier spectrum $Y(\omega)$ of y(t) can then be expressed in terms of the spectrum $X(\omega)$ of the input as

$$Y(\omega) = H(\omega) \cdot X(\omega) \tag{2}$$

where $H(\omega)$ is the transfer function corresponding to h(t).

By processing the linearly distorted output y(t) by another linear network it is possible to remove the linear distortion from y(t). The resulting output is then identical to x(t). The second network is in this case called a linear equalizer.

Figure 3 illustrates a linear equalizer. The transfer function of the equalizer is denoted by $H_e(\omega)$ and its output by z(t). The spectraum $Z(\omega)$ of z(t) is given by

R-1211
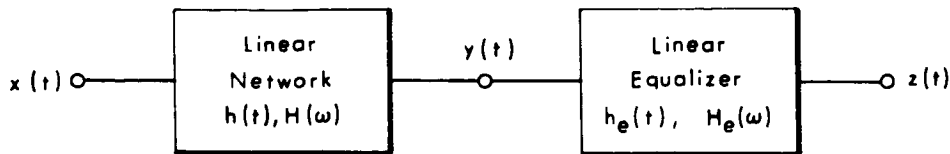
Fig. 3 Linear Network with Equalizer.

$$Z(\omega) = H(\omega) \, H_e(\omega) \, X(\omega) \tag{3}$$

From the condition that $Z(\omega) = X(\omega)$ we obtain the transfer function of the linear equalizer

$$H_e(\omega) = 1/H(\omega) \tag{4}$$

$H_e(\omega)$ might not be physically realizable. However, it should be noted that relation (4) has to be satisfied only for frequencies over which $X(\omega)$ has appreciable components. Thus, even if $H_e(\omega)$ is not realizable, it may still be possible to realize a network which satisfies (4) over the frequency range of $X(\omega)$. This is sufficient for successful equalization of y(t).

Denoting by $h_e(t)$ the impulse response of a linear equalizer which satisfies (4), we may write

$$z(t) = \int_{-\infty}^{\infty}\int h_e(\tau_2) \, h(\tau_1) \, x(t-\tau_1-\tau_2) \, d\tau_1 \, d\tau_2 = x(t) \tag{5}$$

Thus, the operation of $h_e(t)$ "undoes" the operation of h(t) on x(t).

In this connection, it is of interest to recall how a linear-distorting operation affects the power-density spectrum of a random signal. If the power-density spectrum of a random input signal x(t) is denoted by $S_x(\omega)$ and the transfer function of the linear network is $H(\omega)$, then the power-density spectrum $S_y(\omega)$ of the output is given by

$$S_y(\omega) = |H(\omega)|^2 S_x(\omega) \tag{6}$$

2.2 Distortion in Memoryless Nonlinear Systems

A memoryless nonlinear system may be defined by a nonlinear operation, the output of which is completely independent of the frequency of the input signal

16

and only dependent on the instantaneous value of the input signal. Thus, the so-called "static" input-output characteristic does not change with the speed of variation of the input signal. Or in other words, the dynamic and static nonlinear characteristics are always identical for this type of nonlinear system.

The transfer relation of a memoryless nonlinear system is of the form

$$y(t) = F[x(t)] \tag{7}$$

where $F[\cdot]$ denotes a nonlinear <u>function</u>.* Figure 4 shows a typical graph of the nonlinear characteristic of a memoryless nonlinearity. In order to analyze the operation of a memoryless nonlinearity it is frequently advantageous to perform

R -1212
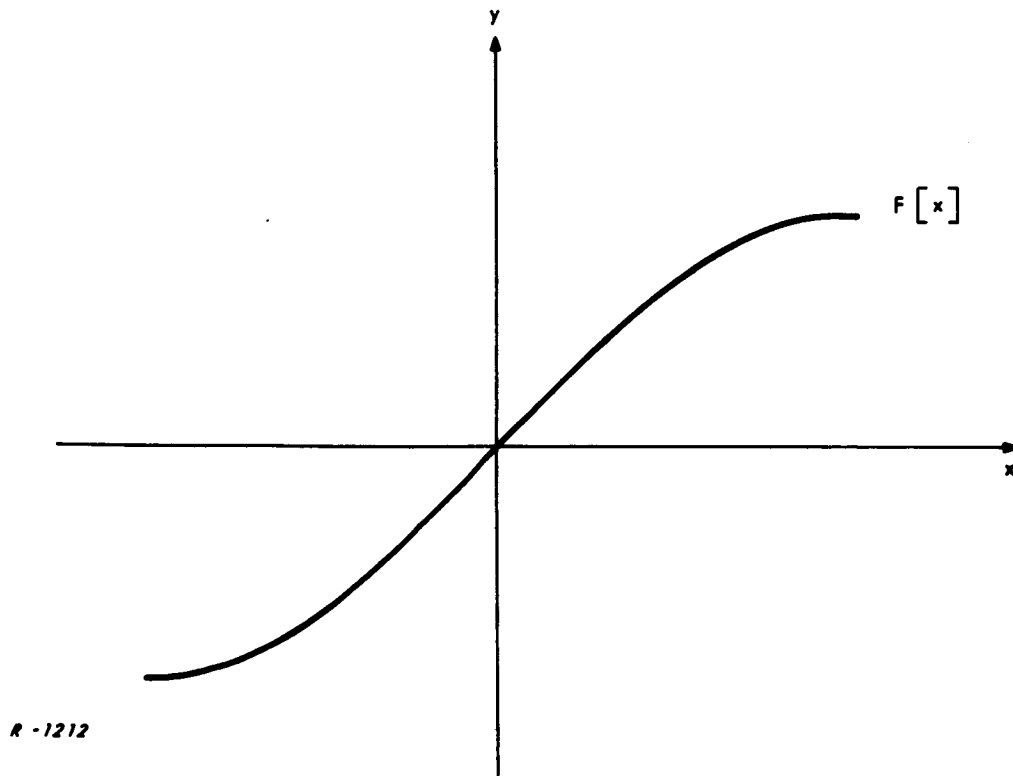
Fig. 4 Characteristic of a Memoryless
Nonlinear System.

---

* By "function", we mean a one-to-one correspondence between the values of $y(t)$ and $x(t)$ at any given instant t.

a power series expansion of the nonlinear characteristic. One such expansion is the familiar Taylor series. Thus, if the input variable x is defined so that $F[x] = 0$ for $x = 0$, then the Taylor series (if it exists) for $F[x]$ about the point $x = 0$ is of the form

$$F[x] = \sum_{n=1}^{\infty} \frac{1}{n!} \left(\frac{d^n F[x]}{dx^n} \right)_{x=0} \cdot x^n$$

$$= \left(\frac{dF[x]}{dx} \right)_{x=0} x + \left(\frac{d^2 F[x]}{dx^2} \right)_{x=0} \cdot \frac{x^2}{2!} + \left(\frac{d^3 F[x]}{dx^3} \right)_{x=0} \cdot \frac{x^3}{3!} \cdots$$

(8)

When the distortion is small the Taylor series converges rapidly and only a few terms are necessary to characterize the nonlinear operation.

Characteristic of nonlinear operations is the creation, in the output, of new spectral components that did not exist at the input. This phenomenon is often called spectral spreading. For illustration, let the nonlinear characteristic be a simple squaring operation $F[x] = x^2$. Assume that the input is a zero-mean gaussian process x(t) with the autocorrelation function $R_x(\tau)$ and power-density spectrum $S_x(\omega)$. Then the output signal is

$$y(t) = x^2(t) \tag{9}$$

and the output autocorrelation function $R_y(\tau)$ is obtained from[*]

$$R_y(\tau) = \overline{y(t)\, y(t+\tau)} = \overline{x^2(t)\, x^2(t+\tau)} \tag{10}$$

Using the rule for the average of the product of gaussian variables (see Ref. 4) Eq. (10) becomes

$$R_y(\tau) = \overline{x^2(t)} \cdot \overline{x^2(t+\tau)} + \overline{2[x(t)\, x(t+\tau)]}^2$$

$$= R_x^2(0) + 2R_x^2(\tau) \tag{11}$$

*The over-bar denotes statistical average.

The power-density spectrum $S_y(\omega)$ of y(t) is obtained from $R_y(\tau)$ by means of the cosine Fourier transform

$$S_y(\omega) = \int_{-\infty}^{\infty}\left\{R_x^2(0) + 2R_x^2(\tau)\right\}\cos(\omega\tau)\,d\tau \qquad (12)$$

The first term in the integral of Eq. (12) corresponds to a dc component and yields an impulse at $\omega = 0$ in $S_y(\omega)$, while the second term results in the convolution of $S_x(\omega)$ with itself, so that

$$S_y(\omega) = R_x^2(0) \cdot \delta(\omega) + 2S_x(\omega) \otimes S_x(\omega) \qquad (13)$$

where $\delta(\omega)$ is an impulse (i.e., discrete spectral line) at $\omega = 0$, and $\otimes$ denotes convolution in the frequency domain, i.e.,

$$S_x(\omega) \otimes S_x(\omega) = \int_{-\infty}^{\infty}S_x(p - \omega)S_x(p)\,dp \qquad (14)$$

To illustrate Eq. (13), let the power-density spectrum of x(t) be rectangular and defined by (see Fig. 5)

$$S_x(\omega) = \begin{cases} a/2 & \text{for } |\omega| < \omega_c \\ 0 & \text{for } |\omega| \geq \omega_c \end{cases} \qquad (15)$$

where a/2 is the power density and ω_c is the cutoff frequency. Carrying out the convolution of Eq. (14) yields

$$S_y(\omega) = \begin{cases} (a\omega_c)^2\{\delta(\omega) + 1 - |\omega/2\omega_c|\} & \text{for } |\omega| < 2\omega_c \\ 0 & \text{for } |\omega| \geq 2\omega_c \end{cases} \qquad (16)$$

which is illustrated in Fig. 5. It can be seen that the squaring operation has created new spectral components which were absent in the input. We shall perform similar but more general computations in Sec. 4.

19
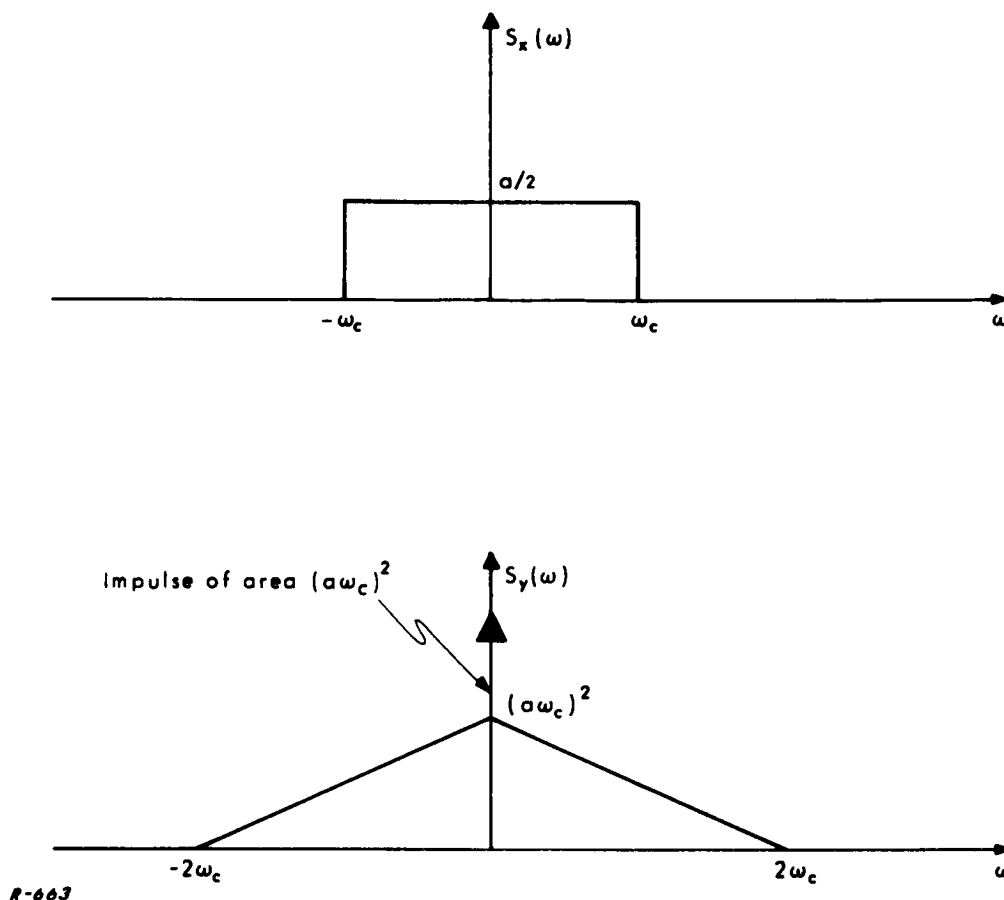
Fig. 5 Input and Output Power-density Spectra for a Gaussian Signal Passed Through a Squaring Operation.

An equalizing system for the distortion caused by a memoryless non-linear system is also a memoryless nonlinear system. The desired nonlinear characteristic $G[\cdot]$ of the equalizing network should be

$$G[y] = x \tag{17}$$

Thus, $G[\cdot]$ is the inverse function of $F[\cdot]$; as for example, $\arcsin[\cdot]$ is the inverse function of $\sin[\cdot]$ (principal value). Figure 6 shows the inverse characteristic to the characteristic of Fig.5, and Fig.7 shows how the equalizing system is used. When the distorting system is characterized in terms of a
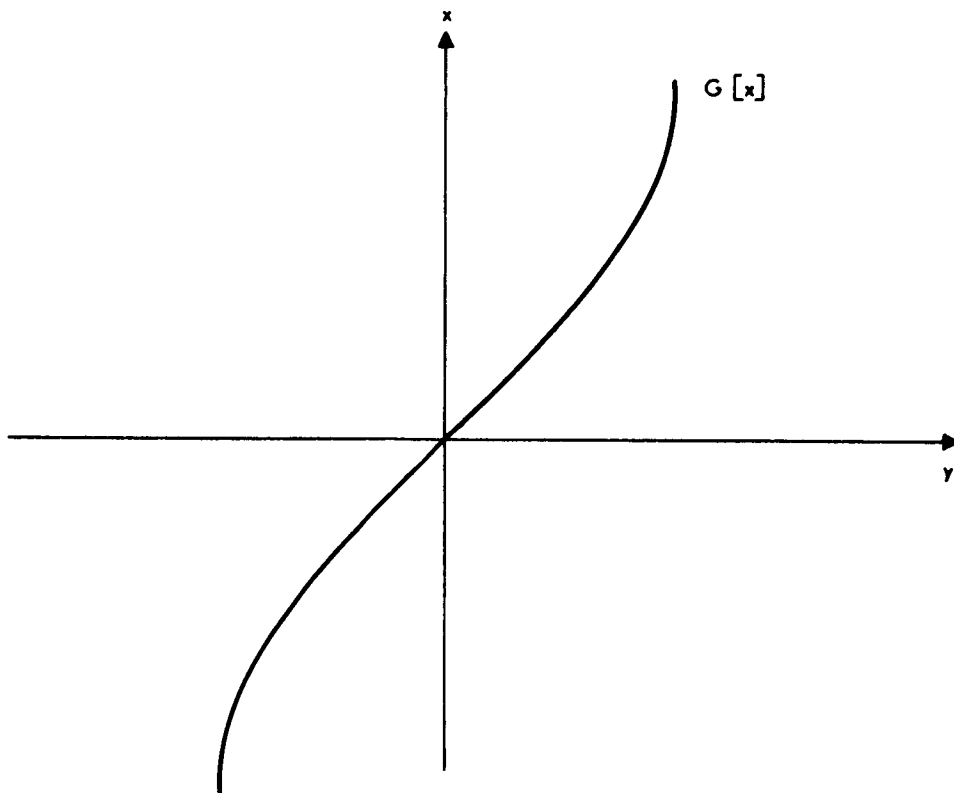
Fig. 6 Characteristic of a Memoryless Nonlinear
Equalizing System, Corresponding to the
Nonlinear System of Fig. 4.
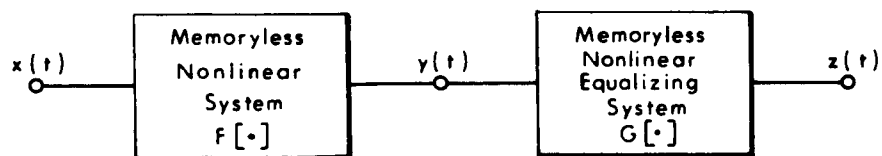
Fig. 7 Memoryless Nonlinear System with Equalizer.

21

Taylor series, the inverse characteristic (in terms of another Taylor series) can be found by reversion of the series (see Ref. 5).

2.3 Distortion in Nonlinear Systems with Memory

A nonlinear system with memory may be defined by a nonlinear operation whose output is dependent on the speed of variation of the input signal. In that case the dynamic characteristic is quite different from the static characteristic. For example, such a system may not distort a slowly varying signal but may cause appreciable distortion in a rapidly varying signal.

The relation between output and input of a nonlinear system with memory can be expressed in terms of a nonlinear functional equation. A nonlinear functional equation is an equation in which the output and input functions are related by means of a nonlinear integro-differential equation. Thus, when an explicit input-output relation exists, then this relation can be expressed as

$$y(t) = F\{x\} \tag{18}$$

where $F\{\cdot\}$ denotes a nonlinear functional.[*]

A nonlinear system with memory usually comprises nonlinearities without memory and linear filters. Figure 8 shows, as a simple example, the block diagram of such a system. The only nonlinearity in this system is the
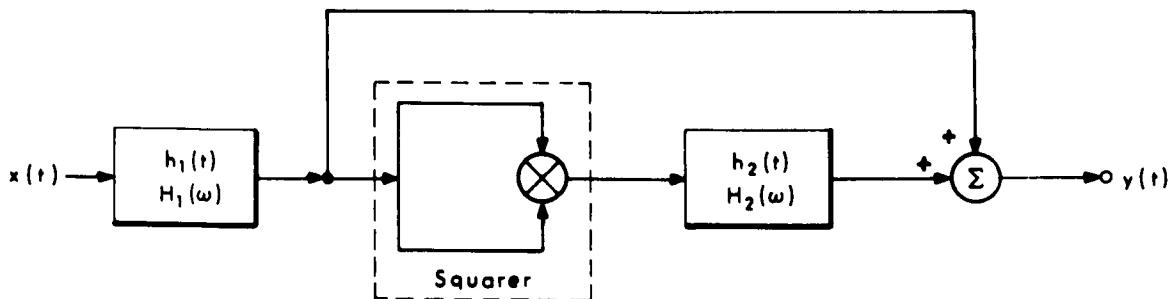
Fig. 8 A Nonlinear System with Memory.

[*]By "functional" we mean here that the value of y(t) at any given instant t
 is determined by the values of x(t) at all past instants of time as well as
 at present instant t. Hence the use of the word "memory" in this context.

22

squaring operation. The transfer relation for this network in functional form is

$$y(t) = \int_{-\infty}^{\infty} h_1(\tau) \, x(t-\tau) \, d\tau + \int_{-\infty}^{\infty} h_2(\tau_1) \left[\int_{-\infty}^{\infty} h_1(\tau_2) \, x(t-\tau_2-\tau_1) \, d\tau_2 \right]^2 d\tau_1$$

$$= \int_{-\infty}^{\infty} h_1(\tau) \, x(t-\tau) \, d\tau + \iiint_{-\infty}^{\infty} h_2(\tau_1) \, h_1(\tau_3) \, h_1(\tau_2) \, x(t-\tau_3-\tau_1) \, x(t-\tau_2-\tau_1)$$
$$d\tau_1 \, d\tau_2 \, d\tau_3 \quad (19)$$

The first term, which is a linear functional, represents a linearly distorted version of x(t). The second term, which is a nonlinear functional of second order, yields a nonlinear distortion component.

To illustrate how the output power spectrum may be obtained in such a case, consider x(t) as a zero-mean gaussian process with autocorrelation function $R_x(\tau)$ and power-density spectrum $S_x(\omega)$. The output y(t) may be written

$$y(t) = y_1(t) + y_2(t) \quad (20)$$

where $y_1(t)$ and $y_2(t)$ represent the first and second functionals of (19) respectively. Then the autocorrelation function $R_y(\tau)$ of y(t) is

$$R_y(\tau) = \overline{y(t) \, y(t+\tau)} = \overline{y_1(t) \, y_1(t+\tau)}$$

$$+ \overline{y_1(t) \, y_2(t+\tau)} + \overline{y_2(t) \, y_1(t+\tau)} + \overline{y_2(t) \, y_2(t+\tau)}. \quad (21)$$

According to the rule for the average of products of gaussian variables (Ref. 4), the average of an odd order product of zero-mean gaussian variables is zero. Since $y_1(t)$ is of first order in x(t) and $y_2(t)$ is of second order in x(t), the two middle terms in Eq. (21) are zero. Hence

$$R_y(\tau) = \overline{y_1(t) \, y_1(t+\tau)} + \overline{y_2(t) \, y_2(t+\tau)} \triangleq R_1(\tau) + R_2(\tau) \quad (22)$$

The two terms of Eq. (22) will be evaluated separately.

$$R_1(\tau) = \overline{y_1(t)\, y_1(t+\tau)} = \int_{-\infty}^{\infty}\!\!\int h_1(\tau_1) h_1(\tau_2) \overline{x(t-\tau_1)\, x(t+\tau-\tau_2)}\; d\tau_1\, d\tau_2$$

$$= \int_{-\infty}^{\infty}\!\!\int h_1(\tau_1)\, h_1(\tau_2)\, R_x(\tau+\tau_1-\tau_2)\; d\tau_1\, d\tau_2 \qquad (23)$$

and

$$R_2(\tau) = \overline{y_2(t)\, y_2(t+\tau)}$$

$$= \iiint_{-\infty}^{\infty}\!\!\iiint h_2(\tau_1)\, h_2(\tau_4)\, h_1(\tau_3)\, h_1(\tau_2)\, h_1(\tau_5)\, h_1(\tau_6)$$

$$\cdot \overline{x(t-\tau_3-\tau_1)\, x(t-\tau_2-\tau_1)\, x(t+\tau-\tau_6-\tau_4)\, x(t+\tau-\tau_5-\tau_4)}\; d\tau_1 \ldots d\tau_6$$

$$= \iiint_{-\infty}^{\infty}\!\!\iiint h_2(\tau_1)\, h_2(\tau_4)\, h_1(\tau_3)\, h_1(\tau_6)\, h_1(\tau_2)\, h_1(\tau_5)$$

$$\cdot \left[R_x(\tau_3-\tau_2)\, R_x(\tau_6-\tau_5) + 3 R_x(\tau-\tau_6+\tau_4+\tau_3+\tau_1)\, R_x(\tau-\tau_5-\tau_4+\tau_2+\tau_1) \right] d\tau_1 \ldots d\tau_6.$$

$$(24)$$

The power-density spectrum $S_y(\omega)$ of the output is obtained as the cosine Fourier transform of the autocorrelation function $R_y(\tau)$. Denoting the spectra corresponding to $R_1(\tau)$ and $R_2(\tau)$ by $S_1(\omega)$ and $S_2(\omega)$ respectively we get

$$S_y(\omega) = \int_{-\infty}^{\infty} R_1(\tau) \cos(\omega\tau)\, d\tau + \int_{-\infty}^{\infty} R_2(\tau) \cos(\omega\tau)\, d\tau = S_1(\omega) + S_2(\omega)$$

$$(25)$$

Carrying out the Fourier transformations on Eqs. (23) and (24) results in

$$S_1(\omega) = |H_1(\omega)|^2\, S_x(\omega) \qquad (26)$$

and

$$S_2(\omega) = |H_2(0)|^2 \cdot \left\{ \int_{-\infty}^{\infty} |H_1(\omega)|^2 S_x(\omega)\, d\omega \right\}^2 \cdot \delta(\omega)$$

$$+ 3|H_2(\omega)|^2 \left\{ |H_1(\omega)|^2 S_x(\omega) \otimes |H_1(\omega)|^2 S_x(\omega) \right\} \qquad (27)$$

where, as before, $\delta(\omega)$ is an impulse at $\omega = 0$ and $\otimes$ denotes convolution in the frequency domain.

$S_1(\omega)$ corresponds to the linearly distorted replica of the input signal spectrum, and may be considered as the desired part of the output spectrum. The first term of $S_2(\omega)$ is a dc component which may be considered harmless, while the part of the second term which falls within the frequency region of $S_x(\omega)$ is the spectrum of the intermodulation distortion. We may now define a new function of frequency, called the intermodulation-to-signal power-density ratio, as the second term of $S_2(\omega)$ divided by $S_1(\omega)$

$$I/S = \frac{3|H_2(\omega)|^2\{|H_1(\omega)|^2 S_x(\omega) \otimes |H_1(\omega)|^2 S_x(\omega)\}}{|H_1(\omega)|^2 S_x(\omega)} \tag{28}$$

Thus, the I/S ratio represents the degree to which the desired output spectrum at any given frequency has been contaminated by intermodulation distortion.

To illustrate Eqs. (26)-(28), let us consider the input x(t) to be a <u>white</u> gaussian random process, so that $S_x(\omega) = N_o$, and let the two filters be identical single-pole networks

$$H_1(\omega) = H_2(\omega) = \frac{1}{j\omega + \alpha} \tag{29}$$

so that

$$|H_1(\omega)|^2 = |H_2(\omega)|^2 = \frac{1}{\omega^2 + \alpha^2} \tag{30}$$

Now, the second term of $S_2(\omega)$ becomes

$$3|H_2(\omega)|^2\{H_1(\omega) S_x(\omega) \otimes |H_1(\omega)|^2 S_x(\omega)\} = 3N_o^2 (\frac{1}{\omega^2 + \alpha^2})\{(\frac{1}{\omega^2 + \alpha^2}) \otimes (\frac{1}{\omega^2 + \alpha^2})\} \tag{31}$$

The convolution is readily computed by first taking its inverse Fourier transform, recognizing that the inverse transform of $|H_1(\omega)|^2$ is $\frac{1}{2\alpha} e^{-\alpha|t|}$, then transforming back to the frequency domain. The results of the computations in Eqs. (26)-(28) are then

$$S_1(\omega) = \frac{N_o}{\omega^2 + \alpha^2} \tag{32}$$

$$S_2(\omega) = \frac{\pi N_o^2}{\alpha^5} \delta(\omega) + \frac{3N_o^2}{\alpha} \left(\frac{1}{\omega^2 + \alpha^2} \right) \left(\frac{1}{\omega^2 + (2\alpha)^2} \right) \qquad (33)$$

$$I/S = \frac{3N_o}{\alpha} \left(\frac{1}{\omega^2 + (2\alpha)^2} \right) \qquad (34)$$

Eqs. (32)-(34) are plotted in Fig. 9. It is noteworthy that the computation of the convolution in Eq. (31) was greatly facilitated by the whiteness assumption. Had the input process been other than white, it would probably be necessary to compute the convolution by numerical means. We shall encounter similar computational difficulties in Sec. 5.

When the characteristic of the memoryless nonlinearity portion of a nonlinear system with memory can be expanded in a Taylor series as in Eq. (8), the input-output relationship can be written in terms of a so-called functional Taylor series, in which the terms are functionals of increasing order. We shall derive such an expansion in Sec. 3 for the modulation transfer relationship in an FM system. This will enable the derivation of distortion equalizer structures for this type of nonlinearity with memory.
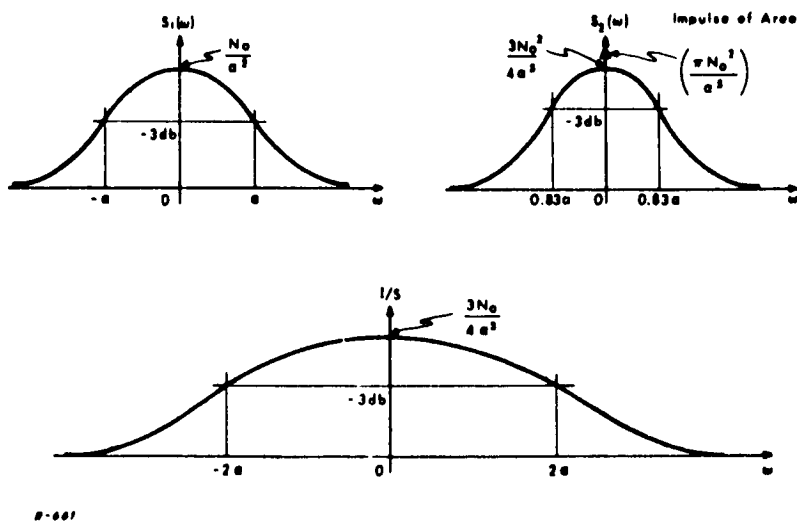
Fig. 9 Output Power-density Spectra, When Input to System of Fig. 8 is White Gaussian Noise.

3. PREDETECTION FILTERING AND INTERMODULATION DISTORTION

The purpose of this chapter is to identify the distortion mechanisms inherent in predetection filters, and to formulate the analytical tools necessary to deal with them. We begin by deriving a transfer relation of a general angle-modulation system.

3.1   The Transfer Relation of an Angle-Modulation System

An angle-modulation system comprises three main subsystems, as depicted in Fig. 10. Here the angle modulator and demodulator subsystems (which are assumed ideal) perform nonlinear operations. If the filter between these two subsystems is very broadband, then the distortion (or spectrum-spreading) introduced by the angle modulator is perfectly equalized by the FM demodulator. However, if the filter alters the RF signal in any way other than by pure attenuation or pure time delay, then the demodulator is no longer a perfect equalizer for the filter output signal, and distortion of the demodulated output signal results.

An angle-modulated signal can be expressed as:

$$u(t) = A \sin [\omega_c t + \phi(t)] \tag{35}$$

where A is the amplitude, ω_c is the angular frequency of the carrier and $\phi(t)$ is the instantaneous phase modulation. With an ideal frequency modulator the relation between the input video signal x(t) and the phase $\phi(t)$ is given by

$$\phi(t) = \omega_e \int_{-\infty}^{t} x(\tau) \, d\tau$$

or $$\tag{36}$$

$$\frac{d\phi(t)}{dt} = \omega_e x(t)$$

If we normalize the video signal x(t) so that its mean is zero and its mean-square is unity, then ω_e represents the rms frequency deviation. By expanding the sine, Eq. (35) can also be expressed as
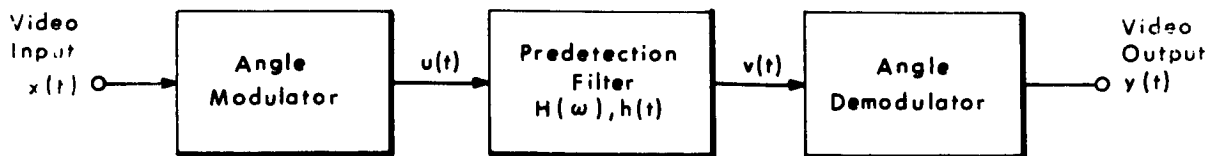
R-1208

Fig. 10 Simplified Block Diagram of an Angle-modulated System.

$$u(t) = A\{\cos \phi(t) \sin \omega_c t + \sin \phi(t) \cos \omega_c t\} \tag{37}$$

It is clear from Eq. (37) that the frequency modulated signal may be viewed as the result of nonlinear amplitude modulation of two quadrature carriers of identical frequency. The mathematical operations of the frequency modulation process are illustrated in Fig. 11. Here the video signal x(t) is first passed through an integrator after which it is fed to two memoryless nonlinearities having the characteristics cos [·] and sin [·]. The outputs from these nonlinearities are then multiplied by the two quadrature components of the carrier. Phase modulation differs only in that $\phi(t)$ is the input video signal, and $\theta(t)$ is the output video signal.

The angle-modulated RF signal passes through the predetection filter, whose output can be expressed as

$$v(t) = B(t) \sin [\omega_c t + \theta(t)] \tag{38}$$

where B(t) is the amplitude modulation introduced by the filter and $\theta(t)$ is the instantaneous phase modulation of the RF signal after filtering. In order to express B(t) and $\theta(t)$ in terms of the input to the filter, we first express v(t) in terms of u(t) by the convolution

$$v(t) = \int_{-\infty}^{\infty} h(\tau) u(t-\tau) \, d\tau \tag{39}$$

where h(t) is the RF impulse response of the filter. Combining Eqs. (37), (38) and (39) results in
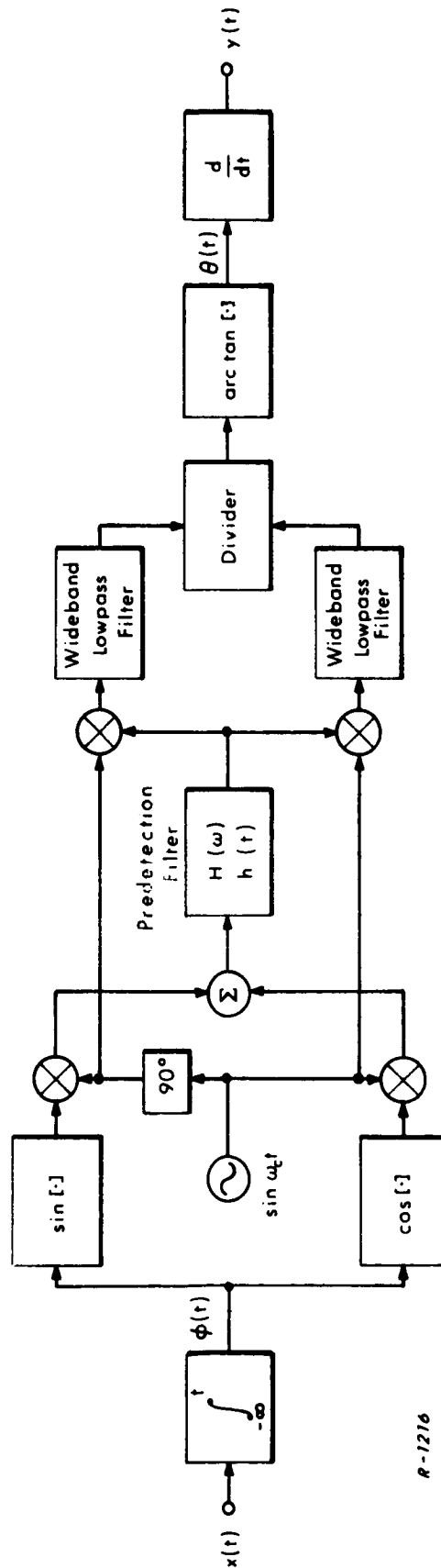
Fig. 11 Block Diagram Illustrating the Mathematical Operations in an FM System.
(Applies to a PM system if the integrator and differentiator are eliminated.)

R-1216

$$v(t) = B(t) \sin \left[\omega_c t + \theta(t) \right] =$$

$$A \int_{-\infty}^{\infty} h(\tau) \left\{ \cos \phi(t-\tau) \sin \omega_c(t-\tau) + \sin \phi(t-\tau) \cos \omega_c(t-\tau) \right\} d\tau \qquad (40)$$

The desired transfer relation directly relates the output phase modulation $\theta(t)$ to the input phase modulation $\phi(t)$. To derive such a relation, we need a low-frequency model of the predetection filter. The filter impulse response $h(t)$ can be written in terms of its low-frequency <u>cophasal</u> and <u>quadrature</u> components $h_p(t)$ and $h_q(t)$ in the following manner

$$h(t) = 2h_p(t) \cos \omega_c t + 2h_q(t) \sin \omega_c t \qquad (41)$$

Let the filter transfer function $H(\omega)$ be expressed as

$$H(\omega) = \begin{cases} H_1(\omega) & \text{for } \omega > 0 \\ H_2(\omega) & \text{for } \omega < 0 \end{cases} \qquad (42)$$

where $H_1(\omega)$ and $H_2(\omega)$ are the positive- and negative-frequency parts of $H(\omega)$ (See Fig. 12). Then it can be shown (see Ref. 6, page 131) that the lowpass transfer functions $H_p(\omega)$ and $H_q(\omega)$ corresponding to $h_p(t)$ and $h_q(t)$ are given by

$$H_p(\omega) = \frac{H_1(\omega + \omega_c) + H_2(\omega - \omega_c)}{2} \qquad (43)$$

$$H_q(\omega) = \frac{H_2(\omega - \omega_c) - H_1(\omega + \omega_c)}{2j} \qquad (44)$$

Figure 12 illustrates how $H_p(\omega)$ and $H_q(\omega)$ are determined by combinations of shifted replicas of $H_1(\omega)$ and $H_2(\omega)$. It is clear from Eq. (44) and Fig. 12 that
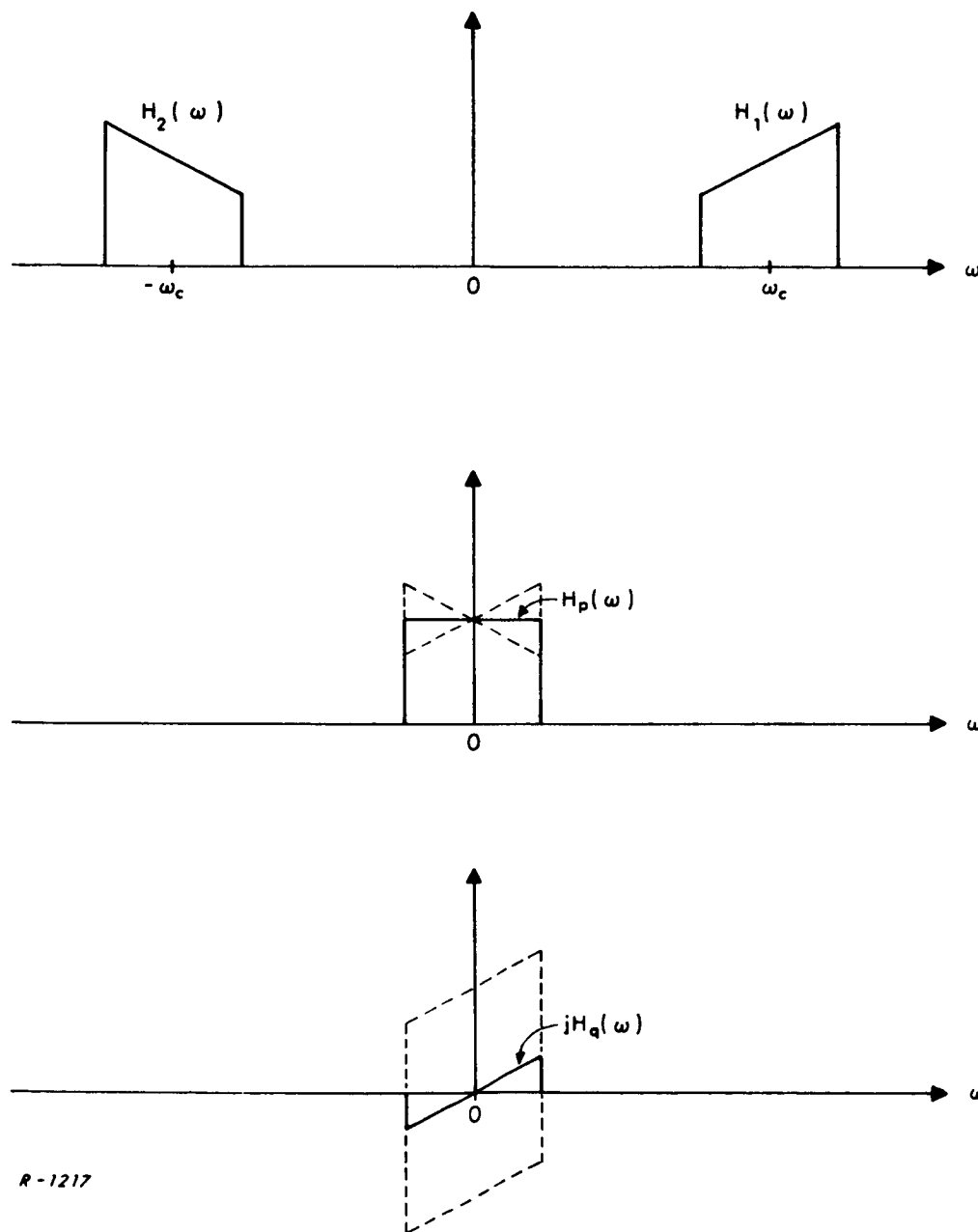
Fig. 12   Illustration of the Operations in Eqs. (43) and (44).

R -1217

$$H_q(0) = \int_{-\infty}^{\infty} h_q(t)\, dt = 0 \qquad (45)$$

and that a filter with a perfectly symmetric characteristic about its center frequency will have $H_q(\omega)$ equal to zero everywhere. Thus, $H_p(\omega)$ represents the symmetric part and $H_q(\omega)$ the antisymmetric part of the predetection filter. Moreover, since the video signal is not affected by the absolute gain and phase levels of the predetection filter we may set

$$|H(\omega_c)| = H_p(0) = \int_{-\infty}^{\infty} h_p(t)\, dt = 1 \qquad (46)$$

and

$$\underline{/\!\!\!\_}\, H(\omega_c) \triangleq \Phi(\omega_c) = 0 \qquad (47)$$

without any loss of generality. $\Phi(\omega)$ has been defined in Eq. (47) to be the phase characteristic of the predetection filter.

Combining Eqs. (40) and (41) and realizing that both $H_p(\omega)$ and $H_q(\omega)$ reject double-frequency components at $\omega = 2\omega_c$, we obtain the cophasal and quadrature components of the filter output after some trigonometric manipulations

$$v(t) = B(t) \sin\left[\omega_c t + \theta(t)\right] =$$

$$A \sin \omega_c t \left\{ \int_{-\infty}^{\infty} h_p(\tau) \cos \phi(t-\tau) + \int_{-\infty}^{\infty} h_q(\tau) \sin \phi(t-\tau)\, d\tau \right\}$$

$$+ A \cos \omega_c t \left\{ \int_{-\infty}^{\infty} h_p(t) \sin \phi(t-\tau)\, d\tau - \int_{-\infty}^{\infty} h_q(\tau) \cos \phi(t-\tau)\, d\tau \right\}$$

$$(48)$$

We are now able to express the amplitude modulation $B(t)$ and the phase modulation $\theta(t)$ of the output RF signal in the following forms

$$\frac{B^2(t)}{A^2} = \{ \int_{-\infty}^{\infty} h_p(t) \cos \phi(t-\tau) \, d\tau + \int_{-\infty}^{\infty} h_q(\tau) \sin \phi(t-\tau) \, d\tau \}^2$$

$$+ \{ \int_{-\infty}^{\infty} h_p(t) \sin \phi(t-\tau) \, d\tau - \int_{-\infty}^{\infty} h_q(\tau) \cos \phi(t-\tau) \, d\tau \}^2 \tag{49}$$

and

$$\theta(t) = \arctan \frac{\int_{-\infty}^{\infty} h_p(\tau) \sin \phi(t-\tau) \, d\tau - \int_{-\infty}^{\infty} h_q(\tau) \cos \phi(t-\tau) \, d\tau}{\int_{-\infty}^{\infty} h_p(\tau) \cos \phi(t-\tau) \, d\tau + \int_{-\infty}^{\infty} h_q(\tau) \sin \phi(t-\tau) \, d\tau} \tag{50}$$

Equation (49) expresses the PM-to-AM conversion introduced by the predetection filter. If the demodulator is not completely amplitude insensitive (i.e., if the amplitude limiters are not ideal) then some of this AM will appear in the video output as intermodulation distortion. In the present context, however, we can assume that the limiters perform ideally and turn our attention to the desired transfer relation expressed in Eq. (50).

An ideal angle demodulator extracts $\theta(t)$ from the RF signal, then differentiates the output to yield the frequency modulation. The mathematical operations of the angle demodulation process are illustrated in Fig. 11. Here the quadrature components of the filter output are resolved by multipliers, followed by wideband lowpass filters which filter out the $2\omega_c$ components in the multiplier outputs. The ratio of the resulting signals is then formed in a divider and passed through a memoryless nonlinearity having an arctangent characteristic. According to Eq. (50) the output from this nonlinearity is $\theta(t)$, which is the PM video signal. The FM video signal $y(t)$ is obtained by differentiating $\theta(t)$.

At this point it should be noted that no approximations have been used to derive Eq. (50); this equation is perfectly general. Nevertheless, its complexity necessitates

finding less complicated approximations to it. As has been discussed in Sec. 1.5, there exist two cases for which the transfer relation can be simplified considerably. These cases are the narrowband angle modulation case and the quasi-stationary case. When these cases do not apply, the transfer relation can still be simplified if it is known that the distortion is relatively small, as will be shown in Sec. 3.4.

3.2   The Transfer Relation for Narrowband Angle Modulation

Narrowband angle modulation is the case in which the resulting phase deviation is so small compared to one radian that $\cos \phi(t) \approx 1$ and $\sin \phi(t) \approx \phi(t)$, so that Eq. (37) can be written approximately

$$u(t) \approx A[\sin \omega_c t + \phi(t) \cos \omega_c t] \tag{51}$$

The right side of Eq. (51) is identical to the expression for an AM signal, except that the carrier component ($\sin \omega_c t$) is phase shifted by 90°. The angle-modulated signal can thus be viewed as the result of a linear modulation operation. In particular, FM with deviation ratio much smaller than unity fits into this category.

By following the same analytical procedure as in Sec. 3.1, we can easily show that the phase modulation at the output of the predetection filter may be expressed as

$$\theta(t) = \int_{-\infty}^{\infty} h_p(\tau)\, \phi(t-\tau)\, d\tau \tag{52}$$

Similarly the FM demodulated output is

$$y(t) = \int_{-\infty}^{\infty} h_p(\tau)\, x(t-\tau)\, d\tau \tag{53}$$

It is clear from Eqs. (52) and (53) that the predetection filter has a linear-filtering effect on the modulation just like a video filter. Thus no intermodulation distortion is caused by the filter in this case, irrespective of its phase characteristic. The same conclusion holds true for amplitude-modulated signals.

3.3 The Transfer Relation in the Quasi-Stationary Case

The quasi-stationary case is met when the video bandwidth is much smaller than the predetection-filter bandwidth, or equivalently when $\phi(t-\tau)$ changes much more slowly with time than $h_p(\tau)$ or $h_q(\tau)$ in Eq.(50). This is the case if the FM deviation ratio (or the phase deviation) is much greater than unity. We may approximate $\phi(t-\tau)$ by the first two terms of its Taylor series expansion in this case:

$$\phi(t-\tau) \approx \phi(t) - \tau \, \frac{d\phi(t)}{dt} \tag{54}$$

By inserting Eq.(54) in Eq.(50), we show in Appendix A that the output phase modulation is

$$\theta(t) \approx \phi(t) + \Phi \left[\omega_e x(t) + \omega_c \right] \tag{55}$$

or the output frequency modulation is

$$y(t) \approx x(t) + \frac{1}{\omega_e} \frac{d}{dt} \left\{ \Phi \left[\omega_e x(t) + \omega_c \right] \right\} \tag{56}$$

where $\Phi(\omega)$ is the phase characteristic of the predetection filter. The instantaneous frequency of the FM signal may be viewed as tracing the phase characteristic of the predetection filter. The distortion is represented by the second terms in Eqs.(55) and (56), and is entirely determined by the (memoryless) nonlinearities in the filter phase characteristic $\Phi(\omega)$. It is not affected by the filter amplitude characteristic.

In further analysis of the quasi-stationary case, it will be convenient to employ a power series expansion of the nonlinear phase characteristic $\Phi(\omega)$ of the form

$$\Phi(\omega) = \sum_{i=0}^{\infty} c_i \left(\frac{\omega - \omega_c}{B} \right)^i \tag{57}$$

where we define B as <u>half</u> the bandwidth of the predetection filter, and c_i as the power-series coefficients. Now, the first term c_o represents the carrier phase shift which we have already set to zero in Eq. (47). Moreover, the second term $c_1(\omega-\omega_c/B)$ represents overall group delay which does not produce distortion, so we may set c_1 to zero without loss of generality. One familiar power series which takes the form of Eq. (57) is the Taylor series (see Eq.(8)). In this case the c_i's are the Taylor coefficients given by

$$c_i = \frac{1}{i!} \cdot \frac{d^i \Phi(\omega)}{d(\omega/B)^i} \bigg|_{\omega = \omega_c} \tag{58}$$

It is well known that the FM distortion can be decreased by linearizing the filter phase characteristic, without changing the amplitude characteristic, by the use of <u>group-delay equalizing networks.</u> These networks are allpass networks with a phase characteristic such that the composite phase characteristic of the filter in cascade with the equalizing network is as close to linear as possible. Some telemetry predetection tape recorders presently incorporate phase equalizers.

Another way of removing FM distortion is using a <u>nonlinear video equalizer.</u> This type of equalizer operates on the demodulated video signal in a nonlinear manner to remove the distortion. A nonlinear video equalizer for the quasi-stationary case, obtained by inverting Eq. (56), is shown in Fig. 13.
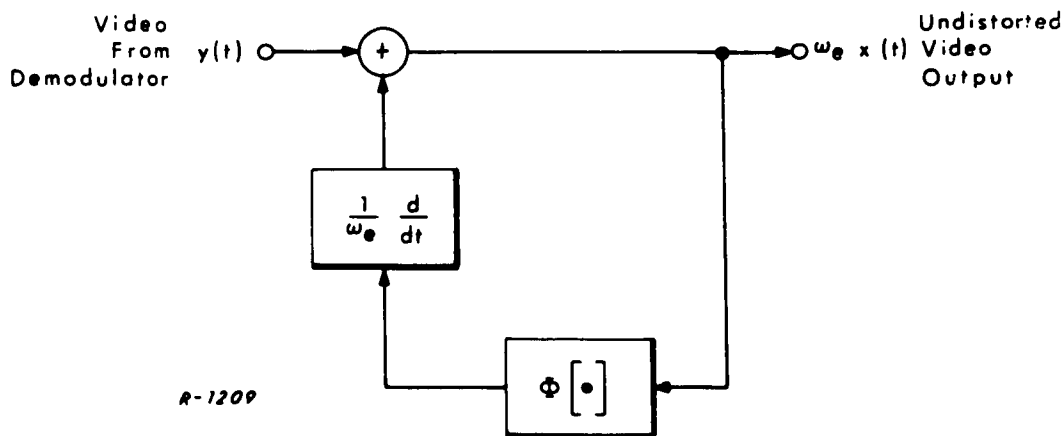
Fig. 13 Nonlinear Video Equalizer for Distortion
in the Quasi-stationary Case.

It consists of a feedback loop containing a memoryless nonlinearity $\Phi[\cdot]$ which is a replica of the phase characteristic of the predetection filter, and a differentiator. If the phase characteristic is closely simulated, this non-linear equalizer can remove most of the quasi-stationary FM distortion caused by the predetection filter.

3.4 Approximation to the Transfer Relation in the General Case

The narrowband and quasi-stationary cases result in simple forms of the transfer relation. However, in many operational telemetry systems, the deviation ratios are such that these cases do not apply. It is, therefore, necessary to make use of the exact relation (Eq. (50)). Since all practical systems work with a fairly small amount of distortion, it is possible to make an approximation to the exact relation which is valid when the resulting video distortion is small. This approximation is obtained in the form of a functional Taylor series expansion[7].

We begin by expanding the cosine and sine functions in their Taylor series up to third order, and inserting into Eq. (50):

$$\tan \theta(t) \cong \frac{\int_{-\infty}^{\infty} \{h_p(\tau)[\phi(t-\tau) - \phi^3(t-\tau)/6] - h_q(\tau)[1 - \phi^2(t-\tau)/2]\}\, d\tau}{\int_{-\infty}^{\infty} \{h_p(\tau)[1 - \phi^2(t-\tau)/2] + h_q(\tau)[\phi(t-\tau) - \phi^3(t-\tau)/6]\}\, d\tau} \tag{59}$$

Utilizing Eqs. (45) and (46), we reduce Eq. (59) to

$$\tan \theta(t) = \frac{\int_{-\infty}^{\infty} \{h_p(\tau)[\phi(t-\tau) - \phi^3(t-\tau)/6] + h_q(\tau)\phi^2(t-\tau)/2\}\, d\tau}{1 + \int_{-\infty}^{\infty} \{h_q(\tau)[\phi(t-\tau) - \phi^3(t-\tau)/6] - h_p(\tau)\phi^2(t-\tau)/2\}\, d\tau} \tag{60}$$

Expanding the denominator in a binomial series and multiplying by the numerator yields

$$\tan \theta(t) = \int_{-\infty}^{\infty} h_p(\tau) \, \phi(t-\tau) \, d\tau + (1/2) \int_{-\infty}^{\infty} h_q(\tau) \, \phi^2(t-\tau) \, d\tau$$

$$- \int_{-\infty}^{\infty}\int h_q(\tau_1) \, h_p(\tau_2) \, \phi(t-\tau_1) \, \phi(t-\tau_2) \, d\tau_1 \, d\tau_2 - (1/6) \int_{-\infty}^{\infty} h_p(\tau) \, \phi^3(t-\tau) \, d\tau$$

$$- (1/2) \int_{-\infty}^{\infty}\int h_q(\tau_1) \, h_q(\tau_2) \, \phi(t-\tau_1) \, \phi^2(t-\tau_2) \, d\tau_1 \, d\tau_2$$

$$+ (1/2) \int_{-\infty}^{\infty}\int h_p(\tau_1) \, h_p(\tau_2) \, \phi(t-\tau_1) \, \phi^2(t-\tau_2) \, d\tau_1 \, d\tau_2$$

$$+ \int_{-\infty}^{\infty}\int\int h_p(\tau_1) \, h_q(\tau_2) \, h_q(\tau_3) \, \phi(t-\tau_1) \, \phi(t-\tau_2) \, \phi(t-\tau_3) \, d\tau_1 \, d\tau_2 \, d\tau_3 \quad (61)$$

We now use the Taylor series expansion of the arctangent function

$$\arctan x = x - \frac{x^3}{3} + \ldots \quad (62)$$

to obtain the functional Taylor series for $\theta(t)$ valid up to third order in $\phi(t)$:

$$\theta(t) = \theta_1(t) + \theta_2(t) + \theta_3(t) + \ldots \quad (63)$$

After some algebraic manipulation, these terms are found to be

$$\theta_1(t) = \int_{-\infty}^{\infty} h_p(\tau) \, \phi(t-\tau) \, d\tau \quad (64)$$

$$\theta_2(t) = 1/2 \int_{-\infty}^{\infty} h_q(\tau) \left[\phi(t-\tau) - \theta_1(t) \right]^2 \, d\tau \quad (65)$$

$$\theta_3(t) = -1/6 \int_{-\infty}^{\infty} h_p(\tau) \left[\phi(t-\tau) - \theta_1(t) \right]^3 \, d\tau$$

$$- \theta_2(t) \int_{-\infty}^{\infty} h_q(\tau) \left[\phi(t-\tau) - \theta_1(t) \right] \, d\tau \quad (66)$$

$$\vdots$$

$\theta_1(t)$ represents the "linearly distorted" term, $\theta_2(t)$ the second-order distortion term, and $\theta_3(t)$ the third-order distortion term. Higher-order terms are readily obtained by including more terms in each of the preceding steps. However, when the distortion is small it consists mainly of second- and third-order terms, and Eq. (63) is an adequate approximation to the exact transfer relation. The output FM video is, of course, the time derivative of Eq. (63).

Most RF filters used in angle modulation systems are designed (and aligned) to have symmetrical frequency characteristics with respect to the carrier frequency. The amplitude characteristic of such a filter is an even function and the phase characteristic an odd function in frequency with respect to the carrier frequency, in which case it can readily be shown that

$$h_q(t) = 0 \tag{67}$$

Consequently, the terms of the functional series for $\theta(t)$ in the case of a symmetric filter reduce to

$$\theta_1(t) = \int_{-\infty}^{\infty} h_p(\tau) \, \phi(t-\tau) \, d\tau \tag{68}$$

$$\theta_2(t) = 0 \tag{69}$$

$$\theta_3(t) = -1/6 \int_{-\infty}^{\infty} h_p(\tau) \left[\phi(t-\tau) - \theta_1(t) \right]^3 \, d\tau \tag{70}$$

$$\vdots$$

Thus the second-order distortion term $\theta_2(t)$ is caused entirely by filter asymmetry.

Just as we were able to derive the transfer relation for the quasi-stationary case from that for the general case by utilizing Eq. (54), it is noteworthy that we can derive each term of the Taylor series of the former from the corresponding term of the functional Taylor series of the latter. Thus, it is easy to show that the c_3 term in the expansion of Eq. (55) corresponds to the third-order term (Eq. (66) or (70)).

A nonlinear video equalizer which would remove distortion up to third order for symmetrical filters can be derived in the form of a feedback loop that solves Eq. (70) for $\phi(t)$. Figure 14 shows the block diagram for this equalizer. The demodulated FM signal $y(t)$ is first passed through an integrator and a linear adder, followed by a filter whose transfer function is the reciprocal of the lowpass equivalent $H_p(\omega)$ of the predetection filter. Then the signal is fed back through paths which contain filters and nonlinear operational circuits. After differentiation an output signal is obtained which would be almost distortion free up to third order.

The distortion equalizer depicted in Fig. 14 contains a filter with transfer function $1/H_p(\omega)$. Such a filter is not physically realizable, but filters can be synthesized to approximate it (see Sec. 2.1.). Complete distortion equalization would not result, of course.
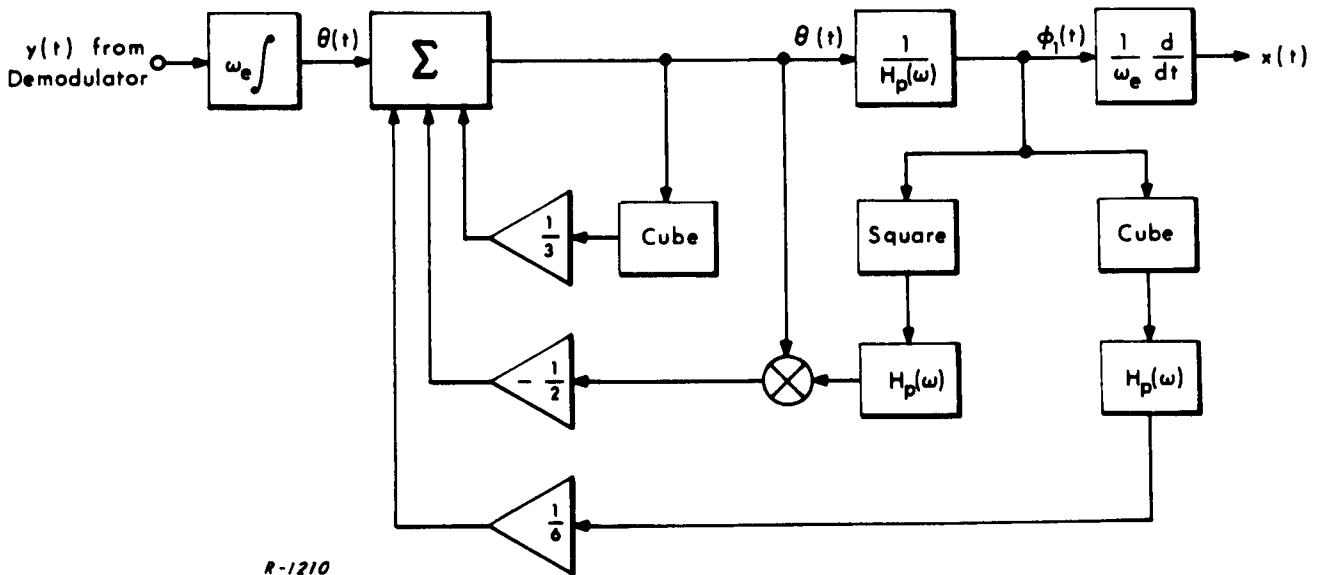
Fig. 14 Nonlinear Video Equalizer for Removal of Third-order
Distortion Caused by Symmetrical Predetection Filters
in the General Case.

4. INTERMODULATION-DISTORTION SPECTRUM, QUASI-STATIONARY CASE

In the previous section we have described the distortion mechanisms involved in the filtering of an angle-modulated signal, and identified the dominant intermodulation distortion terms in the video output under various conditions. We begin this section by selecting a suitable measure of intermodulation distortion, and describe a simple method of measuring it. The remainder of the section is devoted to the analytical prediction of the measurements in the quasi-stationary case.

4.1   Spectral Characterization of Intermodulation Distortion

The obvious way to measure overall intermodulation distortion in the telemetry system depicted in Fig. 1 is to connect the output of the transmitter via an attenuator to the input of the receiver. (This, of course, will not take into account the distortion caused by the antenna feeders and the propagation medium.) Then all but one of the data channels are fed with appropriate signals and the output power of the empty channel is measured. Since the output from the empty channel is only intermodulation distortion (assuming negligible interchannel crosstalk), one can compute an intermodulation noise-to-signal power ratio (I/S ratio) for the particular data channel by dividing the measurement obtained in the unloaded channel by the signal power measured when the particular data channel is fully loaded. From the measurements of the I/S ratio for each channel a bar graph can be plotted showing the I/S ratio versus the frequency location of the channel in the video spectrum.

In order to simplify and standardize the measurement of intermodulation noise, the video signal at the input to the FM modulator is conveniently simulated by a gaussian noise process covering the bandwidth of the video signal. It can be shown that the statistical properties of gaussian noise are very similar to a complex multichannel (FDM) video signal. Thus it is meaningful to simulate the video signal in a telemetry system by a gaussian process. When this <u>noise-loading</u>

technique is used, it is necessary to shape the power-density spectrum of the applied noise signal with a filter so that the resulting signal has approximately the same power-density spectrum as the actual video signal.

Figure 15 shows a block diagram of the noise-loading technique. In order that the intermodulation distortion noise at the demodulator output be measured, an "empty channel" has to be simulated in the input spectrum by a narrowband reject filter (see Fig. 16). The power measured in a corresponding narrow band-pass filter at the output constitutes the intermodulation distortion noise power. By switching out the reject filter it is possible to measure the signal power in the bandpass filter and compute the I/S ratio. If this measurement is performed for different video frequencies a curve of I/S density ratio versus video frequency can be constructed as shown in Fig. 17. This curve exhibits the increased intermodulation noise with the video frequency commonly encountered in FM systems.

In addition to being analytically convenient, the noise-loading approach greatly simplifies experimental verification. Intermodulation distortion tests can be standardized and the measurements easily reproduced. In contrast, we believe that the customary method of simulating the video signal by a set of un-modulated subcarriers is inadequate. It is both mathematically intractable (except in the trivial case of one or two subcarriers) and experimentally cumbersome.
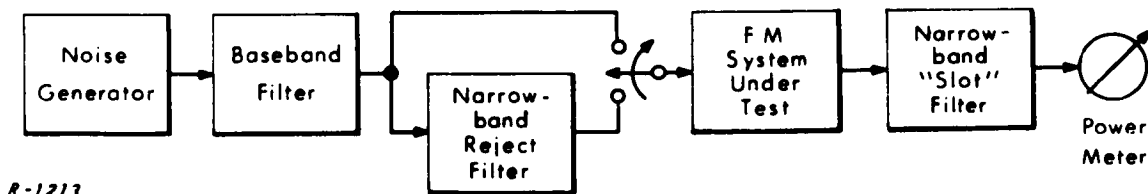
Fig. 15 Noise-loading Technique for Measurement
of Intermodulation Distortion.
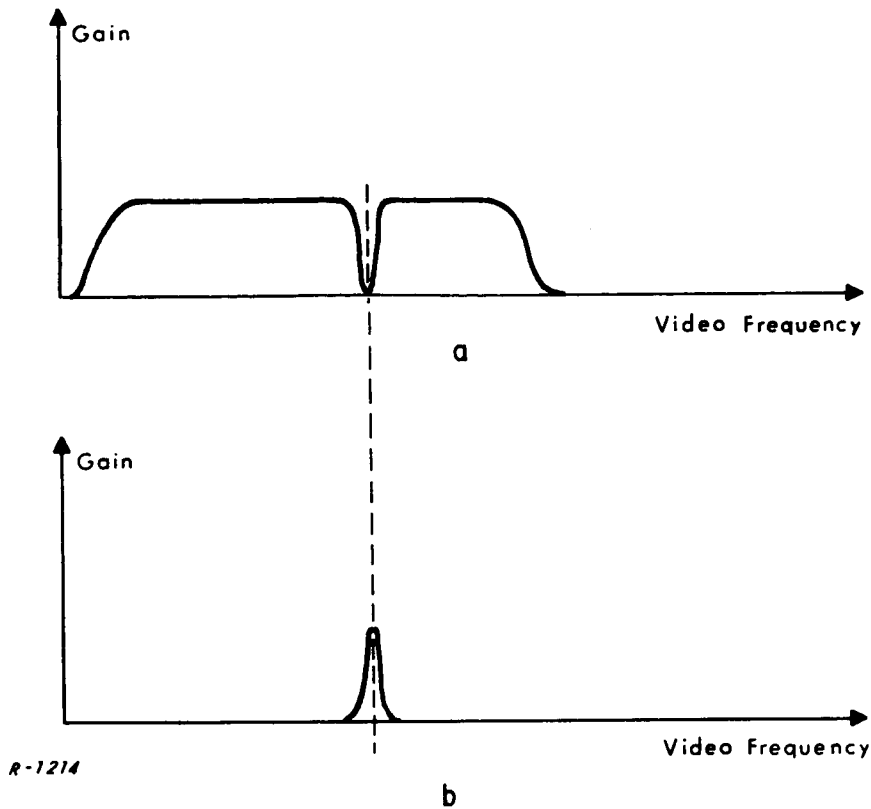
Fig. 16 a) Amplitude Characteristic of Spectral-shaping
Filter for the Noise-loading Technique.

b) Amplitude Characteristic of Narrowband
"Slot" Filter.
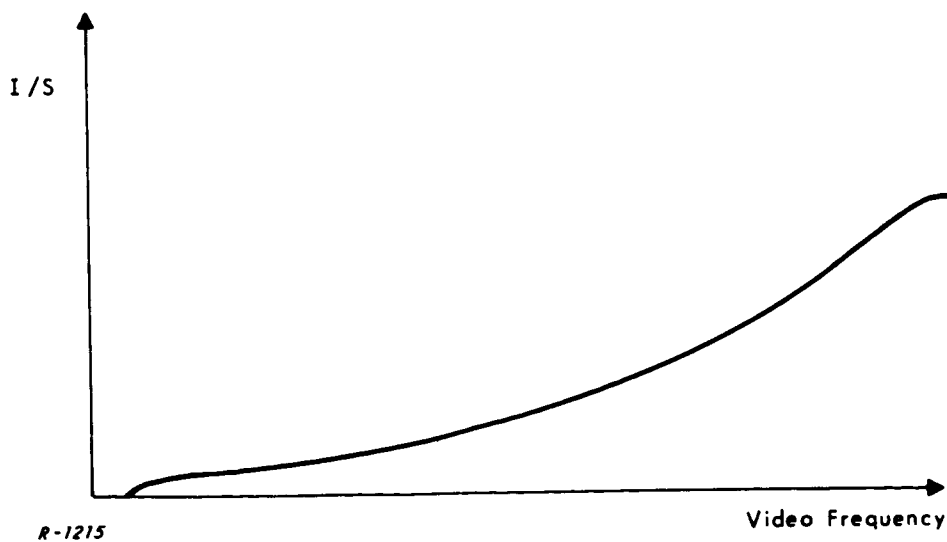
Fig. 17 Typical Curve of Intermodulation Noise-to-signal
Ratio vs Video Frequency.

43

Because of the relative simplicity of the noise-loading test it is very common to specify intermodulation distortion in terms of a gaussian noise input signal (as, for example, in FDM/FM telephony). It would be very useful to be able to predict the amount of intermodulation distortion in a given system caused by a given phase nonlinearity, so that the susceptibility of the design to this type of distortion could be determined prior to the construction of the equipment. In the remaining sections of this chapter we present effective analytical techniques for evaluating the intermodulation distortion spectrum in the quasi-stationary case, in terms of the parameters of the filter and the video signal.

4.2   Distortion Spectrum: Power Series Technique

We wish to compute the power-density spectrum of the intermodulation distortion represented by the second term of Eq. (56). It is convenient to begin by computing the power density spectrum of the PM distortion term of Eq. (55). The procedure is to represent this term by a power series in $x(t)$, then find its autocorrelation function $R_\theta(\tau)$ in terms of the autocorrelation function $R_x(\tau)$ of the input FM video signal and the coefficients of the power series. Fourier transformation of $R_\theta(\tau)$ yields the power-density spectrum I_θ of the PM distortion. Finally, the PM distortion term is simply related to the FM distortion term by scaling and differentiation; consequently their power-density spectra are also simply related by

$$I_y = (\frac{\omega}{\omega_e})^2 I_\theta \qquad (71)$$

This yields the desired distortion spectrum, which when divided by the input video spectrum S_x yields the I/S ratio.

We begin by combining the power series of $\Phi(\omega)$ given by Eq. (57) with the PM distortion term of Eq. (55):

$$\Phi[\omega_e x(t) + \omega_c] = \sum_{i=0}^{\infty} c_i [\frac{\omega_e}{B} x(t)]^i \qquad (72)$$

Now, Thomson[8] has shown that for gaussian inputs

$$R_\theta(\tau) = \sum_{n=0}^{\infty} n! \, R_x^n(\tau) \left[\sum_{k=0}^{\infty} \frac{(n+2k)!}{2^k k! \, n!} \, c_{n+2k} \left(\frac{\omega_e}{B} \right)^{n+2k} \right]^2 \quad (73)$$

The zero order term n=0 represents the dc component of the output which is of no practical interest and may be dropped. The first-order term n=1 is a linear undistorted component, so we drop it in computing the distortion spectrum.

Next, we employ the following Fourier transformation to obtain the power-density spectrum

$$S(\nu) = \int_{-\infty}^{\infty} R(\tau) \cos \hat{\omega} \nu \tau \, d\tau \quad (74)$$

For convenience, we have defined a normalized video frequency variable $\nu = \omega/\hat{\omega}$, where $\hat{\omega}$ is the video signal bandwidth. Thus $S_x(\nu)$ is nonzero in the range $0 \le |\nu| \le 1$, and zero otherwise. Applying Eq. (74) to Eq. (73) yields the PM distortion spectrum

$$I_\theta(\nu) = \sum_{n=2}^{\infty} n! \, S_x^{(n)}(\nu) \left[\sum_{k=0}^{\infty} \frac{(n+2k)!}{2^k k! \, n!} \, c_{n+2k} \left(\frac{\omega_e}{B} \right)^{n+2k} \right]^2 \quad (75)$$

where

$$S_x^{(n)}(\nu) \triangleq \underbrace{S_x(\nu) \boxtimes S_x(\nu) \boxtimes \dots \boxtimes S_x(\nu)}_{n \text{ terms}}$$

denotes the $(n-1)^{th}$ convolution of $S_x(\nu)$ with itself.

Finally, we use Eq. (71) and divide by $S_x(\nu)$ to obtain the I/S ratio as a function of normalized video frequency

$$\frac{I_y(\nu)}{S_x(\nu)} = \left(\frac{\hat{\omega}\nu}{\omega_e} \right)^2 \sum_{n=2}^{\infty} n! \, \frac{S_x^{(n)}(\nu)}{S_x(\nu)} \left[\sum_{k=0}^{\infty} \frac{(n+2k)!}{2^k k! \, n!} \, c_{n+2k} \left(\frac{\omega_e}{B} \right)^{n+2k} \right]^2$$

$$(76)$$

It is instructive to write out a few distortion terms from Eq. (76):

$$I_y(\nu) = 2! \, (\frac{\hat{\omega}}{B})^2 \, (\frac{\omega_e}{B})^2 \nu^2 \, S_x^{(2)}(\nu) \, [\, c_2 + 6 \, c_4 (\frac{\omega_e}{B})^2 + 45 \, c_6 (\frac{\omega_e}{B})^4 + \ldots]^2$$

$$+ \, 3! \, (\frac{\hat{\omega}}{B})^2 \, (\frac{\omega_e}{B})^4 \nu^2 \, S_x^{(3)}(\nu) \, [\, c_3 + 10 \, c_5 (\frac{\omega_e}{B})^2 + 105 \, c_7 (\frac{\omega_e}{B})^4 + \ldots]^2$$

$$+ \, 4! \, (\frac{\hat{\omega}}{B})^2 \, (\frac{\omega_e}{B})^6 \nu^2 \, S_x^{(4)}(\nu) \, [\, c_4 + 15 \, c_6 (\frac{\omega_e}{B})^2 + \ldots]^2$$

$$+ \, 5! \, (\frac{\hat{\omega}}{B})^2 \, (\frac{\omega_e}{B})^8 \nu^2 \, S_x^{(5)}(\nu) \, [\, c_5 + 21 \, c_7 (\frac{\omega_e}{B})^2 + \ldots]^2$$

$$+ \, \ldots \ldots \tag{77}$$

The first line of Eq. (77) represents second-order distortion, the second line represents third-order distortion, etc. It can be seen that an even-power coefficient (c_i) contributes only to all even-ordered distortion up to order i, while an odd-power coefficient (c_j) contributes only to all odd-ordered distortion up to order j. Now, a symmetric filter has an antisymmetric phase characteristic $\Phi(\omega)$, so that all its even-power coefficients vanish. Consequently a symmetric filter will introduce only odd-ordered distortion. Furthermore, it can be seen from Eq. (77) that all the contributions to a given order of distortion accumulate coherently (i.e. voltages add) whereas different orders of distortion accumulate incoherently (i.e. powers add). This is a curious but established property of nonlinear systems with gaussian inputs.

We now have in Eq. (76) a general result relating the intermodulation-distortion spectrum to the parameters of the filter and the video signal. The input video spectrum comes in only in the form of multiple convolutions, while the filter characteristic comes in only as constant factors determined by the phase power-series coefficients. Thus, given a video spectrum, we first compute the necessary convolutions (which can often be obtained in closed form).

Then, by using enough power-series coefficients of the phase till the weighted sum of coefficients in Eq. (76) converges, we can immediately write down the distortion spectrum. Any change of filter characteristic or video spectrum would not necessitate an elaborate recomputation.

4.3 Distortion Spectrum: Hermite-Polynomials Technique

The power-density spectrum of the intermodulation distortion may be computed with the aid of the Hermite-Polynomials technique due to Thomson[8]. This technique has certain advantages which we discuss below over the power-series technique. The same procedure as that of the previous section is used here, except that the PM distortion term of Eq. (55) is represented by a series of Hermite polynomials in $x(t)$:

$$\Phi[\omega_e x(t) + \omega_c] = \sum_{i=0}^{\infty} h_i H_i[x(t)] \tag{78}$$

The Hermite polynomials are given generally by

$$e^{-x^2/2} H_i(x) = (-1)^i \frac{d^i}{dx^i} e^{-x^2/2} \tag{79}$$

The first few polynomials are easily seen to be

$$H_0(x) = 1$$
$$H_1(x) = x$$
$$H_2(x) = x^2 - 1 \tag{80}$$
$$H_3(x) = x^3 - 3x$$
$$\vdots$$

The corresponding Hermite coefficients h_i of Eq. (78) are well-known to be

$$h_i = \frac{1}{i!\sqrt{2\pi}} \int_{-\infty}^{\infty} \Phi[\omega_e x + \omega_c] e^{-x^2/2} H_i(x) dx \tag{81}$$

47

Now, Thomson[8] has shown that for gaussian inputs

$$R_\theta(\tau) = \sum_{n=0}^{\infty} n! \, h_n^2 \, R_x^n(\tau) \tag{82}$$

Again, we ignore the zero- and first-order terms since they do not represent intermodulation distortion. Applying the Fourier transformation of Eq. (74) to Eq. (82) yields the PM distortion spectrum

$$I_\theta(\nu) = \sum_{n=2}^{\infty} n! \, h_n^2 \left(\frac{\omega_e}{B}\right)^{2n} S_x^{(n)}(\nu) \tag{83}$$

Finally, we use Eq. (71) and divide by $S_x(\nu)$ to obtain the I/S ratio as a function of normalized video frequency

$$\frac{I_y(\nu)}{S_x(\nu)} = \left(\frac{\hat{\omega}\nu}{\omega_e}\right)^2 \sum_{n=2}^{\infty} n! \, h_n^2 \left(\frac{\omega_e}{B}\right)^{2n} \frac{S_x^{(n)}(\nu)}{S_x(\nu)} \tag{84}$$

It is instructive to write out a few distortion terms from Eq. (84):

$$\begin{aligned}
I_y(\nu) = \; & 2! \left(\frac{\hat{\omega}}{\omega_e}\right)^2 \nu^2 \, h_2^2 \, S_x^{(2)}(\nu) \\
& + 3! \left(\frac{\hat{\omega}}{\omega_e}\right)^2 \nu^2 \, h_3^2 \, S_x^{(3)}(\nu) \\
& + 4! \left(\frac{\hat{\omega}}{\omega_e}\right)^2 \nu^2 \, h_4^2 \, S_x^{(4)}(\nu) \\
& + \; . \; . \; . \; .
\end{aligned} \tag{85}$$

Comparison of Eq. (85) with Eq. (77) reveals the simplification of the final result achieved by the Hermite-polynomials technique. In place of the infinite sum of power coefficients appearing in each term of Eq. (77), there is now in Eq. (85) a single Hermite coefficient determining the distortion-power level of

of a given order. Thus, each term in the series of Hermite-polynomials Eq. (78) is associated with an intermodulation-distortion product of a given order.

If the predetection-filter phase characteristic $\Phi(\omega)$ is available in the form of an analytical expression, it is relatively easy to compute the power-series coefficients c_i. The computation of the Hermite coefficients h_i from Eq. (81) may prove a more difficult matter. On the other hand, if $\Phi(\omega)$ is available in empirical form, say as a graph of direct measurements, then numerical techniques can readily be applied to accurately compute h_i from Eq. (81). Numerical techniques for computing power-series coefficients are subject to significant approximation errors. Thus, the Hermite polynomials technique is particularly suited to the processing of experimental data.

5. INTERMODULATION-DISTORTION SPECTRUM, GENERAL CASE

We pointed out in Sec. 3 that the deviation ratios employed in many operational telemetry systems are such that the narrowband and quasi-stationary approximations to the transfer relation do not apply. In such a situation, we must resort to the functional Taylor series approximation (Eqs. (63)-(66)) to the general transfer relation. In this section we compute the intermodulation-distortion spectrum in the general case, both for asymmetric filters and for symmetric filters.

5.1   Distortion Spectrum: Asymmetric Filter

For the case of an asymmetric predetection filter, we assume that the distortion is low enough and that the filter is asymmetric enough so that the first two terms in the series of Eq. (63) suffice for an adequate approximation to the transfer relation. Thus, we wish to compute the power-density spectrum of the intermodulation distortion contained in the output phase

$$\theta(t) \cong \theta_1(t) + \theta_2(t) \tag{86}$$

The procedure is the same as that used in Sec. 4.2, but the details of the computations are different since we must now analyze nonlinearity with memory.

We begin by forming the autocorrelation function from Eq. (86)

$$R_\theta(\tau) = \overline{\theta(t)\,\theta(t+\tau)} = \overline{\theta_1(t)\,\theta_1(t+\tau)} + \overline{\theta_2(t)\,\theta_2(t+\tau)}$$

$$+ \ \overline{\theta_1(t)\,\theta_2(t+\tau)} + \overline{\theta_1(t+\tau)\,\theta_2(t)} \tag{87}$$

It can be shown[4] that the last two terms in Eq. (87) are equal to zero, because they involve averages of odd-order products of gaussian random processes. The first term in Eq. (87) is easily seen to depend only on the first power of $R_\phi(\tau)$, so it does not contribute to intermodulation distortion and may be dropped.

With the aid of Eq. (65) and the notation

$$\psi(t, \sigma) = [\phi(t - \sigma) - \theta_1(t)] \qquad (88)$$

we can now write

$$R_\theta(\tau) = \overline{\theta_2(t) \, \theta_2(t + \tau)}$$

$$= \frac{1}{4} \int\!\!\int_{-\infty}^{\infty} h_q(\tau_1) \, h_q(\tau_2) \, \overline{\psi^2(t, \tau_1) \, \psi^2(t + \tau, \tau_2)} \, d\tau_1 \, d\tau_2 \qquad (89)$$

Since $\psi(t, \sigma)$ is a gaussian random process over the time-variable t, we may employ the rule for the average of the product of gaussian processes of Eq. (11) to get

$$R_\theta(\tau) = \frac{1}{4} \int\!\!\int_{-\infty}^{\infty} h_q(\tau_1) \, h_q(\tau_2) \, [\, R_\psi^2(0; \tau_1, \tau_2) + 2 R_\psi^2(\tau; \tau_1, \tau_2)\,] \, d\tau_1 \, d\tau_2 \qquad (90)$$

The notation $R_\psi(\tau; \tau_1, \tau_2)$ is used for the cross-correlation function of $\psi(t, \tau_1)$ and $\psi(t, \tau_2)$. The first term in Eq. (90) is a constant that does not contribute to inter-modulation distortion, so it too is dropped.

Next, we evaluate $R_\psi(t; \tau_1, \tau_2)$ in terms of $R_\phi(\tau)$ for insertion in Eq. (90).

$$R_\psi(\tau; \tau_1, \tau_2) = \overline{\psi(t, \tau_1) \, \psi(t + \tau, \tau_2)}$$

$$= \overline{\phi(t - \tau_1) \, \phi(t + \tau - \tau_2)}$$

$$+ \int\!\!\int_{-\infty}^{\infty} h_p(\tau_3) \, h_p(\tau_4) \, \overline{\phi(t - \tau_3) \, \phi(t + \tau - \tau_4)} \, d\tau_3 \, d\tau_4$$

$$- \int_{-\infty}^{\infty} h_p(\tau_3) \, \overline{\phi(t - \tau_3) \, \phi(t + \tau - \tau_2)} \, d\tau_3$$

$$- \int_{-\infty}^{\infty} h_p(\tau_4) \, \overline{\phi(t - \tau_1) \, \phi(t + \tau - \tau_4)} \, d\tau_4$$

$$= R_\phi(\tau + \tau_1 - \tau_2) + \int\!\!\int_{-\infty}^{\infty} h_p(\tau_3) \, h_p(\tau_4) \, R_\phi(\tau + \tau_3 - \tau_4) \, d\tau_3 \, d\tau_4$$

$$- \int_{-\infty}^{\infty} h_p(\tau_3) \, R_\phi(\tau + \tau_3 - \tau_2) \, d\tau_3 - \int_{-\infty}^{\infty} h_p(\tau_4) \, R_\phi(\tau + \tau_1 - \tau_4) \, d\tau_4 \qquad (91)$$

Inserting this expression into the second term of Eq. (90) and Fourier transforming yields, after some algebraic manipulation, the PM distortion spectrum

$$I_\theta(\omega) = \frac{1}{2} |H_q(\omega)|^2 [S_\phi(\omega) \otimes S_\phi(\omega)]$$

$$- \text{Re}\{H_q^*(\omega)[H_p(\omega) S_\phi(\omega) \otimes H_q(\omega) S_\phi(\omega)]\}$$

$$+ |H_q(\omega)|^2 S_\phi(\omega) \otimes |H_p(\omega)|^2 S_\phi(\omega)$$

$$+ H_q(\omega) H_p^*(\omega) S_\phi(\omega) \otimes H_p(\omega) H_q^*(\omega) S_\phi(\omega) \qquad (92)$$

where the asterisk denotes complex conjugate. $S_\phi(\omega)$ is the power-density spectrum of the phase modulation $\phi(t)$, which is simply related to that of the frequency modulation by

$$S_\phi(\omega) = (\frac{\omega_e}{\omega})^2 S_x(\omega) \qquad (93)$$

Finally, multiplication of Eq. (92) by $(\omega/\omega_e)^2$ as indicated in Eq. (71) yields the desired FM distortion spectrum, which in turn may be divided by the input video spectrum $S_x(\omega)$ to obtain the I/S ratio.

We now have in Eq. (92) an exact relationship between the intermodulation-distortion spectrum in the second-order term and convolutions of the input video spectrum and the filter transfer functions $H_p(\omega)$ and $H_q(\omega)$. These convolutions would have to be evaluated numerically for each combination of input video spectrum and predetection filter of interest. Such computations could prove arduous enough to require a digital computer. In the next section we derive an approximation which greatly reduces this computational complexity.

5.2   Approximation to the Distortion Spectrum: Asymmetric Filter

The first approximation is to insert into the expression for $R_\psi(\tau; \tau_1, \tau_2)$ (Eq. (91)) the following truncated Taylor series for $R_\phi(\tau + \Delta)$

$$R_\phi(\tau + \Delta) \cong R_\phi(\tau) + \Delta R_\phi^i(\tau) + \frac{\Delta^2}{2!} R_\phi^{1i}(\tau) + \frac{\Delta^3}{3!} R_\phi^{iii}(\tau)$$

$$+ \frac{\Delta^4}{4!} R_\phi^{iv}(\tau) + \frac{\Delta^5}{5!} R_\phi^{v}(\tau) + \frac{\Delta^6}{6!} R_\phi^{vi}(\tau) \tag{94}$$

where $R_\phi^i(\tau)$ is the first derivative of $R_\phi(\tau)$, etc. The dummy variable Δ is set appropriately for each term in Eq. (91) (e.g. $\Delta = (\tau_1 - \tau_2)$ in the first term). Collecting terms containing the same derivatives of $R_\phi(\tau)$, we find that those containing $R_\phi(\tau)$ and $R_\phi^i(\tau)$ vanish, and we denote the remaining terms by T's so that

$$R_\psi(\tau; \tau_1, \tau_2) \cong T_2 + T_3 + T_4 + T_5 + T_6 \tag{95}$$

In writing the expressions for the various T's, we notice that they involve the moments m_i of the impulse response $h_p(t)$ of the symmetric part of the predetection filter

$$m_i = \int_{-\infty}^{\infty} t^i h_p(t) \, dt \tag{96}$$

It is desirable to replace the m_i's by more convenient parameters of the filter. First we note that the moments are related to derivatives of the symmetric filter transfer function by (see Ref. 6, p. 16)

$$m_i = j^i \left. \frac{d^i H_p(\omega)}{d\omega^i} \right|_{\omega = 0} \tag{97}$$

Next, we write a power series for $H_p(\omega)$ in the form

$$H_p(\omega) = 1 + a_2(\omega/B)^2 + ja_3(\omega/B)^3 + a_4(\omega/B)^4 + ja_5(\omega/B)^5 + \ldots \qquad (98)$$

The term $a_1(\omega/B)$ has been left out of (98) since it can be made to vanish by cascading a suitable time-advance with the predetection filter without changing the intermodulation distortion. Now, by comparing (97) and (98) with a Taylor series in the form of Eq. (8) we can identify the power coefficients a_i as proportional to the moments m_i

$$m_i = \begin{cases} j^i i! \; a_i/B^i \, , & i \text{ even} \\ j^{i+1} i! \; a_i/B^i \, , & i \text{ odd} \end{cases} \qquad (99)$$

We use Eq. (99) to express the T's in Eq. (95) in terms of the a_i's.

The next step is to take the square of Eq. (95) in order to insert the result in the second term of Eq. (90). All terms in the square of Eq. (95) of the form $T_r T_s$, with $(r+s)$ odd, are dropped because they can be shown to correspond to imaginary distortion power. The second approximation of this computation is to assume that all terms having $(r+s)$ greater than eight are negligibly small. We are thus left with

$$R_\psi^2(\tau; \tau_1, \tau_2) \cong T_2^2 + T_3^2 + T_4^2 + 2T_2 T_4 + 2T_2 T_6 + 2T_3 T_5 \qquad (100)$$

Inserting Eq. (100) into the second term of Eq. (90), we notice that $R_\theta(\tau)$ now involves the moments n_i of the impulse response $h_q(t)$ of the anti-symmetric part of the predetection filter

$$n_i = \int_{-\infty}^{\infty} t^i h_q(t) \, dt \qquad (101)$$

Again, it is desirable to replace the n_i's by power coefficients as we did for the m_i's. If we write a power series for $H_q(\omega)$ is the form

$$H_q(\omega) = jb_1(\omega/B) + b_2(\omega/B)^2 + jb_3(\omega/B)^3 + b_4(\omega/B)^4 + jb_5(\omega/B)^5 + \ldots \quad (102)$$

we can readily identify the power coefficients b_i as proportional to the moments n_i

$$n_i = \begin{cases} j^i \, i! \quad b_i/B^i \, , & i \text{ even} \\ j^{i+1} i! \, b_i/B^i \, , & i \text{ odd} \end{cases} \quad (103)$$

We use Eq. (103) to express $R_\theta(\tau)$ in terms of the b_i's.

We are now left with an expression for the autocorrelation function $R_\theta(\tau)$ of the intermodulation distortion in terms of the a_i's, b_i's and various derivatives of $R_\phi(\tau)$. The Fourier transformation of Eq. (74) is applied to $R_\theta(\tau)$ to obtain the power density spectrum. Finally, we use Eq. (71) and divide by $S_x(\nu)$ to obtain the I/S ratio as a function of the normalized video frequency ν. Long algebraic manipulations were required to perform all the computations. The final result is given on the next page as Eq. (105). The following is a short-ened version obtained by neglecting T-products having (r+s) greater than six

$$I/S \approx \frac{(\hat{\omega}/B)^2 (\omega_e/B)^2 \nu^2}{S_x(\nu)} \left\{ \left[S_x(\nu) \otimes S_x(\nu) \right] \right.$$

$$\left[2b_2^2 + (\hat{\omega}/B)^2 \nu^2 \left(3a_2 b_1 b_2 + 2a_2 b_2^2 - \tfrac{1}{2} a_2^2 b_1^2 - a_2^2 b_2 - 6 b_2 b_4 - \tfrac{9}{2} b_3^2 \right) \right]$$

$$\left. + \left[S_x(\nu) \otimes \nu^2 S_x(\nu) \right] (\hat{\omega}/B)^2 \left(2a_2^2 b_2 - 4a_2 b_2^2 - 4a_3 b_1 b_2 - 4b_2 b_4 \right) \right\} \quad (104)$$

$$\frac{I}{S} = \frac{(\hat{\omega}/B)^2 (\omega_e/B)^2 \, \nu^2}{S_x(\nu)} \cdot$$

$$\Big\{ \; [S_x(\nu) \otimes S_x(\nu)] \, (2b_2^2)$$

$$+ (\hat{\omega}/B)^2 \nu^2 \, [S_x(\nu) \otimes S_x(\nu)] \, (-\tfrac{1}{2}a_2^2 b_1^2 - a_2^2 b_2 + 3a_2 b_1 b_3 + 2a_2 b_2^2 - 6b_2 b_4 - \tfrac{9}{2}b_3^2)$$

$$+ (\hat{\omega}/B)^4 \nu^4 \, [S_x(\nu) \otimes S_x(\nu)] \, (\tfrac{1}{4}a_2^2 b_1^2 b_3 + a_2^2 b_2 b_4 - \tfrac{1}{16}a_2 a_3 b_1 b_2 + \tfrac{3}{4}a_2 a_3 b_3 - \tfrac{1}{4}a_2 a_4^2 b_1 + \tfrac{1}{2}a_2 a_4 b_2 - \tfrac{15}{4}a_2 b_1 b_5$$

$$-\tfrac{5}{2}a_2 b_2 b_4 - \tfrac{3}{4}a_2 b_2 b_3 + \tfrac{3}{2}a_3 b_1 b_4 - \tfrac{3}{4}a_3 b_2 b_3 + \tfrac{15}{2}b_2 b_6 + \tfrac{45}{4}b_3 b_5 + 6b_4^2)$$

$$+ (\hat{\omega}/B)^2 \, [S_x(\nu) \otimes \nu^2 S_x(\nu)] \, (2a_2^2 b_2 - 4a_3 b_1 b_2 - 4a_2 b_2^2 - 4b_2 b_4)$$

$$+ (\hat{\omega}/B)^4 \, [\nu^2 S_x(\nu) \otimes \nu^2 S_x(\nu)] \, (\tfrac{1}{2}a_2^4 - 2a_2^3 b_2 - 2a_2^2 a_3 b_1 + 2a_2^2 b_1 b_3 + 2a_2^2 b_2^2 + \tfrac{7}{2}a_2 a_2^2 b_2 + \tfrac{3}{2}a_2 a_3 b_1 b_2 + \tfrac{3}{2}a_2 a_3 b_3 - \tfrac{3}{2}a_2 a_4 b_1 - 3a_2 a_4 b_2$$

$$+ \tfrac{5}{2}a_2 b_1 b_5 + 3a_2 b_2 b_4 - \tfrac{3}{2}a_2 a_3 b_3 - \tfrac{3}{2}a_2 a_3 b_3 + \tfrac{1}{8}a_3^2 b_1^2 - \tfrac{1}{4}a_3 b_2 - \tfrac{1}{2}a_3 b_1 b_4 - \tfrac{5}{2}a_3 b_2 b_3 - 5b_2 b_6 - \tfrac{15}{2}b_3 b_5 - 2b_4^2)$$

$$+ (\hat{\omega}/B)^4 \, [S_x(\nu) \otimes \nu^4 S_x(\nu)] \, (-\tfrac{1}{2}a_2^2 b_1 b_3 - 2a_2^2 b_4 + \tfrac{1}{2}a_2 a_3 b_1 b_2 - \tfrac{9}{2}a_2 a_3 b_3 + \tfrac{3}{2}a_2 a_4 b_1 - a_2 a_4 b_2 - \tfrac{5}{2}a_2 b_1 b_5 + 5a_2 b_2 b_4$$

$$+ \tfrac{3}{2}a_2 b_2 b_3 + a_3^2 b_1 - a_3 b_1 b_4 + \tfrac{3}{2}a_3 b_2 b_3 - 6a_4 b_1 b_3 + 4a_5 b_1 b_2 + 9b_2 b_6 + \tfrac{15}{2}b_3 b_5 + 4b_4^2) \Big\}$$

$$(105)$$

We now have in Eqs. (104) and (105) an approximate result relating the intermodulation-distortion spectrum in the second-order term to the parameters of the filter and the video signal. The input video spectrum comes in only in the form of convolutions, while the filter characteristic comes in only as constant factors determined by power-series coefficients. Thus, given a video spectrum, we first compute the necessary convolutions (which can often be obtained in closed form). Then, by inserting numerical values for filter power-series coefficients into either Eq. (104) or (105), we can immediately write down the distortion spectrum. Any change of filter characteristic or video spectrum would not necessitate an elaborate recomputation. Furthermore, the dependence of distortion spectrum on $B, \hat{\omega}$ and ω_e is explicitly indicated in Eqs. (104) and (105). These equations would be most useful in evaluating the distortion introduced by highly unsymmetrical filters.

5.3 Distortion Spectrum: Symmetric Filter

For the case of a symmetric predetection filter, we assume that the distortion is low enough so that the first and third term in the series of (63) suffice for an adequate approximation to the transfer relation. We know that the second term $\theta_2(t)$ vanishes in this case, and that $\theta_1(t)$ and $\theta_3(t)$ are given by Eqs. (68) and (70). Thus, we wish to compute the power-density spectrum of the intermodulation distortion contained in the output phase

$$\theta(t) \cong \theta_1(t) + \theta_3(t) \tag{106}$$

The procedure is exactly the same as that used in Sec. 5.2.

We begin by forming the autocorrelation function from Eq. (106)

$$R_\theta(\tau) = \overline{\theta(t)\theta(t+\tau)} = \overline{\theta_1(t)\theta_1(t+\tau)} + \overline{\theta_3(t)\theta_3(t+\tau)}$$
$$+ \overline{\theta_1(t)\theta_3(t+\tau)} + \overline{\theta_1(t+\tau)\theta_3(t)} \tag{107}$$

All but the second term of Eq. (107) are readily seen[4] to depend only on the first power of $R_\phi(\tau)$, so they do not contribute to intermodulation distortion and may be dropped.

With the aid of Eqs. (70) and (88) we can now write

$$R_\theta(\tau) = \overline{\theta_3(t)\,\theta_3(t+\tau)}$$

$$= \frac{1}{36} \int_{-\infty}^{\infty}\!\!\int h_p(\tau_1)\,h_p(\tau_2)\,\overline{\psi^3(t,\tau_1)\,\psi^3(t+\tau,\tau_2)}\,d\tau_1\,d\tau_2 \qquad (108)$$

We employ the rule for the average of the product of gaussian processes[4] to get

$$R_\theta(\tau) = \frac{1}{36} \int_{-\infty}^{\infty}\!\!\int h_p(\tau_1)\,h_p(\tau_2)\Big[9R_\psi^2(0;\tau_1,\tau_2)\,R_\psi(\tau;\tau_1,\tau_2) + 6R_\psi^3(\tau;\tau_1,\tau_2)\Big]d\tau_1\,d\tau_2$$

$$(109)$$

The first term in Eq. (109) is easily seen to depend only on the first power of $R_\phi(\tau)$, so it too is dropped because it does not contribute to intermodulation distortion.

Inserting the expression for $R_\psi(\tau;\tau_1,\tau_2)$ from Eq. (91) into the second term of Eq. (109) and Fourier transforming yields, after some algebraic manipulation, the PM distortion spectrum

$$I_\theta(\omega) = (1/6)\,|H_p(\omega)|^2\big\{S_\phi(\omega)\boxtimes S_\phi(\omega)\boxtimes S_\phi(\omega)\big\}$$

$$+ (2/3)\,\big\{|H_p(\omega)|^2 S_\phi(\omega)\boxtimes |H_p(\omega)|^2 S_\phi(\omega)\boxtimes |H_p(\omega)|^2 S_\phi(\omega)\big\}$$

$$+ (1/2)\big\{|H_p(\omega)|^2 S_\phi(\omega)\boxtimes |H_p(\omega)|^2\,[S_\phi(\omega)\boxtimes S_\phi(\omega)]\big\}$$

$$+ (2/3)\,\mathrm{Re}\big\{H_p^*(\omega)\,[H_p(\omega)\,S_\phi(\omega)\boxtimes H_p(\omega)\,S_\phi(\omega)\boxtimes H_p(\omega)\,S_\phi(\omega)]\big\}$$

$$-\mathrm{Re}\big\{H_p^*(\omega)\,[H_p(\omega)\,S_\phi(\omega)\boxtimes H_p(\omega)\{S_\phi(\omega)\boxtimes S_\phi(\omega)\}]\big\}$$

$$-2\mathrm{Re}\big\{|H_p(\omega)|^2 S_\phi(\omega)\boxtimes H_p^*(\omega)\,[H_p(\omega)\,S(\omega)\boxtimes H_p(\omega)\,S_\phi(\omega)]\big\}$$

$$+ \int\!\!\int_{-\infty}^{\infty} H_p^*(\omega-p)\,H_p^*(p)\,H_p(\omega-s)\,H_p(s)\,S_\phi(\omega-p-s)\,S_\phi(p)\,S_\phi(s)\,dp\,ds$$

$$(110)$$

$S_\phi(\omega)$ is power-density spectrum of the phase modulation $\phi(t)$, which is simply related to that of the frequency modulation by Eq. (93). Finally, multiplication of Eq. (110) by $(\omega/\omega_e)^2$ as indicated in Eq. (71) yields the desired FM distortion spectrum, which in turn may be divided by the output video spectrum $S_x(\omega)$ to obtain the I/S ratio.

We now have in Eq. (110) an exact relationship between the inter-modulation-distortion spectrum in the third-order term and double-convolutions of the input video spectrum and the filter transfer function $H_p(\omega)$. These convolutions would have to be evaluated numerically for each combination of input video spectrum and predetection filter of interest. Such computations could prove arduous enough to require a digital computer. In the next section we derive an approximation which greatly reduces this computational complexity.

5. 4   Approximation to the Distortion Spectrum: Symmetric Filter

The approximation procedure is the same as that used in Sec. 5.2. We take the cube of Eq. (95), with T's expressed in terms of the a's, in order to insert the result in the second term of Eq. (109). Again, we drop all terms of the form $T_q T_r T_s$, with (q+r+s) odd, because they can be shown to correspond to imaginary distortion power. We also assume that all terms having (q+r+s) greater than ten are negligibly small. We are thus left with

$$R_\psi^3(\tau; \tau_1, \tau_2) \cong T_2^3 + 3T_2^2 T_4 + 3T_2 T_3^2 + 3T_2 T_4^2 + 3T_3^2 T_4 + 6T_2 T_3 T_5 + 3T_2^2 T_6 \tag{111}$$

Inserting Eq. (111) into the second term of Eq. (109), we notice that $R_\theta(\tau)$ again involves the moments m_i, so we employ Eq. (99) once more to replace the m_i's by a_i's. We are then left with an expression for $R_\theta(\tau)$ in terms of the a_i's and various derivatives of $R_\phi(\tau)$. The Fourier transformation of Eq. (74) is applied to $R_\theta(\tau)$ to obtain the power density spectrum. Finally, we use Eq. (71) and divide by $S_x(\nu)$ to obtain the I/S ratio as a function of ν. Long

algebraic manipulations were required to perform all the computations. The final result is given on the next page as Eq. (113). The following is a shortened version obtained by neglecting T-products having $(q + r + s)$ greater than eight

$$I/S = \frac{(\hat{\omega}/B)^2 (\omega_e/B)^4 \nu^2}{S_x(\nu)} \left\{ [S_x(\nu) * S_x(\nu) * S_x(\nu)] \right.$$

$$[6a_3^2 + (\hat{\omega}/B)^2 \nu^2 (30a_3 a_5 + 24a_4^2 - 8a_2^2 a_4 - 6a_2 a_3^2 - \tfrac{2}{3} a_2^4)]$$

$$\left. + [S_x(\nu) * S_x(\nu) * \nu^2 S_x(\nu)] (\hat{\omega}/B)^2 (30a_3 a_5 + 6a_2 a_3^2) \right\} \qquad (112)$$

We now have in Eqs. (112) and (113) an approximate result relating the intermodulation-distortion spectrum in the third-order term to the parameters of the filter and the video signal. The input video spectrum comes in only in the form of double convolutions, while the filter characteristic comes in only as constant factors determined by power-series coefficients. Thus, given a video spectrum, we first compute the necessary double convolutions (which can often be obtained in closed form). Then, by inserting numerical values for filter power-series coefficients into either Eq. (112) or (113), we can immediately write down the distortion spectrum. Any change of filter characteristic or video spectrum would not necessitate an elaborate recomputation. Furthermore, the dependence of distortion spectrum on B, $\hat{\omega}$ and ω_e is explicitly indicated in Eqs. (112) and (113).

$$I/S = \frac{(\hat{\omega}/B)^2 (\omega_e/B)^4 \nu^2}{S_x(\nu)} \Bigg\{$$

$$+ (\hat{\omega}/B)^2 \nu^2 \,[S_x(\nu) \otimes S_x(\nu) \otimes S_x(\nu)]\,(6a_3^2)$$

$$+ (\hat{\omega}/B)^2 \,[S_x(\nu) \otimes S_x(\nu) \otimes S_x(\nu)]\,(30a_3 a_5 + 24a_4^2 - 8a_2^2 a_4 - 6a_2 a_3^2 + \tfrac{2}{3}a_2^4)$$

$$+ (\hat{\omega}/B)^2 \,[S_x(\nu) \otimes S_x(\nu) \otimes \nu^2 S_x(\nu)]\,(30a_3 a_5 + 6a_2 a_3^2)$$

$$+ \tfrac{1}{6}(\hat{\omega}/B)^4 \nu^4 \,[S_x(\nu) \otimes S_x(\nu) \otimes S_x(\nu)]\,(-a_2^5 + 16a_2^3 a_4 + \tfrac{21}{2}a_2^2 a_3^2 - 60a_2^2 a_6 - \tfrac{15}{2}a_2 a_3 a_5 - 60a_2 a_4^2$$
$$+ \tfrac{9}{2}a_3^2 a_4 + \tfrac{315}{2}a_3 a_7 + 360a_4 a_6 + 15a_5^2)$$

$$+ \tfrac{1}{6}(\hat{\omega}/B)^4 \nu^2 \,[S_x(\nu) \otimes S_x(\nu) \otimes \nu^2 S_x(\nu)]\,(6a_2^5 - 60a_2^3 a_4 - 45a_2^2 a_3^2 - 180a_2^2 a_6 + 45a_2 a_3 a_5 + 144a_2 a_4^2$$
$$+ 27a_3^2 a_4 + 945a_3 a_7 + 1080a_4 a_6 + 450a_5^2)$$

$$+ \tfrac{1}{6}(\hat{\omega}/B)^4 \,[S_x(\nu) \otimes \nu^2 S_x(\nu) \otimes \nu^2 S_x(\nu)]\,(6a_2^5 - 72a_2^3 a_4 - 39a_2^2 a_3^2 + 375a_2 a_3 a_5 + 216a_2 a_4^2$$
$$+ 9a_3^2 a_4 + 315a_3 a_7 + 150a_5^2)$$

$$+ \tfrac{1}{6}(\hat{\omega}/B)^4 \,[S_x(\nu) \otimes S_x(\nu) \otimes \nu^4 S_x(\nu)]\,(-3a_2^5 + 36a_2^3 a_4 - \tfrac{3}{2}a_2^2 a_3^2 - \tfrac{39}{2}a_2 a_3 a_5 - 108a_2 a_4^2$$
$$- \tfrac{81}{2}a_3^2 a_4 + \tfrac{189}{2}a_3 a_7 + 75a_5^2 \Bigg)\Bigg\}$$

$$(113)$$

6. CONCLUSIONS

The effect of predetection-filter characteristics on telemetry-data quality has been studied. Intermodulation distortion was recognized as the primary data-degrading effect, and was characterized in terms intermodulation distortion spectrum under noise-loading conditions. The noise-loading technique was shown to be:

a) Realistic, in that it is capable of simulating typical multi-channel telemetry signals,

b) Practical, in that consistent and meaningful laboratory measurements can readily be obtained, and

c) Analytically tractable, in that the results of measurements can be mathematically predicted, and the dependence of distortion on important system parameters (such as filter bandwidth, video-signal bandwidth and deviation) is explicitly determined.

The distortion mechanism in the predetection filter is found to hinge on the ratio of video-signal bandwidth to filter bandwidth. Two cases are identified: the quasi-stationary case, when this ratio is much less than unity, and the general case when it is not. In the quasi-stationary case, the distortion is determined entirely by the filter phase characteristic, whereas in the general case the whole transfer function determines the distortion. The distortion spectrum is computed for each case, and the contributions caused by lack of filter symmetry are isolated.

One interesting question has not been answered, namely: under exactly what conditions is the quasi-stationary approach invalid? Or alternatively: how large is the error in the distortion spectrum computed on the quasi-stationary basis when the bandwidth ratio is not much less than unity? It is likely that the error will remain small until the ratio of bandwidths approaches one half. Further, there is some reason to believe that the distortion spectrum computed on the quasi-stationary basis will always be smaller than the actual level.

In practice, IF amplifier-filters must satisfy three performance requirements:

a) Adequate adjacent channel rejection,

b) Low noise bandwidth, and

c) Low data distortion.

Each design represents a compromise between a) and b) on the one hand and c) on the other. The designer must be able to predict the performance of his design, in order to ensure that his compromise is acceptable, consistent and attainable. The results of the present study enable such a prediction, once the numerical computations for the specific filter design and signal parameters are performed. It would be very helpful to the designer to have at his disposal a "catalog" of popular IF filter designs (e.g. Butterworth, Gaussian etc.) with their associated performance parameters including intermodulation-distortion levels.

APPENDIX A

DERIVATION OF THE QUASI-STATIONARY TRANSFER RELATION

We wish to derive Eq. (55) from the general transfer relation in Eq.(50). Inserting Eq. (54) in Eq. (50), utilizing the trigonometric identities for the sine and cosine of the difference of two angles, and then dividing numerator and denominator by $\cos \phi(t)$ yields

$$\tan \theta (t) = \frac{\left[\tan \phi(t) \int h_p(\tau) \cos (\tau \dot{\phi} (t)) d\tau - \int h_p(\tau) \sin (\tau \dot{\phi} (t)) d\tau \right.}{\left[\int h_p(\tau) \cos (\tau \dot{\phi}(t)) d\tau + \tan \phi(t) \int h_p(\tau) \sin (\tau \dot{\phi}(t)) d\tau \right.}$$

$$\frac{\left. - \int h_q(\tau) \cos (\tau \dot{\phi}(t)) d\tau - \tan \phi(t) \int h_q(\tau) \sin (\tau \dot{\phi}(t)) d\tau \right]}{\left. + \tan \phi(t) \int h_q(\tau) \cos (\tau \dot{\phi}(t)) - \int h_q(\tau) \sin (\tau \dot{\phi}(t)) d\tau \right]} \qquad (A-1)$$

Now, recognize the following Fourier transforms:

$$\mathrm{Re}\left[H_p(\dot{\phi}) \right] = \int h_p(\tau) \cos (\tau \dot{\phi}) d\tau \qquad (A-2)$$

$$\mathrm{Im}\left[H_p(\dot{\phi}) \right] = - \int h_p(\tau) \sin (\tau \dot{\phi}) d\tau \qquad (A-3)$$

$$\mathrm{Re}\left[H_q(\dot{\phi}) \right] = \int h_q(\tau) \cos (\tau \dot{\phi}) d\tau \qquad (A-4)$$

$$\mathrm{Im}\left[H_q(\dot{\phi}) \right] = - \int h_q(\tau) \sin (\tau \dot{\phi}) d\tau \qquad (A-5)$$

Substituting from Eqs. (A-2) - (A-5) into (A-1), and dividing numerator and denominator by $\left\{ \mathrm{Re}\left[H_p(\dot{\phi}) \right] + \mathrm{Im}\left[H_q(\dot{\phi}) \right] \right\}$ we get

$$\tan \theta(t) = \frac{\dfrac{\mathrm{Im}\left[H_p(\dot{\phi}) \right] - \mathrm{Re}\left[H_q(\dot{\phi}) \right]}{\mathrm{Re}\left[H_p(\dot{\phi}) \right] + \mathrm{Im}\left[H_q(\dot{\phi}) \right]} + \tan \phi(t)}{1 - \dfrac{\mathrm{Im}\left[H_p(\dot{\phi}) \right] - \mathrm{Re}\left[H_q(\dot{\phi}) \right]}{\mathrm{Re}\left[H_p(\dot{\phi}) \right] + \mathrm{Im}\left[H_q(\dot{\phi}) \right]} \cdot \tan \phi (t)} \qquad (A-6)$$

The similarity of Eq. (A-6) to the trigonometric identity

$$\tan(\alpha + \beta) = \frac{\tan \alpha + \tan \beta}{1 - \tan \alpha \tan \beta} \tag{A-7}$$

is exploited to conclude that

$$\theta(t) = \arctan \frac{\text{Im}\left[H_p(\dot{\phi})\right] - \text{Re}\left[H_q(\dot{\phi})\right]}{\text{Re}\left[H_p(\dot{\phi})\right] + \text{Im}\left[H_q(\dot{\phi})\right]} + \phi(t) \tag{A-8}$$

With the aid of Eqs. (3.10) and (3.11) we can write

$$\text{Im}\left[H_p(\dot{\phi})\right] - \text{Re}\left[H_q(\dot{\phi})\right] = \text{Im}\left[H_1(\dot{\phi} + \omega_c)\right] \tag{A-9}$$

$$\text{Re}\left[H_p(\dot{\phi})\right] + \text{Im}\left[H_q(\dot{\phi})\right] = \text{Re}\left[H_1(\dot{\phi} + \omega_c)\right] \tag{A-10}$$

Therefore

$$\theta(t) = \arctan \frac{\text{Im}\left[H_1(\dot{\phi} + \omega_c)\right]}{\text{Re}\left[H_1(\dot{\phi} + \omega_c)\right]} + \phi(t) \tag{A-11}$$

The arc tan is immediately recognized to be the phase characteristic $\Phi[\dot{\phi} + \omega_c]$, and use of Eq. (36) finally yields the desired Eq. (55).

REFERENCES

1. Magnusson, R. I., "Intermodulation Noise in Linear FM Systems," Proc. I.E.E., Monograph No. 459E (Vol. 109C, pp. 32-44), July 1961.

2. Magnusson, R. I., "On Intermodulation Noise and Group-Delay in Wide-band Radio-Relay Systems Carrying Frequency-Division Multiplex Telephony," Transactions of Chalmers University of Technology, Gothenburg, Sweden, No. 285, Avd. Elektrotechnik 74, 1964.

3. Baghdady, E. J., Lectures on Communication System Theory, McGraw-Hill, New York, 1961.

4. Laning, J. H. and R. H. Battin, Random Processes in Automatic Control, McGraw-Hill Book Company, Inc., New York, N.Y., p. 82, 1956.

5. Dwight, H. B., Tables of Integrals and Other Mathematical Data, The Macmillan Company, New York, N.Y., Fourth Edition, p. 11, 1961.

6. Papoulis, A., The Fourier Integral and Its Applications, McGraw-Hill, New York, 1962.

7. Van Trees, H. L., "Functional Techniques for the Analysis of the Non-linear Behavior of Phase-Locked Loops," IEEE Proc., 52, 8, pp. 894-911, August 1964.

8. Thomson, W. E., "The Response of a Non-Linear System to Random-Noise," Proc. I.E.E., Monograph No. 106R (Vol. 102C, pp. 46-48), September 1954.

PART II

COMPUTATION AND SPECIFICATION OF INTERMODULATION DISTORTION

1. INTRODUCTION

1.1 Purpose

This part comprises the fifth final task report on the results of a program of investigations carried out at ADCOM, Inc. under Contract No. NAS-5-9742 for NASA. This work was conducted in close coordination with, and in direct support of, activities of members of the RF Systems Branch, Advanced Development Division of the Goddard Space Flight Center.

The effort during the period from 1 September 1965 to the end of the period of performance was allocated exclusively to performing Task I of the study program. This report documents this effort.

1.2 Scope

This task of the study program called for the application of the analyses developed under Task II (Part I of this report) of intermodulation distortion caused by phase nonlinearities to

    a) analyze nonlinearities in demodulators,

    b) study overall filter design problems, e.g., shape factor vs. phase linearity, and

    c) compile a catalog of commonly used predetection filters along with their intermodulation distortion levels.

We begin in Sec. 2 by reviewing the results on the quasi-stationary approximation which were presented in Part I. We explain in detail how to use these results to compute actual intermodulation distortion levels. In Sec. 3 we compute the shape of the I/S spectrum corresponding to a rectangular video spectrum with and without ideal preemphasis (Fig. 2).

The effect of filter type on the level of distortion is evaluated in Sec. 3. Here we catalog the various types of predetection filters commonly incorporated into telemetry receivers, giving their transfer functions, phase characteristics and group delay characteristics. The distortion levels are determined by the power series coefficients of the phase characteristics. These are tabulated for the various filters in Tables 1, 4 and 5.

The computation of distortion levels caused by filters consisting of several cascaded stages is treated in Sec. 5. Great simplification of the computations is achieved if the stages are identical. We then give concise information as to the bandwidth of the cascade in terms of the bandwidth of each of the identical stages. Selected experimental results are cited in Sec. 6 to demonstrate the adequacy of the quasi-stationary approximation for the prediction of I/S ratios in most telemetry applications.

A good filter design must perform other functions in addition to reducing intermodulation distortion. The tradeoffs between distortion and these other performance criteria are considered in Sec. 7. Comprehensive tradeoff results are tabulated in Tables 7, 8 and 9. These tables can be used to formulate meaningful and effective specifications for predetection filters. The specification methods are explained in Sec. 8, where we express a preference for performance specifications over design specifications.

The application of the noise-loading technique to evaluation of distortion caused by nonlinear modulators and demodulators is covered in Secs. 9 and 10. We derive a general result in Sec. 9 relating the resulting I/S ratio to the power-series coefficients of the modem nonlinearity. Then in Sec. 10 we prove that the intermodulation distortion waveforms generated by the modem and the predetection filters are uncorrelated, so that their I/S ratios add on a power basis.

Finally, we sum up the achievements of the study in Sec. 11, and discuss the possible improvements that could be introduced in the design of predetection filters for future telemetry systems. We recommend analytical and experimental efforts to develop these filters, and identify some of the more promising avenues of attack.

2. THE QUASI-STATIONARY APPROXIMATION

When the video bandwidth is much smaller than the predetection-filter bandwidth, we showed in Sec. 3.3 of Part I that the modulation transfer relation is closely approximated by

$$\theta(t) \approx \phi(t) + \Phi[\omega_e x(t) + \omega_c] \tag{1}$$

for the phase modulation, or

$$y(t) \approx x(t) + \frac{1}{\omega_e} \frac{d}{dt}\left\{\Phi[\omega_e x(t) + \omega_c]\right\} \tag{2}$$

for the frequency modulation. The distortion is represented by the second terms in Eqs. (1) and (2), and is entirely determined by the nonlinearities in the filter phase characteristic $\Phi(\omega)$. It is not affected by the filter amplitude characteristic in this approximation.

We introduced in Section 4 of Part I the noise-loading technique for the spectral characterization of the intermodulation distortion. We employed a power-series expansion of the nonlinear phase characteristic $\Phi(\omega)$ of the form

$$\Phi(\omega) = \sum_{i=0}^{\infty} c_i \left(\frac{\omega - \omega_c}{B}\right)^i \tag{3}$$

where we defined B as <u>half</u> the bandwidth of the predetection filter, and c_i as the power-series coefficients. We were then able to show that the ratio of intermodulation-distortion power to signal power is given generally by

$$\frac{I_y(\nu)}{S_x(\nu)} = \left(\frac{\hat{\omega}\nu}{\omega_e}\right)^2 \sum_{n=2}^{\infty} n! \frac{S_x^{(n)}(\nu)}{S_x(\nu)} \left[\sum_{k=0}^{\infty} \frac{(n+2k)!}{2^k k! \, n!} c_{n+2k}\left(\frac{\omega_e}{B}\right)^{n+2k}\right]^2 \tag{4}$$

It is instructive to write out a few distortion terms from Eq. (4)

$$I_y(\nu) = 2! \left(\frac{\hat{\omega}}{B}\right)^2 \left(\frac{\omega_e}{B}\right)^2 \nu^2 S_x^{(2)}(\nu) \left[c_2 + 6 c_4 \left(\frac{\omega_e}{B}\right)^2 + 45 c_6 \left(\frac{\omega_e}{B}\right)^4 + \ldots\right]^2$$

$$+ 3! \left(\frac{\hat{\omega}}{B}\right)^2 \left(\frac{\omega_e}{B}\right)^4 \nu^4 S_x^{(3)}(\nu) \left[c_3 + 10 c_5 \left(\frac{\omega_e}{B}\right)^2 + 105 c_7 \left(\frac{\omega_e}{B}\right)^4 + \ldots\right]^2$$

$$+ 4! \left(\frac{\hat{\omega}}{B}\right)^2 \left(\frac{\omega_e}{B}\right)^6 \nu^2 S_x^{(4)}(\nu) \left[c_4 + 15 c_6 \left(\frac{\omega_e}{B}\right)^2 + \ldots\right]^2$$

$$+ 5! \left(\frac{\hat{\omega}}{B}\right)^2 \left(\frac{\omega_e}{B}\right)^8 \nu^2 S_x^{(5)}(\nu) \left[c_5 + 21 c_7 \left(\frac{\omega_e}{B}\right)^2 + \ldots\right]^2$$

$$+ \ldots \tag{5}$$

The first line of Eq. (5) represents second-order distortion, the second line represents third-order distortion, etc. It can be seen that an even-power coefficient (c_i) contributes only to all even-ordered distortion up to order i, while an odd-power coefficient (c_j) contributes only to all odd-ordered distortion up to order j.

Now, most predetection filters used in telemetry systems are designed (and aligned) to have symmetrical frequency characteristics with respect to the center frequency. A symmetric filter has an anti-symmetric phase characteristic $\Phi(\omega)$, so that all its even-order coefficients vanish. Consequently a symmetric filter will introduce only odd-ordered distortion. Comparing the various odd-order terms in Eq. (5), we see that successive terms are reduced in magnitude by the factor $(\omega_e/B)^4$ which is usually a very small number. Thus the third-order term will usually predominate over the fifth- and higher-order terms. Therefore the I/S ratio for symmetric filters is given approximately by

$$\frac{I_y(\nu)}{S_x(\nu)} \approx 3! \left(\frac{\hat{\omega}}{B}\right)^2 \left(\frac{\omega_e}{B}\right)^4 \frac{\nu^2 S_x^{(3)}(\nu)}{S_x(\nu)} \left[c_3 + 10 c_5 \left(\frac{\omega_e}{B}\right)^2 + 105 c_7 \left(\frac{\omega_e}{B}\right)^4 + \ldots\right]^2 \tag{6}$$

We now have in Eq. (6) a general result relating the intermodulation-distortion spectrum to the parameters of the filter and the video signal. The spectrum of the input video signal appears only in the form of a double convolution. The factor in which this appears

$$\frac{\nu^2 S_x^{(3)}(\nu)}{S_x(\nu)} \tag{7}$$

completely determines the shape of the distortion spectrum over the video band. The effect of input spectral shape on distortion spectral shape is discussed in the next section. The magnitude of the distortion is determined in part by the factor

$$3! \left(\frac{\hat{\omega}}{B}\right)^2 \left(\frac{\omega_e}{B}\right)^4 \tag{8}$$

which involves only the normalized video bandwidth $(\hat{\omega}/B)$ and the normalized rms deviation (ω_e/B). The other factor determining the magnitude is

$$\left[c_3 + 10 c_5 \left(\frac{\omega_e}{B}\right)^2 + 105 c_7 \left(\frac{\omega_e}{B}\right)^4 + \ldots\right]^2 \tag{9}$$

which involves the filter phase coefficients in conjunction with the normalized rms deviation. The type of filter influences the magnitude of the distortion spectrum solely through this factor. Section 4 presents the coefficients for the various filter types commonly used in telemetry systems, and Sec. 5 discusses the manner in which distortion accumulates in a cascade of filter stages.

The three factors identified above (Eqs. (7) through (9)) may be obtained readily in decibels and added to obtain the I/S ratio. The first factor (Eq. (7)) can be taken directly from Fig. 2 for any desired value of ν. The second factor (Eq. (8)) requires only a rapid calculation and conversion to dB's. The third factor (Eq. (9)) is tabulated in Sec. 7 for various filter types and for selected values of $\left(\frac{\omega_e}{B}\right)$. Interpolation may give sufficient accuracy for intermediate values of $\left(\frac{\omega_e}{B}\right)$; if not, the coefficients c_i are available for direct calculation in Sec. 4.

3. THE EFFECT OF VIDEO SPECTRUM SHAPE

In Eq. (7) of the preceding section we identified the factor which determines the shape of the I/S curve of the video band. In this section we consider two possible input spectra and calculate the shape of the resulting I/S curves. The two input spectra are shown in Fig. 1. The rectangular spectrum results when a rectangular video spectrum is applied directly to the FM transmitter. The parabolic spectrum results when a rectangular video spectrum is passed through an ideal preemphasis network before FM modulation. (Alternately, it represents applying a rectangular video spectrum directly to a PM modulator.) Both spectra are normalized to have unit area in the (S, ν) plane and hence unity power in the video signal.

For these two spectra, the double convolutions in Eq. (7) are given in the range of interest by:

Rectangular Spectrum:

$$S_x^{(3)}(\nu) = S_x(\nu) \boxtimes S_x(\nu) \boxtimes S_x(\nu) = \frac{1}{8}(3 - \nu^2) \qquad |\nu| < 1 \qquad (10)$$

Parabolic Spectrum:

$$S_x^{(3)}(\nu) = S_x(\nu) \boxtimes S_x(\nu) \boxtimes S_x(\nu) = \frac{27}{8}\left(\frac{1}{40} + \frac{\nu^2}{3} - \frac{\nu^4}{4} + \frac{\nu^8}{840}\right) \qquad |\nu| < 1 \qquad (11)$$

Substitution of these results into Eq. (7) gives the curves shown in Fig. 2 for the two cases. As can be seen, ideal preemphasis has reduced distortion at the upper end of the video band by a few dB. This may be significant when a peak I/S criterion is to be met. However, this has been at the cost of significantly higher distortion at the lower video frequencies. The cross-over point where the two spectra yield equal distortion is about $\nu = 0.7$.

More complicated preemphasis schemes are frequently employed in telemetry systems. It is difficult to evaluate the resulting distortion spectra in closed form; but results can readily be obtained by performing the double convolutions on a digital computer. Nevertheless, results obtained for a rectangular spectrum should be considered representative for most practical situations.
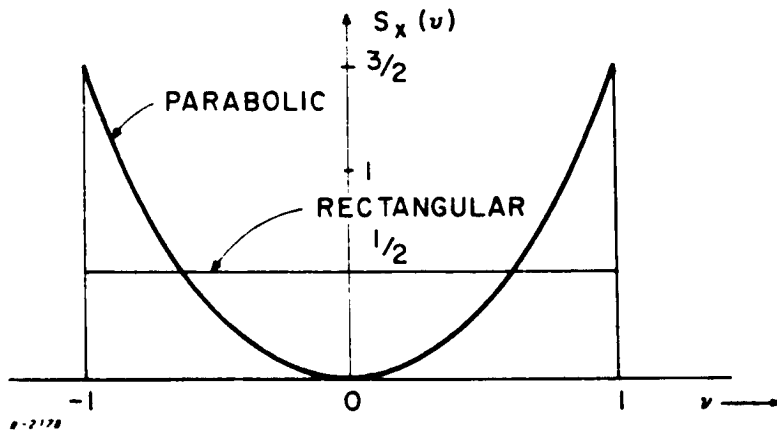
Fig. 1 Rectangular and Parabolic Input Spectra.
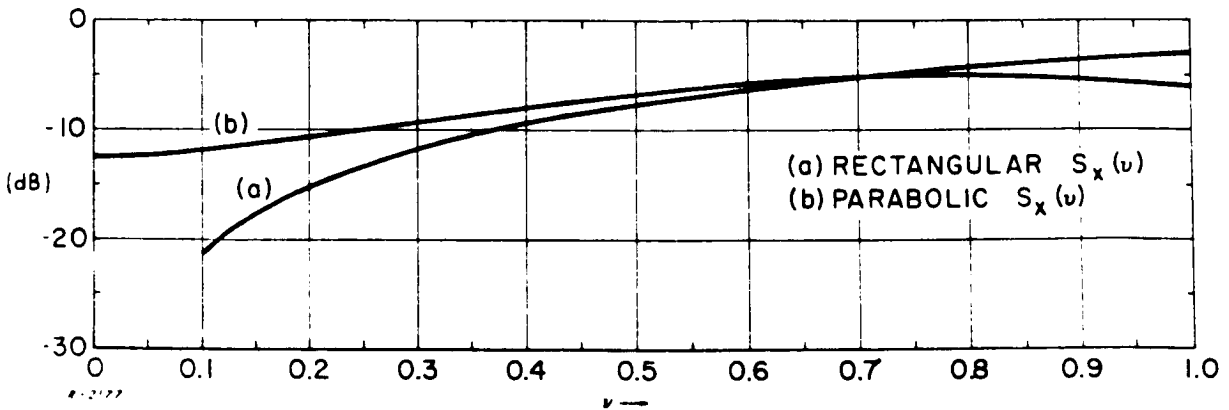
Fig. 2 $\dfrac{\nu^2 S_x^{(3)}(\nu)}{S_x(\nu)}$ vs ν for Different Input Spectra.

4. THE EFFECT OF FILTER TYPE

In this section we tabulate phase coefficients c_i defined by the series representation of Eq. (3). These coefficients depend only upon the type (e.g., Butterworth) and order of the filter. We consider three types of filters commonly employed in telemetry receivers; namely Butterworth filters of various orders, Bessel filters of various orders, and double-tuned circuits with various coupling coefficients.

In addition to the phase coefficients of Eq. (3) we will present appropriate curves of group delay, defined as the derivative of the phase characteristic

$$T_d(\omega) = \frac{d}{d\omega} \Phi(\omega) \tag{12}$$

In writing expressions for the transfer functions and group-delay characteristics of various filters, we make one simplifying assumption throughout; namely, that the relative bandwidth of the filter is small, so that the familiar lowpass-to-bandpass reactance transformation becomes a simple frequency translation (see Ref. 4, Sec. 11-9).

The group delay is used because it is an easy parameter to measure and it presents the nonlinearities of the phase characteristic in a manner in which they are most evident. A nonflat group-delay characteristic contains all the data-degrading features of the corresponding nonlinear phase characteristic. Measurement of the group delay permits a comparison with the theoretically predicted group-delay characteristics to assess the effects of misalignment, and also enables the computation of the resultant intermodulation distortion.

The first filter type we consider is the Butterworth filter, which is defined by the maximally-flat amplitude characteristic

$$|H_n(\omega)|^2 = \frac{1}{1 + \left((\omega - \omega_c)/B\right)^{2n}} \tag{13}$$

where 2B is the 3 dB bandwidth and n is the order of the filter. The phase and group-delay characteristics of this filter are given by: (Ref. 3)

$$\Phi(\omega) = \sum_{m=0}^{\infty} \frac{\left((\omega - \omega_c)/B\right)^{2m+1}}{(2m+1) \sin (2m+1)\pi/2n} \quad \text{radians} \tag{14}$$

and

$$T_d(\omega) = \sum_{m=0}^{\infty} \frac{\left((\omega - \omega_c)/B\right)^{2m}}{\sin (2m+1)\pi/2n}$$

$$= \frac{1}{1 + \left((\omega - \omega_c)/B\right)^{2n}} \sum_{m=0}^{n-1} \frac{\left((\omega - \omega_c)/B\right)^{2m}}{\sin (2m+1)\pi/2n} \quad \text{seconds} \tag{15}$$

This group-delay characteristic is plotted in normalized form in Fig. 3 for orders from 1 to 6. The coefficients c_i for the Butterworth filters are listed in Table 1. The general expression is readily found from Eq. (14) to be

$$c_{(2i+1)} = \frac{1}{(2i+1) \sin\dfrac{(2i+1)\pi}{2n}} \qquad i = 0, 1, \ldots \tag{16}$$

The second filter type we study is the Bessel or linear-phase filter. This filter has the property of a maximally-linear phase characteristic and is defined by the transfer function (Ref. 4, pp 499-500)

$$H_n(\omega) = \frac{a_o}{y_n(u)} \tag{17}$$

where the y_n are the Bessel polynomials whose coefficients are listed in Table 2 for n from 1 to 6. The phase and group-delay characteristics corresponding
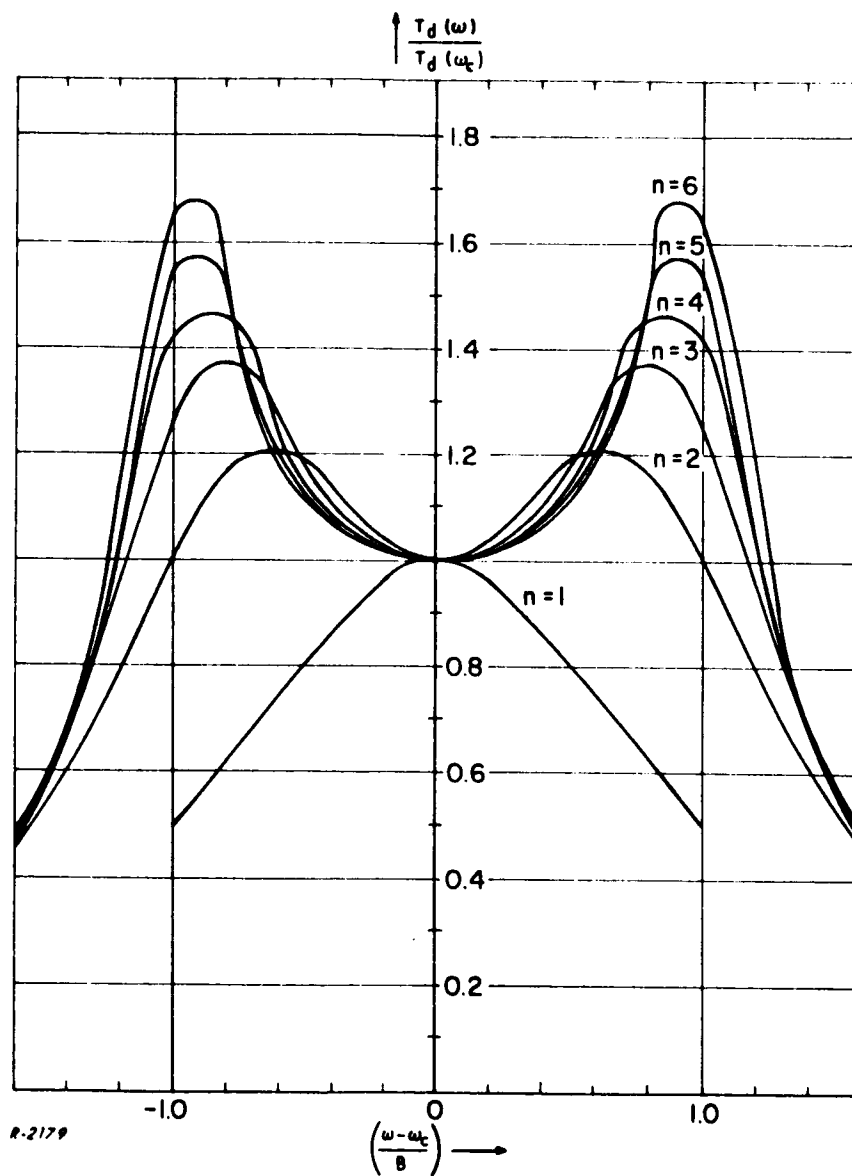
Fig. 3 Normalized Group Delay for Butterworth
Filters of Various Orders

R-2179

Table 1

PHASE COEFFICIENTS OF BUTTERWORTH FILTERS
OF VARIOUS ORDERS

	n=1	n=2	n=3	n=4	n=5	n=6
c_1	1.00	1.414	2.00	2.61	3.24	3.86
c_3	-0.333	0.471	0.333	0.361	0.412	0.471
c_5	0.200	-0.283	0.400	0.216	0.200	0.207
c_7	-0.143	-0.202	-0.286	0.373	0.177	0.552
c_9	0.111	0.157	-0.111	-0.283	0.360	0.157
c_{11}	-0.0909	0.129	-0.182	-0.0984	-0.294	0.351

Table 2

COEFFICIENTS OF THE BESSEL POLYNOMIALS

$$y_n(x) = x^n + a_{n-1} x^{n-1} + \ldots + a_o$$

n	a_o	a_1	a_2	a_3	a_4	a_5
1	1					
2	3	3				
3	15	15	6			
4	105	105	45	10		
5	945	945	420	105	15	
6	10,395	10,395	4,725	1,260	210	21

to Eq.(16) can be shown to be (Refs. 2 and 4)

$$\Phi(\omega) = u - \tan^{-1} \frac{J_{n+1/2}(u)}{(-1)^n J_{-n-1/2}(u)} \quad \text{radians} \quad (18)$$

and

$$T_d(\omega) = T_d(\omega_c) \left(1 - \frac{1}{u^2 \{ \frac{\pi}{2u} [J_{-n-1/2}^2(u) + J_{n+1/2}^2(u)] \}}\right) \text{seconds} \quad (19)$$

where $T_d(\omega_c)$ is the group delay at center frequency and J denotes spherical Bessel functions of the first kind. The argument $u = (\omega - \omega_c) T_d(\omega_c)$ used in Eqs.(17) through (19) is a normalized frequency. It can be converted to the more convenient $(\omega - \omega_c)/B$ using the relationship

$$\frac{\omega - \omega_c}{B} = (\omega - \omega_c) T_d(\omega_c) \times \frac{1}{B T_d(\omega_c)} \quad (20)$$

where the product $B T_d(\omega_c)$ is fixed for a given order and may be found from Table 3. (A more extensive table of these time-bandwidth products in available in Ref. 2, p. 502.)

The group-delay characteristics given by Eq.(19) are plotted in normalized form in Fig. 4 with $(\omega - \omega_c)/B$ as abscissa. It can readily be seen that the Bessel filters give a much flatter group-delay curve than the Butterworth filters of Fig. 3. This, of course, is because the design criterion of the Butterworths is maximally-flat _amplitude_ rather than maximally-flat _group delay_ as in the Bessel filters.

Table 4 lists the coefficients for Bessel filters or order n. Since the Bessel filters have maximally-linear phase characteristics, the first nonzero coefficient after c_1 is c_{2n+1}, c_1 is given by (Ref. 4)

$$c_1 = B T_d(\omega_c) \quad (21)$$

Table 3

TIME-BANDWIDTH PRODUCT FOR BESSEL FILTERS

| Order n	$B T_d(\omega_c)$
1	1.00
2	1.36
3	1.75
4	2.13
5	2.42
6	2.70
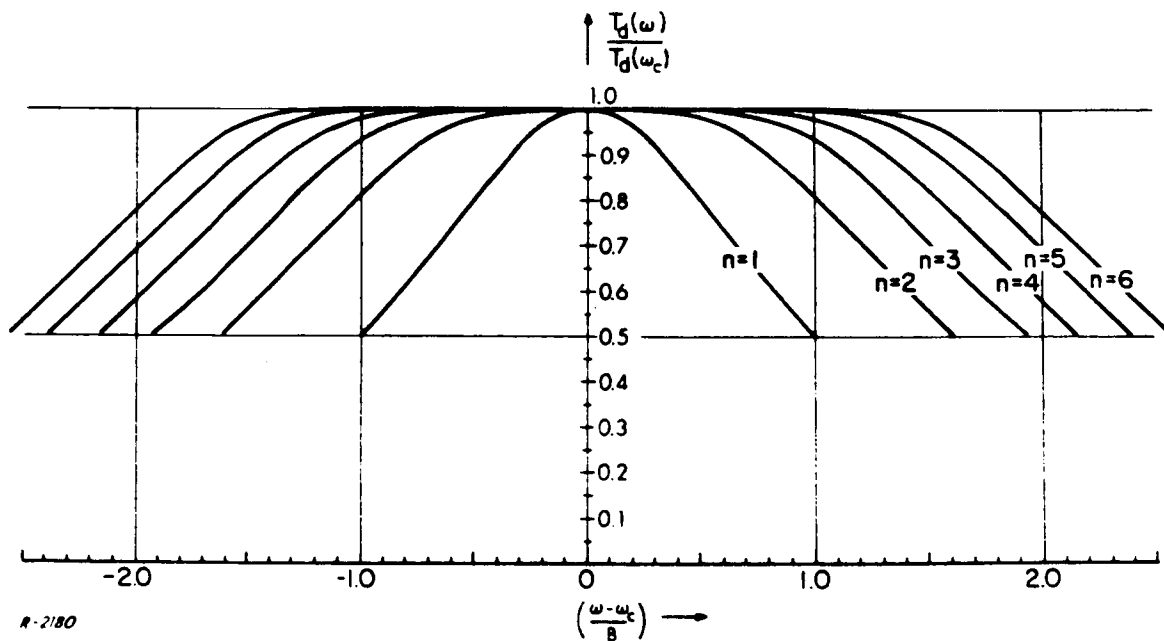
Fig. 4 Normalized Group Delay for Bessel Filters of Various Orders

82

Table 4

PHASE COEFFICIENTS OF BESSEL FILTERS

OF VARIOUS ORDERS

	n=1	n=2	n=3	n=4	n=5	n=6
c_1	1	1·36	1·75	2·13	2·42	2·72
c_3	-0.333	0	0	0	0	0
c_5	0.200	-0.103	0	0	0	0
c_7	-0.143	0.0455	-0.0319	0	0	0
c_9		0	0.0152	-9.05×10^{-3}	0	0
c_{11}			-0.00508	4.82×10^{-3}	-1.70×10^{-3}	0
c_{13}				-2.12×10^{-3}	9.34×10^{-4}	-2.88×10^{-4}
c_{15}					-4.17×10^{-4}	1.66×10^{-4}
c_{17}						-8.61×10^{-5}

The three succeeding nonzero coefficients are (see Ref. 4)

$$c_{2n+1} = - \frac{\left(B\,T_d(\omega_c)\right)^{2n+1}}{(2n+1)\,a_o^2} \tag{22}$$

$$c_{2n+3} = \frac{\left(B\,T_d(\omega_c)\right)^{2n+3}}{(2n+3)\,(2n-1)\,a_o^2} \tag{23}$$

$$c_{2n+5} = - \frac{2(n-2)\left(B\,T_d(\omega_c)\right)^{2n+5}}{(2n-1)^2\,(2n-3)\,(2n+5)\,a_o^2} \tag{24}$$

where the values of $BT_d(\omega_c)$ are listed in Table 3, and those for a_o are listed in Table 2. Formulas for higher-order c_i's have not been obtained because of the computational complexity involved.

The last filter type to be studied is the double-tuned circuit which (near resonance) has the transfer function (Ref. 5, p. 220)

$$H(\omega) = \frac{1}{1 - \frac{f^2(a)}{1+a^2}\left((\omega-\omega_c)/B\right)^2 + j\,\frac{2f(a)}{1+a^2}\left((\omega-\omega_c)/B\right)} \tag{25}$$

where

$$f(a) = \frac{2BQ}{\omega_c} = \sqrt{a^2 - 1 + \sqrt{2(1+a^4)}} \tag{26}$$

where Q is the "quality factor" of each tuned circuit. The parameter $\underline{a}$ is the coupling coefficient, such that

$a < 1$	corresponds to undercoupling,
$a = 1$	corresponds to critical coupling,
$a > 1$	corresponds to overcoupling.

The phase characteristic corresponding to Eq. (25) is

$$\Phi(\omega) = \tan^{-1} \frac{2f(a)(\omega-\omega_c)/B}{f^2(a)\left((\omega-\omega_c)/B\right)^2 - (1+a^2)} \quad \text{radians} \qquad (27)$$

from which we obtain the group delay

$$T_d(\omega) = \frac{2f(a)}{B} \frac{1+a^2 + f^2(a)(\omega-\omega_c/B)^2}{\left[f^2(a)(\omega-\omega_c/B)^2 - (1+a^2)\right]^2 + 4f^2(a)(\omega-\omega_c/B)^2} \text{secs.} (28)$$

This is plotted in normalized form in Fig. 5 for a range of coupling coefficients. Note that the group-delay characteristic appears to be flattest at a coupling coefficient of about 0.6.

Finally, Table 5 shows the coefficients for double-tuned circuits with various values of coupling coefficients. The general formulas for these coefficients have been computed from Eq. (27) to be

$$c_1 = \frac{2}{1+a^2} f(a) \qquad (29)$$

$$c_3 = \frac{2}{(1+a^2)^2} \left(f(a)\right)^3 \left[1 - \frac{4}{3(1+a^2)}\right] \qquad (30)$$

$$c_5 = \frac{2}{(1+a^2)^3} \left(f(a)\right)^5 \left[1 - \frac{4}{1+a^2} + \frac{16}{5(1+a^2)^2}\right] \qquad (31)$$

$$c_7 = \frac{2}{(1+a^2)^4} \left(f(a)\right)^7 \left[1 - \frac{8}{1+a^2} + \frac{16}{(1+a^2)^2} - \frac{64}{7(1+a^2)^3}\right] \qquad (32)$$

$$c_9 = \frac{2}{(1+a^2)^5} \left(f(a)\right)^9 \left[1 - \frac{40}{3(1+a^2)} + \frac{48}{(1+a^2)^2} - \frac{64}{(1+a^2)^3} + \frac{256}{9(1+a^2)^4}\right] \qquad (33)$$

$$c_{11} = \frac{2}{(1+a^2)^6} \left(f(a)\right)^{11} \left[1 - \frac{20}{1+a^2} + \frac{112}{(1+a^2)^2} - \frac{256}{(1+a^2)^3} + \frac{256}{(1+a^2)^4} - \frac{1024}{11(1+a^2)^5}\right]$$

$$(34)$$

where f(a) is given in Eq. (26).

85
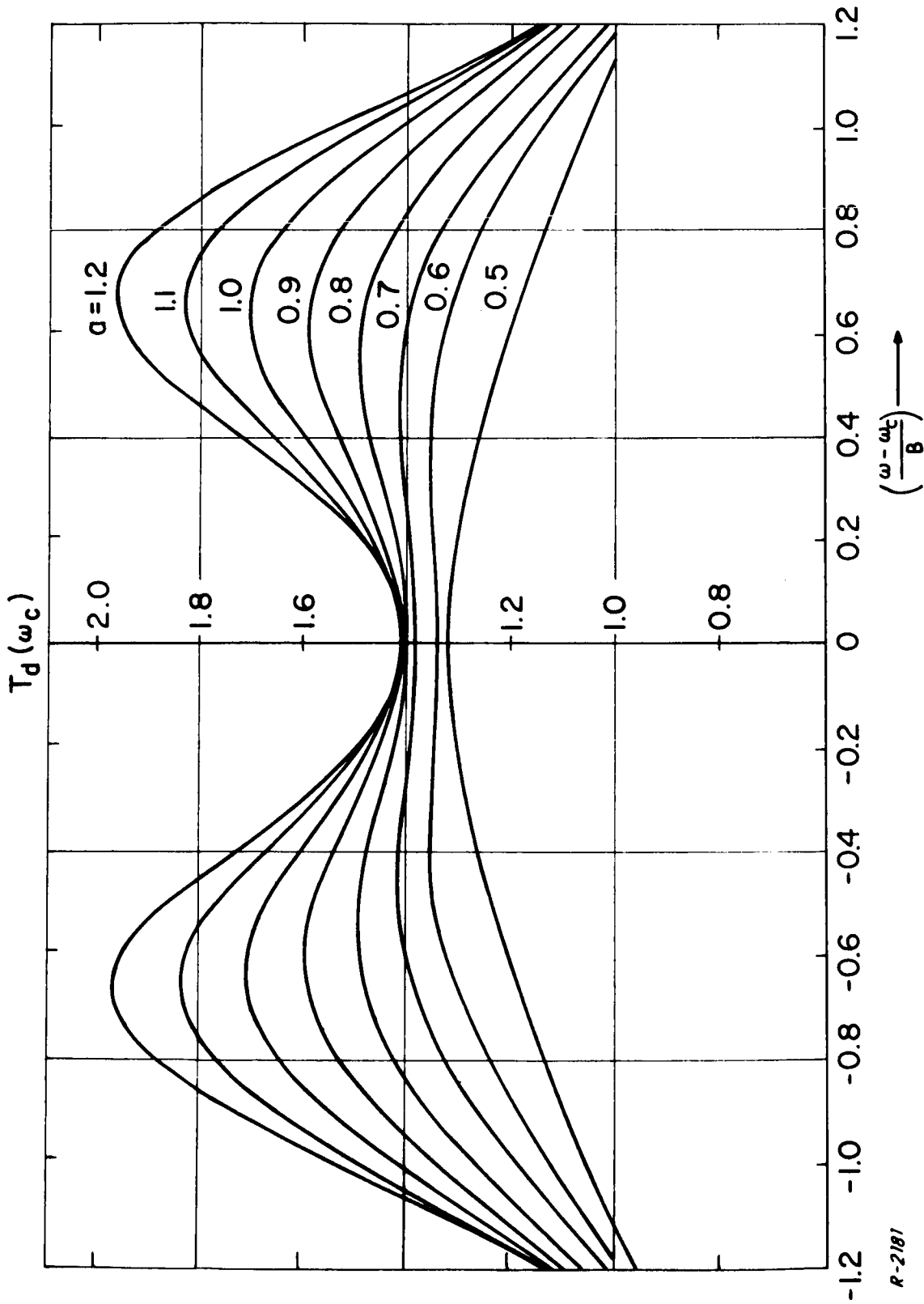
Fig. 5 Group Delay for Double-Tuned Circuits with Various Couplings

R-2181

Table 5

PHASE COEFFICIENTS OF DOUBLE-TUNED CIRCUITS

WITH VARIOUS COUPLING COEFFICIENTS

	a=0.5	a=0.6	a=0.7	a=0.8	a=0.9	a=1.0	a=1.1	a=1.2	a=1.3	a=1.4
c_1	1.346	1.366	1.385	1.401	1.411	1.414	1.411	1.401	1.384	1.363
c_3	-0.0508	-0.0170	0.104	0.211	0.335	0.471	0.615	0.760	0.900	1.031
c_5	-0.0656	-0.116	-0.172	-0.226	-0.267	-0.283	-0.264	-0.204	-0.103	0.036
c_7	0.039	0.0466	0.0373	-0.00144	-0.0803	-0.202	-0.358	-0.529	-0.689	-0.813
c_9	-0.00883	0.00433	0.0346	0.0816	0.132	0.157	0.119	-0.0152	-0.259	-0.602
c_{11}	-0.00301	-0.0141	-0.0260	-0.0297	0.021	0.129	0.296	0.477	0.588	0.540

5. ACCUMULATION OF DISTORTION IN CASCADED FILTER STAGES

When a receiver contains a single predetection filter it is a simple matter to look up the appropriate coefficients in one of the tables of Sec. 4 and insert them into Eq. (6). However, frequently two or more filters are used in cascade; in this case obtaining suitable phase coefficients is not so straight-forward. In this section we consider two approaches: the first is completely general and the second simplifies the calculation when the cascade consists of identical filters.

Consider a cascade of filters having phase characteristics Φ_1, Φ_2, etc. which are expressed as series

$$\Phi_1(\omega) = \sum_{i=1}^{\infty} c_{1,i} \left(\frac{\omega - \omega_c}{B_1} \right)^i$$

$$\Phi_2(\omega) = \sum_{i=1}^{\infty} c_{2,i} \left(\frac{\omega - \omega_c}{B_2} \right)^i$$

$$\vdots$$

(35)

where B_1, B_2, etc. are the half-bandwidths of the individual stages. The cascade will have a phase characteristic $\Phi(\omega)$ equal to the sum of the individual phases

$$\Phi(\omega) = \Phi_1(\omega) + \Phi_2(\omega) + \dots$$

(36)

We can express $\Phi(\omega)$ as a series

$$\Phi(\omega) = \sum_{i=1}^{\infty} c_i \left(\frac{\omega - \omega_c}{B} \right)^i$$

(37)

where B is the overall half-bandwidth of the cascade. Substitution of Eqs. (35) and (37) into (36) gives the coefficients of the cascade in terms of the coefficients of the stages

$$c_1 = c_{1,1}\left(\frac{B}{B_1}\right) + c_{2,1}\left(\frac{B}{B_2}\right) + \cdots$$

$$c_3 = c_{1,3}\left(\frac{B}{B_1}\right)^3 + c_{2,3}\left(\frac{B}{B_2}\right)^3 + \cdots$$

(38)

$$\vdots$$

Therefore <u>to compute the I/S ratio we may consider the cascade as a single filter of bandwidth B having the coefficients c_1, c_3, etc. (given by Eq. (38)) and substitute these values directly into Eq. (6).</u> Note that in order to compute the coefficients it is necessary to know the coefficients and bandwidths of each individual stage as well as the resulting overall bandwidth.

As might be expected, these calculations can be simplified considerably in the case where all stages are identical. If the result of Eq. (38) is simplified to the case of k filters with identical coefficients and equal bandwidths, substitution into Eq. (6) gives the result that <u>the overall I/S ratio is k^2 times the I/S ratio which would be calculated for an individual stage.</u> In other words, we make the calculation assuming one of the individual stages is present and then multiply by k^2. This result is easily verified by noting that the distortion waveforms produced by each stage are identical. These waveforms add in voltage so that the overall distortion waveform is k times that produced by one stage. Therefore the overall distortion power is k^2 times the individual distortion power.

Overall bandwidths of a cascade may be obtained by simple formulae in certain simple cases. In particular, if the cascade consists of k identical stages, each of which is an nth order Butterworth, it can be shown that the overall half-bandwidth is given by

$$B_k = \sqrt[2n]{\sqrt[k]{2} - 1} \; B \tag{39}$$

where B is the half-bandwidth of an individual stage.

Another situation where the bandwidth of a cascade may be found from an explicit equation is the case of k double-tuned stages, each having coupling coefficient $\underline{a}$. We have computed the overall half-bandwidth to be

$$B_k = \frac{\omega_c}{2Q} \sqrt{a^2 - 1 + \sqrt{2^{1/k}(1+a^2)^2 - 4a^2}} \tag{40}$$

Equation (40) is plotted in Fig. 6. The overall half-bandwidth of a single stage is given in terms of the resonant angular frequency ω_c and "quality factor" Q by

$$B = \frac{\omega_c}{2Q} \sqrt{a^2 - 1 + \sqrt{2(1+a)^4}} \tag{41}$$

Equation (41) is, of course, simply a special case of Eq. (40).

Finally we consider the case of a cascade of k Bessel filters of order n. It is well-known that for n sufficiently large the amplitude of a Bessel filter approaches the gaussian shape. In this limit it is easy to show that the bandwidth of a cascade is $1/\sqrt{k}$ times the bandwidth of an individual stage. This result is adequate $n \geq 4$; the exact results for lower values of n have been calculated and are shown in Table 6.
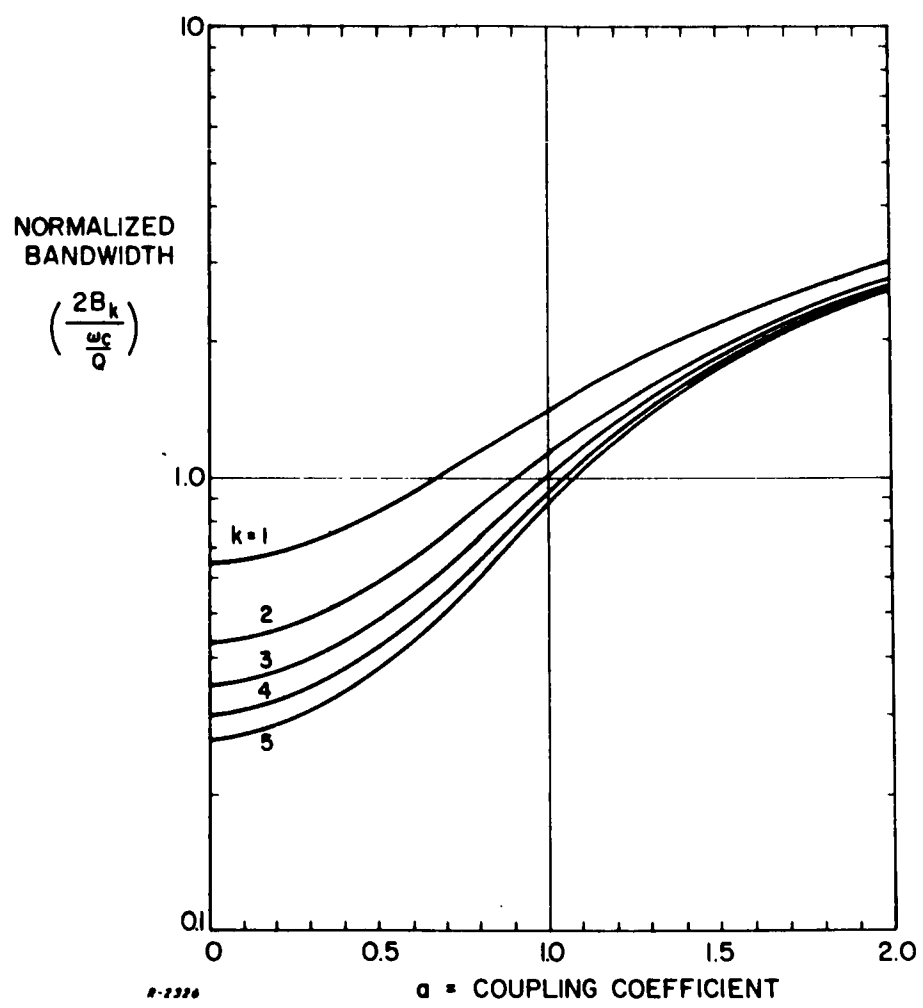
Fig. 6 Bandwidth of k Identical Cascaded Double-Tuned
Circuits as a Function of Coupling Coefficient.

Table 6

BANDWIDTH OF A CASCADE OF k n^{th}-ORDER BESSEL FILTERS

Order of Filter	B_k/B					
	k = Number of Filters Cascaded					
n	k=1	k=2	k=3	k=4	k=5	k=6
1	1	0.643	0.510	0.435	0.384	0.350
2	1	0.71	0.59	0.51	0.47	0.42
3	1	0.74	0.60	0.52	0.48	0.43
4	1	0.72	0.59	0.51	0.46	0.42
limit as $n \rightarrow \infty$	1	0.707	0.577	0.500	0.447	0.408

6. EXPERIMENTAL VERIFICATION OF THE QUASI-STATIONARY RESULTS

Extensive laboratory measurements have been conducted by ADCOM in order to establish the validity of the quasi-stationary results presented in the previous sections. Here we present some selected measurements which demonstrate the agreement between theory and experiment. All measurements presented have been corrected to remove the contributions to the intermodulation distortion caused by modem nonlinearities. (These contributions are considered analytically in Secs. 9 and 10 below.)

The measurements presented here were obtained using second-order Butterworth filters. The second-order Butterworth design is identical with a critically-coupled double-tuned circuit. Theoretical predictions were made using the coefficients from Table 1. Other experimental measurements not cited here have been obtained with many other filter types, including higher-order Butterworth and Bessel designs found in commercial telemetry receivers. The input video spectrum in these tests was rectangular; the shape of the corresponding theoretical I/S curves is shown in Fig. 2.

In the first test we present, the deviation ω_e was held constant and the maximum video frequency $\hat{\omega}$ was adjusted to 40, 85, and 200 kHz. In each case the I/S ratio was measured at various notch locations to determine the I/S spectrum. The experimental points are shown in Fig. 7; the analytical predictions are also plotted for the three values of $\hat{\omega}$. Comparison shows good agreement even for the largest value of $\hat{\omega}$, thus verifying the results of Secs. 2 through 4. The largest value of $\hat{\omega}$ selected represents a normalized maximum video frequency $\hat{\omega}/B$ of approximately unity. It is at such high values of $\hat{\omega}$ that we might expect the quasi-stationary solution to break down and non-quasi-stationary effects to appear. However, this does not appear to be the case for $\hat{\omega}/B$ up to unity, indicating that the quasi-stationary approximation yields satisfactory results under typical telemetry conditions.
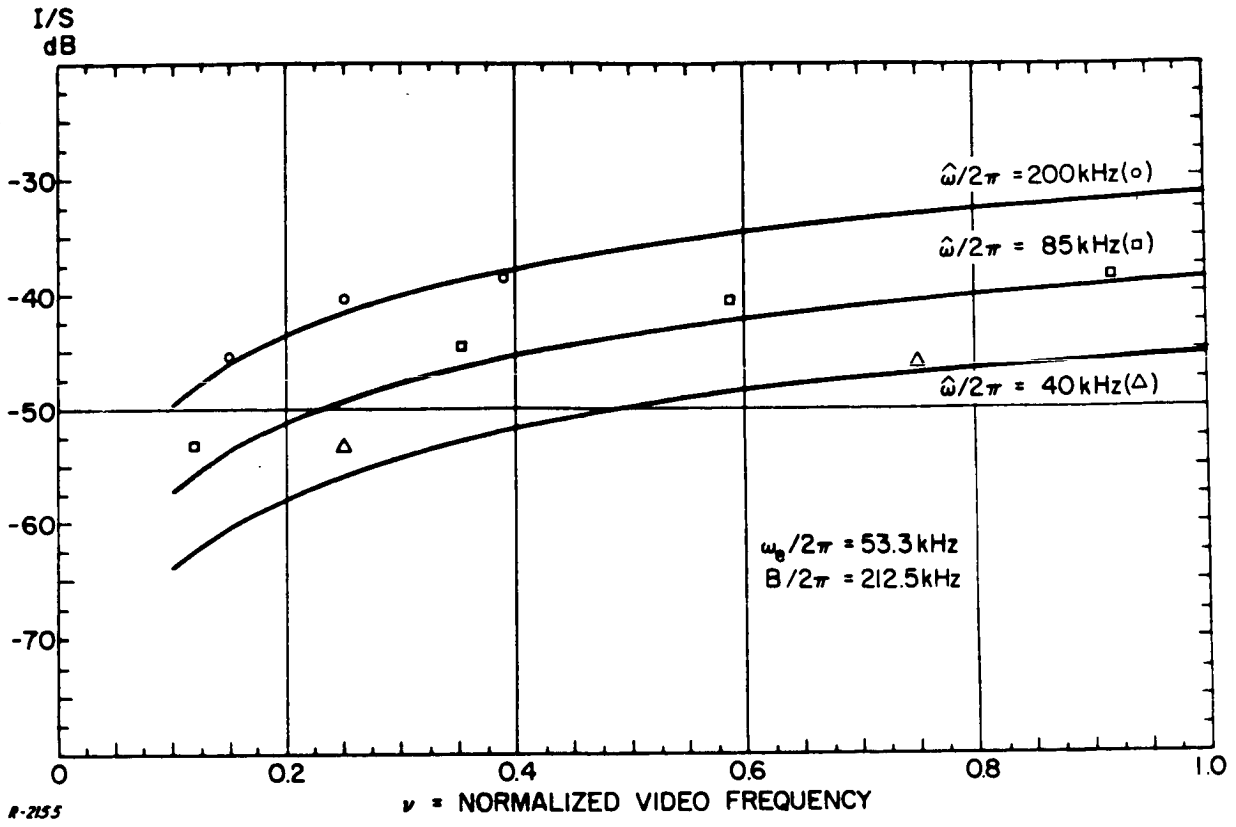
Fig. 7 Measured and Predicted Distortion-to-Signal Ratios
for Different Maximum Video Frequencies, Second-
Order Butterworth Filters.
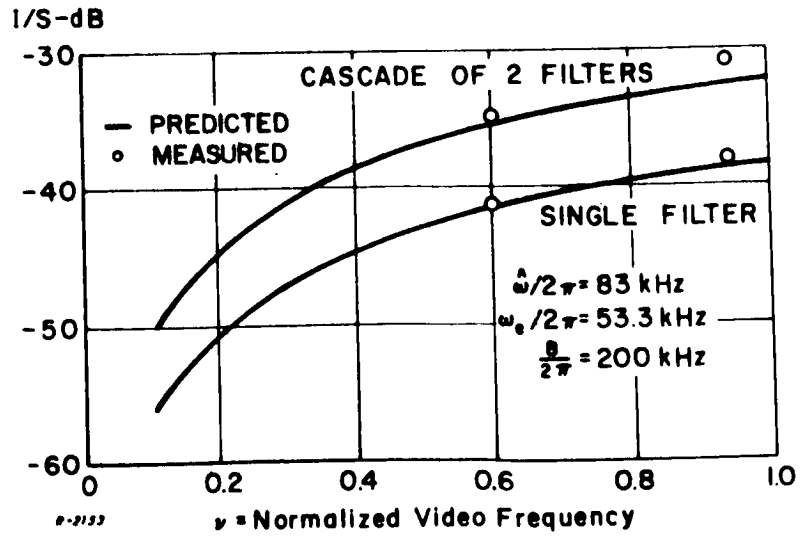
Fig. 8 Distortion-to-Signal Ratio of a Cascade

96

The second test to be cited here investigates the effect of cascading of identical filters. For fixed maximum video frequency and deviation, I/S measurements were made with two identical filters, separately and in cascade. The results (taken with two different notch locations) are plotted in Fig. 8 together with the analytical predictions. The analytical curves are separated by 6 dB since $k^2 = 4$. Agreement with theory is once again excellent, verifying the results of Sec. 5.

7. PERFORMANCE TRADEOFFS FOR PREDETECTION FILTERS

In Sections 2 through 6 we have concentrated on intermodulation distortion in predetection filters. We have developed analytic tools for predicting this distortion, thereby making it possible for the designer to control distortion levels. However, distortion is only one of the measures of performance of a predetection filter; a good design must perform other functions as well as minimizing intermodulation distortion. This brings us to the subject of this section: what are the tradeoffs involved between distortion level on the one hand and other filter performance requirements on the other? To answer this question we will first discuss the various functions of predetection filters and suitable quantitative performance measures for these functions. Then we will present the values of these performance measures for the various filter types catalogued earlier, so that comparisons may be drawn between them.

The primary functions of predetection filters are:

a) to reduce the total additive noise power appearing at the demodulator input,

b) to reject interfering signals from adjacent telemetry bands, and

c) to reject undesired mixer and converter products.

The filters must perform these functions at a minimum cost in data degradation. The functions listed as a) - c) above are best achieved by narrowing the bandwidth and sharpening the skirts of the filter, without causing undue degradation of the telemetry data. Thus, the amplitude characteristic of the filter determines the performance in terms of these functions. On the other hand, we have shown that intermodulation distortion is determined primarily by the degree of nonlinearity of the phase characteristic.

Now, it is well-known that the amplitude characteristic and the group-delay (or phase) characteristic of a filter are intimately related. It follows that fundamental tradeoffs exist between the various filter performance criteria, and that these tradeoffs are determined by the type of filter in question.

The performance measure suitable for characterizing the ability of the filter to reduce additive noise is its noise bandwidth B_n, defined by

$$B_n = \frac{\int_0^\infty |H(\omega)|^2 \, d\omega}{|H(\omega_c)|^2} \quad \text{rad/sec} \tag{42}$$

where $H(\omega)$ is the transfer function of the predetection filter. Any two filters with equal noise bandwidths will have equal mean-square voltages due to additive noise at their outputs, regardless of their exact amplitude characteristics. This makes possible a direct comparison of different filter designs with respect to function a), once appropriate noise bandwidths have been calculated.

The only completely general performance measure for functions b) and c) is the amplitude characteristic of the filter. Knowing this, two filters can be compared by checking to see which has greater attenuation in the frequency region where unwanted signals are likely to fall. If the application is known in detail, so that the location of adjacent channels is fixed, a suitable performance measure would simply be the attenuation at the near edge of the adjacent channel. However, this degree of information is not always available to the designer.

In the absence of complete knowledge as to the frequency location of undesired signals, the performance measure frequently used is the 3 dB bandwidth in conjunction with the shape factor, defined as the ratio of the frequency at the 60 dB attenuation to the frequency at 6 dB attenuation on the skirts of the amplitude characteristic. In the present context, we regard the shape factor as a potentially misleading measure of performance. To illustrate this point, consider a Butterworth filter and a Bessel filter of the same order designed to have

the same intermodulation distortion. With this requirement the Bessel filter will have a considerably smaller 6 dB bandwidth than the Butterworth. Then if we require the two filters to have equal shape factors, this will have the effect of requiring the Bessel filter to have greater skirt attenuation than the Butterworth. This is certainly not the desired objective. Therefore, the shape factor must be used with great care. It is far more meaningful for the designer to work with the attenuation at the frequency of a known undesired signal.

We present here the attainable performance measures computed for three types of predetection filters: Butterworth filters of various orders, Bessel filters of various orders and double-tuned circuits with various coupling coefficients. The results are tabulated in Tables 7, 8 and 9.

The performance measures computed are:

a)   the noise bandwidth B_n, as defined by Eq. (42), and normalized to the 3 dB <u>half</u>-bandwidth B, in rad/sec,

b)   the shape factor, as defined above, and

c)   a factor representing the effect of the filter in determining the I/S ratio in FDM telemetry (see Eq. (9)).

The factor in c) above is presented in dB to facilitate combining it with the other two factors to determine the I/S ratio, as explained in detail in Section 2. Notice that this distortion factor is a function of the ratio of the rms frequency deviation ω_e to the filter half-bandwidth B, so a set of values for a range of ω_e/B is given in each case. As ω_e/B increases, more and more terms in the infinite sum of Eq. (9) are needed to obtain an accurate estimate of the factor in question. The computation of the power-series coefficients $\{c_i\}$ is a mathematically simple but increasingly tedious operation, so we had to content ourselves with those already presented in Tables 1, 4 and 5. This accounts for the convergence inaccuracies indicated in Tables 7-9 by asterisks.

Table 7

PERFORMANCE TRADEOFFS FOR BUTTERWORTH FILTERS

Order n	Shape Factor	B_n/B	Distortion Factor, dB $10\log_{10}\left[c_3+10\,c_5\left(\frac{\omega_e}{B}\right)^2+\ldots\right]^2$			
			$(\omega_e/B)=$ 0.1	$(\omega_e/B)=$ 0.2	$(\omega_e/B)=$ 0.3	$(\omega_e/B)=$ 0.4
1	579	3.14	-10.1	-11.3	-11.2*	**
2	24.0	2.22	-7.1	-9.3	**	**
3	8.34	2.09	-8.6	-7.4	**	**
4	4.91	2.05	-8.3	-6.3	**	**
5	3.57	2.03	-7.2	-5.4	**	**
6	2.89	2.02	-6.1	-3.6	**	**

Table 8

PERFORMANCE TRADEOFFS FOR BESSEL FILTERS

Order n	Shape Factor	B_n/B	Distortion Factor, dB $10\log_{10}\left[c_3+10\,c_5\left(\frac{\omega_e}{B}\right)^2+\ldots\right]^2$			
			$(\omega_e/B)=$ 0.1	$(\omega_e/B)=$ 0.2	$(\omega_e/B)=$ 0.3	$(\omega_e/B)=$ 0.4
1	579	3.14	-10.1	-11.3	-11.2*	**
2	29.4	2.31	-40.1	-29.5	-25.4*	-27.4*
3	10.2	2.15	-70.0	-47.2	-35.5	-23.7*
4	6.23	2.08	-99.5	-64.8	-44.1*	**
5	4.71	2.08	-131.3	-84.8	-56.5*	**
6	3.93	2.08	-163.0	-104.4	-67.5*	**

* Inaccurate due to limited number of terms available.
** Not accurate enough to cite.

Table 9

PERFORMANCE TRADEOFFS FOR
DOUBLE-TUNED CIRCUITS

			Distortion Factor, dB $$10 \log_{10} \left[c_3 + 10 \, c_5 \left(\frac{\omega_e}{B} \right)^2 + \ldots \right]^2$$			
Coupling Coeff. $\underline{a}$	Shape Factor	B_n/B	$(\omega_e/B) =$ 0.1	$(\omega_e/B) =$ 0.2	$(\omega_e/B) =$ 0.3	$(\omega_e/B) =$ 0.4
0.5	28.6	2.33	-24.9	-22.9	-21.1	-17.6*
0.6	27.6	2.30	-44.6	-33.2	-24.5*	-14.9*
0.7	26.5	2.27	-21.2	-27.3	-35.5*	**
0.8	25.6	2.25	-14.5	-18.0	-25.2*	**
0.9	24.8	2.23	-10.3	-12.9	-15.3*	**
1.0	24.1	2.22	-7.1	-9.3	**	**
1.1	23.4	2.23	-4.7	-6.5	**	**
1.2	22.9	2.25	-2.7	-4.3	-3.6*	**
1.3	22.3	2.27	-1.1	-2.5	**	**
1.4	21.9	2.30	0.2	-1.1	**	**

* Inaccurate due to limited number of terms available.
** Not accurate enough to cite.

Fortunately, most telemetry situations employ values of (ω_e / B) not in excess of 0.3, where the tabulated results are generally satisfactory. On the other hand, this factor could be more accurately computed using the Hermite-polynomials technique presented in Section 4.3 of Ref. 1 (see Errata in this report). The factor would then be given by $10 \log_{10} h_3^2$, and h_3 could be computed from Eq. (81) of Ref. 1 using a digital computer. No convergence problems would arise in this case. In fact, we recommend that this alternate procedure be employed in the study of more advanced filter designs.

8. SPECIFICATIONS FOR PREDETECTION FILTERS

The performance tradeoffs presented in the previous section can be used to formulate meaningful and effective specifications for predetection filters. In this section we describe how such specifications may be drawn; but first we must discuss the general nature of specifications in order to motivate the recommended specification procedures.

In general, specifications must be:

a) <u>Self-consistent,</u> so that satisfying one specified criterion does not automatically prevent the satisfaction of another.

b) <u>Attainable,</u> either directly by known techniques, or -- if the specification is stringent enough that it has not been previously attained -- then there must be good reason to believe that it can be attained by some advanced technique.

c) <u>Verifiable,</u> directly or indirectly by standardizable tests.

We shall attempt to satisfy the above requirements in our proposed specification methods. Next, we need to divide specification methods into two types:

a) <u>Performance Specifications</u>

The desired performance characteristics, -- e. g., low intermodulation distortion by the predetection filter -- are specified directly in terms of suitable measures of performance. No attempts are made to indicate the detailed nature of the filters; that is left to the development or design engineer who then has the flexibility to choose whatever design suits him and meets the specification.

b) <u>Design Specifications</u>

The specifier first determines the desired performance characteristics, then determines the corresponding design characteristics -- e. g., phase linearity -- that will ensure the desired performance. This type of specification generally requires accurate analytical or empirical relationships between the performance characteristics and the design characteristics.

This may not be readily available, in general, although the results of this report supply the necessary relationships for the particular problem of phase nonlinearities.

It is frequently necessary in making design specifications to treat a system in its component parts rather than as a whole. This can lead to over-design, especially where the deficiency in the design of one subsystem can be easily compensated in the design of another. Thus, design specifications are generally less desirable than performance specifications because they depend for their effectiveness on the accuracy of the available relationships between performance and design, and because they can lead to overdesign. From the viewpoint of the specifier, they require a greater effort to achieve the same end; whereas from the viewpoint of the design engineer they can restrict flexibility and resourcefulness.

Whatever the merits of the two types of specifications, it is imperative that no system should be specified both in design and in performance, because this can only lead to confusion and waste. A set of specifications should therefore contain no redundancies, whether explicit or implicit.

The general problem of specifications is fundamentally one of establishing quantitative tradeoffs between all the pertinent parameters, such as those presented in Section 7 above. These tradeoffs indicate to the specifier the attainable and self-consistent performance measures which he may select. In the present context of predetection filters we strongly recommend performance specifications, instead of such design specifications as "percent of deviation from phase linearity" or "tolerance on group-delay flatness."

Tables 7, 8 and 9 can be used directly to specify filter performance. Start by determining the requirements placed on the filter by the receiving system. These requirements are usually given in terms of 3 dB bandwidth, and skirt selectivity. Compute the corresponding shape factor. Next, determine the rms frequency deviation ω_e, and the video bandwidth $\hat{\omega}$. Compute the factor given by Eq. (8), and read the second factor representing the effect

of the spectrum-shape from Fig. 2. It will usually be sufficient to consider the I/S ratio at bandedge, so use -3 dB for the second factor. Add these two factors (in dB) to the distortion factors under the appropriate (ω_e/B) in the tables. It should be possible to achieve an I/S ratio at least as good as -50 dB. Now, check in the tables to see that the desired shape factor can be achieved by the filter types capable of better than -50 dB in I/S ratio. Also, check that the resulting noise bandwidth is acceptable. If all these performance criteria are met by one or more filter types listed in the tables, then specify the corresponding numbers for: shape factor, 3 dB bandwidth, noise bandwidth, and I/S ratio. Add some margins to these numbers to allow for slight misalignments and other manufacturing imperfections.

If none of the filter types listed achieves all the performance requirements, then consider either a cascade of identical stages or a more advanced filter design such as those discussed in Section 11 below. In considering cascaded stages, use Eqs. (39) and (40) and Table 6 to compute the 3 dB bandwidth of each stage, then repeat the procedure described above. Use the fact that a cascade of k stages increase the I/S ratio by a factor of k^2 over that of one stage.

The above procedure will ensure that the performance specifications are both self-consistent and attainable. The measurement techniques presented in Section 4.1 of Ref. 1 can be used for acceptance testing and for experimental evaluation of designs. This ensures that the specifications are verifiable by standardizable tests.

In closing this section, a word of caution about a particular type of design specification is in order. It is customary to specify the inband amplitude ripple of various components in a telemetry system. These specifications are frequently quite stringent, e.g., ±0.5 dB over most of the 3 dB bandwidth. Yet, we have been unable to find any direct dependence of data degradation on inband ripple. In fact, Bessel filters are known to have rather large variations

of inband gain, and yet they can achieve very low I/S ratios because of their maximally-flat group-delay characteristics. We must conclude, therefore, that inband ripple specifications are superfluous unless amplitude-modulated signals are used. They may even be damaging if not accompanied by a consistent specification on group-delay variations. That is because in attempting to satisfy a stringent specification on inband ripple, the designer may have to sacrifice group-delay linearity and thus incur greater intermodulation distortion.

9. DISTORTION DUE TO MODULATOR-DEMODULATOR NONLINEARITIES

In this section we consider the intermodulation distortion of a non-ideal modulator-demodulator pair (called modem). The approach used is the same as that used in Ref. 1 in the quasi-stationary case. In this section we proceed under the assumption that no predetection filter is present. In the next section we consider the relationship between modem distortion and predetection filter distortion.

The modem configuration is shown in Fig. 9 where the input "frequency" is $v(t)$, the actual transmitted frequency (a replica of $v(t)$) is $\phi(t)$, and the output "frequency" (a replica of $\phi'(t)$) is $w(t)$. It is reasonable to assume that both the VCO and the discriminator operate without memory, so that we may write the output of each as a power series in the input

$$\phi(t) = e_1 v(t) + e_2 v^2(t) + e_3 v^3(t) + \ldots \tag{43}$$

and

$$w(t) = f_1 \phi(t) + f_2 \phi^2(t) + f_3 \phi^3(t) + \ldots \tag{44}$$

These two series represent the static characteristics of the VCO and discriminator respectively. By combining (43) and (44) we may write a series for the overall characteristic of the modem

$$w(t) = g_1 v(t) + g_2 v^2(t) + g_3 v^3(t) + \ldots \tag{45}$$

where the coefficients g_i can be written in terms of the e's and f's

$$g_1 = e_1 f_1 \tag{46}$$

$$g_2 = e_2 f_1 + e_1^2 f_2 \tag{47}$$

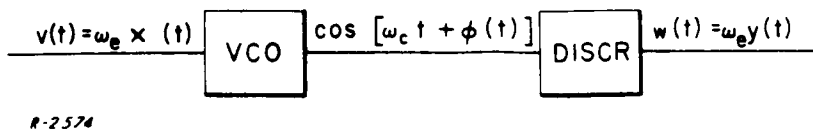$$g_3 = e_3 f_1 + 2 e_1 e_2 f_2 + e_1^3 f_3 \tag{48}$$

etc.

R-2574

Fig. 9 Modem Configuration

If the VCO or discriminator is ideal, the g_i are equal to the f's or the e's respectively. In practice, the w(t) vs v(t) characteristic can be measured to obtain the g's, or the individual characteristics can be measured to obtain the e's and f's which can then be used to calculate the g's.

From Eq. (45) we may write the transfer relation in terms of unity-mean-square variables x(t) and y(t) as

$$y(t) = \frac{1}{\omega_e} \sum_{i=1}^{\infty} g_i [\omega_e x(t)]^i \tag{49}$$

Proceeding exactly as in Sec. 4. 2 of Ref. 1, we find the autocorrelation of the output is given by

$$R_y(\tau) = \frac{1}{\omega_e^2} \sum_{n=0}^{\infty} n! \, R_x^n(\tau) \left[\sum_{j=0}^{\infty} \frac{(n+2j)!}{2^j j! \, n!} g_{n+2j} \omega_e^{n+2j} \right]^2 \tag{50}$$

As before this may be transformed to give the distortion spectrum

$$I_y(\nu) = \frac{1}{\omega_e^2} \sum_{n=2}^{\infty} n! \, S_x^{(n)}(\nu) \left[\sum_{j=0}^{\infty} \frac{(n+2j)!}{2^j j! \, n!} g_{n+2j} \omega_e^{n+2j} \right]^2 \tag{51}$$

We leave the result in this form rather than attempting to single out the dominant terms because it is not clear which terms will dominate in all cases.

10. CORRELATION BETWEEN MODEM DISTORTION AND PREDETECTION-FILTER DISTORTION

In laboratory measurements we have observed a "noise floor" consisting primarily of intermodulation distortion caused by nonlinearities in the modulator and demodulator. When making measurements of the intermodulation distortion caused by a predetection filter, correction must be made to remove the effect of the distortion due to the modem. In making this correction, one faces the question of whether or not distortion waveforms from the two sources are correlated. If these waveforms were exactly correlated, voltage addition would take place. If, as we shall show in this section, the waveforms are completely uncorrelated, power addition occurs.

The system configuration is shown in Fig. 10. If the filter is ideal (no distortion), Eq. (45) holds

$$w(t) = \sum_{n=1}^{\infty} g_n v^n(t) = v(t) + \sum_{n=2}^{\infty} g_n v^n(t) \tag{52}$$

On the other hand, if the modem is ideal and if the quasi-stationary condition holds for the filter, we have

$$\theta(t) = \phi(t) + \sum_{m=1}^{\infty} \frac{c_m}{B^m} \dot{\phi}^m(t) \tag{53}$$

$v(t)$ → VCO → $\cos\left[\omega_c t + \phi(t)\right]$ → FILTER → $\cos\left[\omega_c t + \theta(t)\right]$ → DISCR → $w(t)$
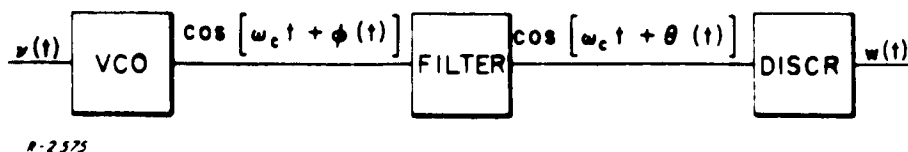
R-2575

Fig. 10 Modem and Predetection Filter.

111

This is simply the transfer relation obtained by combining Eqs. (2) and (3). Differentiating with respect to time yields

$$\dot{\theta}(t) = \dot{\phi}(t) + \sum_{m=1}^{\infty} \frac{mc_m}{B^m} \dot{\phi}^{m-1}(t) \ddot{\phi}(t) \tag{54}$$

Recognizing that $\dot{\phi}(t) = v(t)$ and $\dot{\theta}(t) = w(t)$ (we are assuming ideal VCO and discriminator) we can write this as

$$w(t) = v(t) + \dot{v}(t) \sum_{m=1}^{\infty} \frac{mc_m}{B^m} v^{m-1}(t) \tag{55}$$

Equations (52) and (55) represent the distortion in the two cases of ideal filter and ideal modem.

When neither the modem nor the filter is ideal, and when the distortion is low, it is readily shown that the total distortion is given by the sum of the distortions in (52) and (55). That is,

$$w(t) = v(t) + \sum_{n=2}^{\infty} g_n v^n(t) + \dot{v}(t) \sum_{m=1}^{\infty} \frac{mc_m}{B^m} v^{m-1}(t) \tag{56}$$

This ignores "second-order" distortions such as, for example, the distortion arising in the discriminator and acting upon the distortion waveform produced by the filter. However, in the ordinary situation where "first-order" distortions are at least 20 dB below the signal level, "second-order" distortions will be at least 40 dB below signal level and can be neglected.

If we define new variables $r(t)$ and $s(t)$ for the distortion waveforms

$$r(t) = \sum_{n=2}^{\infty} g_n v^n(t) \tag{57}$$

$$s(t) = \dot{v}(t) \sum_{m=1}^{\infty} \frac{mc_m}{B^m} v^{m-1}(t) \tag{58}$$

112

then the total distortion is $r(t) + s(t)$. To investigate the correlation between the components, we must form the autocorrelation of the total distortion, given by

$$\overline{[r(t)+s(t)][r(t+\tau)+s(t+\tau)]} = \overline{r(t)\,r(t+\tau)} + \overline{r(t)\,s(t+\tau)}$$
$$+ \overline{s(t)\,r(t+\tau)} + \overline{s(t)\,s(t+\tau)} \qquad (59)$$

We first observe that the first and last terms are the autocorrelations of the modem distortion alone and the filter distortion alone. When transformed, they give the distortion spectra calculated in (51) and (1), respectively. Therefore, to show that the two distortions are uncorrelated (and hence their powers add) we must show that the sum of the second and third terms of Eq. (59) is zero. These terms are given by

$$\overline{r(t)\,s(t+\tau)} = \sum_m \sum_n \frac{mc_m g_n}{B^m} \overline{\dot{v}(t+\tau)\,v^{m-1}(t+\tau)\,v^n(t)} \qquad (60)$$

$$\overline{s(t)\,r(t+\tau)} = \sum_m \sum_n \frac{mc_m g_n}{B^m} \overline{\dot{v}(t)\,v^{m-1}(t)\,v^n(t+\tau)} \qquad (61)$$

We will establish that their sum is zero by showing that, for any m and n,

$$\overline{\dot{v}(t+\tau)\,v^{m-1}(t+\tau)\,v^n(t)} = -\overline{\dot{v}(t)\,v^{m-1}(t)\,v^n(t+\tau)} \qquad (62)$$

First recall that for $x_1, x_2, \ldots, x_k$ zero-mean gaussian random variables

$$\overline{x_1, x_2, \ldots, x_k} = \begin{cases} \sum \prod \overline{x_i x_j} & k \text{ even} \\ 0 & k \text{ odd} \end{cases} \qquad (63)$$

where the $\sum \prod$ denotes the sum over all distinguishable products of pairs of x's. For example

$$\overline{x_1 x_2 x_3 x_4} = \overline{x_1 x_2} \cdot \overline{x_3 x_4} + \overline{x_1 x_3} \cdot \overline{x_2 x_4} + \overline{x_1 x_4} \cdot \overline{x_2 x_3} \qquad (64)$$

113

The number of terms will in general be

$$N = k! / (\tfrac{k}{2})! \, 2^{k/2} \tag{65}$$

Note that each x_i appears once in every term.

Applying the above result to Eq. (62) we can write (with the noise-loading technique $v(t)$ and $\dot{v}(t)$ are gaussian random processes) the left-hand side as

$$\overline{\dot{v}(t+\tau) \, v^{m-1}(t+\tau) \, v^{n}(t+\tau)} = \sum_{j=1}^{N} \left\{ \begin{array}{c} \overline{\dot{v}(t+\tau) \, v(t+\tau)} \\ \text{or} \\ \overline{v(t+\tau) \, v(t)} \end{array} \right\} \alpha_{j}(\tau) \tag{66}$$

On the other hand, if we apply (63) to the expectation on the right-hand side of Eq. (61) we find

$$\overline{\dot{v}(t) \, v^{m-1}(t) \, v^{n}(t+\tau)} = \sum_{j=1}^{N} \left\{ \begin{array}{c} \overline{\dot{v}(t) \, v(t)} \\ \text{or} \\ \overline{v(t) \, v(t+\tau)} \end{array} \right\} \beta_{j}(\tau) \tag{67}$$

In both cases the number of terms N is

$$N = \frac{(m+n)!}{\left(\dfrac{m+n}{2}\right)! \; 2^{\frac{m+n}{2}}} \tag{68}$$

If we number terms the same way in Eqs. (66) and (67) we can see that

$$\alpha_{j}(\tau) = \beta_{j}(-\tau) \tag{69}$$

because the left-hand sides of the equations are the same expectation with t and $(t + \tau)$ interchanged. Furthermore, $\alpha_{j}(\tau)$ and $\beta_{j}(\tau)$ are both of the form

$$\overline{v(t) \, v(t)}^{u} \cdot \overline{v(t+\tau) \, v(t)}^{v} \cdot \overline{v(t) \, v(t+\tau)}^{w}, \quad 2(u+v+w) = m+n-2 \tag{70}$$

The derivative of $v(t)$ does not appear because we have factored it out in Eqs. (66) and (67). This form is an even function of τ, so we have

114

$$\alpha_j(\tau) = \alpha_j(-\tau) \tag{71}$$

and

$$\beta_j(\tau) = \beta_j(-\tau) \tag{72}$$

Combining this with Eq. (69) we have

$$\alpha_j(\tau) = \beta_j(\tau) \tag{73}$$

Now we recall another result from the theory of gaussian processes, namely

$$\overline{v(t)\,\dot{v}(t+\tau)} = \frac{d}{d\tau}\,\overline{v(t)\,v(t+\tau)} \tag{74}$$

Since $\overline{v(t)\,v(t+\tau)}$ is an even function of τ this implies that $\overline{v(t)\,\dot{v}(t+\tau)}$ is an odd function of τ; that is

$$\overline{v(t)\,\dot{v}(t+\tau)} = \overline{-v(t+\tau)\,\dot{v}(t)} \tag{75}$$

Combining Eqs. (75) and (73) we see that each term on the right-hand side of Eq. (66) is the negative of the corresponding term on the right-hand side of Eq. (67). Therefore Eq. (62) is proven, and we have established that modem distortion and filter distortion are uncorrelated.

To understand the application of this result, let us consider a typical laboratory situation. An I/S measurement P_T of a predetection filter is made. Then the filter is removed and the measurement repeated, giving a reading P_1 due to the modem alone. Both readings P_T and P_1 are in dB's. Now it is desired to calculate the I/S due to the filter alone, call it P_2. Now we know from the above that

$$P_2 = P_T - P_1 \tag{76}$$

To save many conversions from dB's to numerical values and vice-versa, the nomograph of Fig. 11 may be used. The difference between P_T and P_1 in dB's is used to enter the nomograph on the vertical axis. Then the difference between P_1 and the desired value P_2 can be read in dB's on the horizontal axis.
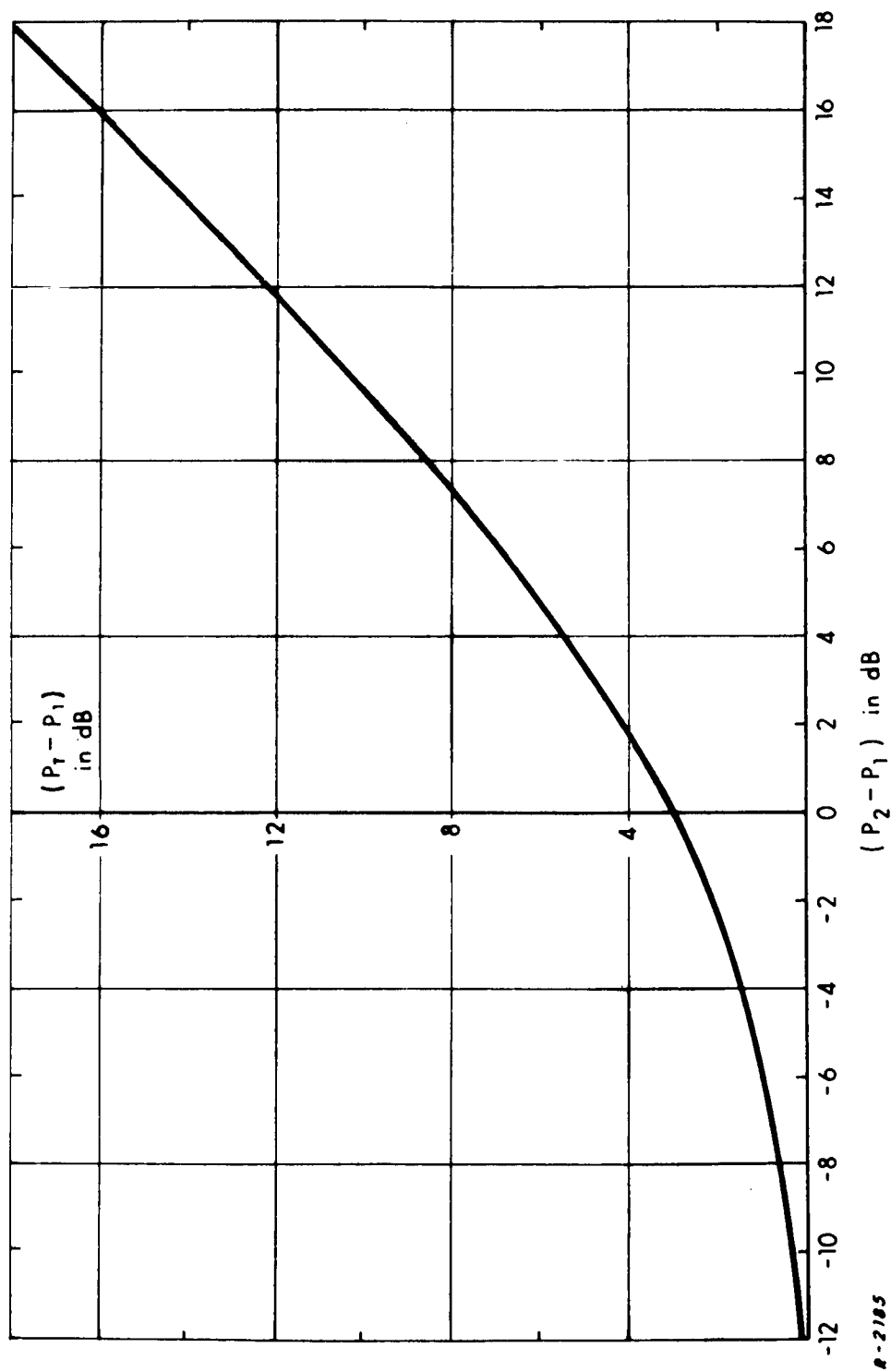
Fig. 11   Nomograph for Accumulation of Distortion.

11. CONCLUSIONS AND RECOMMENDATIONS

We have studied the application of the results obtained earlier in Part I to the overall design and specification of low distortion receivers. We have found that distortion calculations made with these results agree with measurements obtained in the laboratory. Further, we have applied the results to a whole catalog of common filter types and presented the results (Tables 7, 8 and 9), together with other measures of filter performance, in a manner useful to the filter designer unfamiliar with the theory.

The overall results of the study can be utilized in a variety of ways. They can clarify the cause/effect relationships so as to improve the insight of the design engineer. They supply the tools for systematic analytical design to reduce intermodulation distortion. They introduce new experimental techniques for system alignment and for the evaluation of system performance in terms of data quality. And finally, they lead to systematic techniques for system specification and acceptance testing.

Consequently, our primary recommendation is that the techniques, both analytical and experimental, presented in this report and Part I should be utilized to ensure data quality in all phases of telemetry system implementation. This includes system design, analysis, specification, standardization, evaluation, testing, alignment and calibration. We believe the noise-loading technique should fill an urgent need experienced by all those concerned with telemetry systems.

Throughout the study we have emphasized that the principal source of phase nonlinearity and hence of intermodulation distortion is the receiver second IF amplifier/filter. Thus a significant improvement in the linearity of the second IF filter will be reflected directly in an improvement in system data quality. We recommend that future efforts should be directed to the development of such filters for telemetry applications.

There are several methods by which the second IF phase linearity can be improved. Since the inband amplitude characteristic of the IF filter has been shown not to be a significant source of intermodulation distortion in telemetry situations, Bessel filters can be used to achieve the desired linear phase characteristics. Measurements with these have shown distortion to be significantly lower than a Butterworth design with the same 3 dB bandwidth. Theoretical predictions based on perfectly aligned filters indicate even more spectacular capabilities. However, the use of Bessel filters necessitates a sacrifice in skirt selectivity and adjacent channel rejection. For example, a sixth-order Butterworth filter has a 2.89 shape factor while the same order Bessel filter has a shape factor of 3.93, which results in the out-of-band attenuation of the Butterworth being about 25 dB better than the Bessel filter. A compromise between the skirt slectivity and phase linearity is achievable with the Transitional Butterworth-Thomson filters (Ref. 6). These filters can be designed such that their characteristics vary between the Butterworth maximally-flat amplitude response and the Bessel maximally-flat group-delay response as the pole positions are changed. Thus, it is entirely feasible with this form of filter to select any point between the linear phase and flat amplitude designs and arrive at a compromise between these two characteristics. The resulting design trades off adjacent channel rejection for low intermodulation distortion.

A Paynter filter design (Ref. 7) could also be used for the receiver second IF. This design approximates the linear phase characteristic all across the desired band of frequency, giving a low average delay variation as compared with the Bessel design which concentrates on the near center frequency behavior. The Bessel and Paynter filters have the same relationship in phase characteristic that the Butterworth and Chebyshev filters have in amplitude characteristic. The amplitude response of the Paynter filter, however, has less amplitude variation inband and greater attenuation out of band than the Bessel, thus providing an intermediate compromise between the desirable phase characteristic of the Bessel filter and the desirable amplitude characteristics of the Butterworth design.

The obvious drawback in the Bessel, Butterworth-Thomson and Paynter designs is the need to tradeoff linear phase characteristics against flat inband amplitude characteristics and high out-of-band attenuation. This is the same tradeoff encountered in most modern filter design techniques (Butterworth, Chebyshev, etc.). It is a consequence of the minimum-phase assumption which introduces an enormous simplification in the synthesis of realizable filters. The minimum-phase criterion permits the approximation of either the amplitude or phase characteristics of physically realizable filters and then specifies the other in such a way as to ensure relizability. Thus, under a minimum-phase design procedure the amplitude and phase characteristics are interrelated such that simultaneous approximation of both flat amplitude and linear phase characteristics is impossible.

It is possible to simultaneously approximate a linear phase and flat amplitude filter by using a non-minimum phase design technique. One approach using such a procedure has been described by Lerner (Ref. 8) in which a passive network realization using lattice techniques is employed to derive a bandpass filter with flat inband amplitude response and a linear phase characteristic. The skirts of this filter provide at least as much out-of-band attenuation as the same order Butterworth filter for the first 50 dB. This design technique thus holds promise for satisfying both the requirements of adjacent channel rejection and low intermodulation distortion by providing filters with high skirt selectivity and low group-delay variations.

Other techniques for the design of non-minimum phase filter characteristics using the procedures of active network synthesis are under investigation. These include the application of negative impedance converters, controlled sources, and operational amplifiers in the realization of specialized filter characteristics through the independent manipulation of poles and zeroes. Kerwin and Huelsman (Ref. 9) describe such a technique in which high nearband attenuation is achieved. The active network procedures hold particular promise in that they are ideally suited to implementation with integrated circuit techniques,

thus providing the additional benefit of size reduction. Networks using these techniques have been built in the range of hundreds of kHz. However, application in the frequency range of the second IF filters of telemetry receivers has not yet been achieved.

One more technique for achieving linear phase and high out-of-band rejection deserves mention. This method employs a cascade of a linear phase filter which has poor skirt selectivity and out-of-band notch filters to achieve adjacent channel rejection. In principle, this technique is similar to the well-known method of approximating the desired rectangular amplitude characteristic and then compensating the phase nonlinearities by cascading delay equalizing networks. This method is currently being investigated and it remains to be seen if the out-of-band notches can be brought close enough to the desired bandedge to give adequate skirt selectivity without having their phase characteristics affect the inband phase linearity of the filter.

It is clear that many approaches are available for achieving filters with linear phase and high skirt selectivity. Application of these techniques to telemetry receiver designs will permit independent control of the intermodulation distortion and adjacent channel rejection characteristics which are currently interrelated in telemetry systems. We strongly recommend that these approaches be investigated, both analytically and experimentally, for inclusion in future telemetry systems.

It would be useful to subject all of the passive and active filter types outlined here to an analysis using the Hermite Polynomial Technique (presented in Section 4.3 of Part I). This technique is a more convenient method of calculating the distortion factor through which the filter phase characteristic influences the distortion level. This factor, a function of (ω_e / B), serves as a figure of merit for the filter and can be used in conjunction with other parameters such as noise bandwidth and skirt selectivity to select an optimum filter type for telemetry applications.

REFERENCES

1. ADCOM, Inc., "Telemetry Receiver Phase Characteristics and Data Distortion," Draft Final Task Report, Task II, Contract No. NAS5-9742 with Goddard Space Flight Center, March 31, 1965.

2. Weinberg, L., Network Analysis and Synthesis, McGraw-Hill Book Co., Inc., New York, 1962.

3. Orchard, H. J., "The Phase and Envelope Delay of Butterworth and Tchebycheff Filters," IRE Trans. on Circuit Theory, Vol. CT-7, No. 2, pp. 180-181, June 1960.

4. Storch, L., "Synthesis of Constant-Time-Delay Ladder Networks Using Bessel Polynomials," Proc. IRE, Vol. 42, No. 11, pp. 1666-1675, November 1954.

5. Seely, S., Radio Electronics, McGraw-Hill Book Co., Inc., New York, 1956.

6. Peerless, Y. and Murakami, T., "Analysis and Synthesis of Transitional Butterworth-Thomson Filters and Bandpass Amplifiers," RCA Review, pp. 60-94, March 1957.

7. Hansen, P. D., "New Appraches to the Design of Active Filters," The Lightening Empiricist, Vol. 13, Nos. 1 and 2, pp. 3-16, July 1965.

8. Lerner, R. M., "Bandpass Filters with Linear Phase," Proc. IEEE, Vol. 52, pp. 249-268, March 1964.

9. Kerwin, W. J. and Huelsman, L. P., "The Design of High Performance Active R-C Bandpass Filters," IEEE International Convention Record, Vol. 14, Part 10, pp. 74-80, March 1966.